

Alma Mater Studiorum – Università di Bologna

DOTTORATO DI RICERCA IN

Ingegneria Civile, Chimica, Ambientale e dei Materiali

Ciclo XXX

Settore Concorsuale: 08/B2

Settore Scientifico Disciplinare: ICAR/08

GEOMETRICALLY NONLINEAR ANALYSIS OF THIN-WALLED
BEAMS BASED ON THE GENERALIZED
BEAM THEORY

Presentata da: Andrea Walter Ruggerini

Coordinatore Dottorato:

Prof. Luca Vittuari

Relatore:

Prof. Francesco Ubertini

Correlatore:

**Prof. Stefano de Miranda
Ing. Antonio Madeo**

Esame finale anno 2018

Andrea Walter Ruggerini: *Geometrically nonlinear analysis of thin-walled beams based on the Generalized Beam Theory*, A nonlinear beam model incorporating genuine folded-plate concepts , © December 2017

ABSTRACT

The thesis addresses the geometrically nonlinear analysis of thin-walled beams by the Generalized Beam Theory (GBT). Starting from the recent literature, the linear theory is illustrated, along with some issues related to GBT finite element formulation. Potential benefits of using the GBT in design are exemplified with reference to the design of roofing systems. To assess the deterioration of member capacity due to cross-section distortion phenomena, the formulation of a geometrically nonlinear GBT is then pursued. The generalization of the GBT to the nonlinear context is performed by using the Implicit Corotational Method (ICM), devising a strategy to effectively apply the ICM when considering higher order deformation modes. Once, obtained, the nonlinear model has been implemented using a state-of-the-art mixed-stress finite element. The nonlinear finite element is then implemented starting from the linear GBT one. Different numerical tests show the performance of the proposed approach in buckling and path-following analyses.

...

CONTENTS

1	INTRODUCTION	1
2	THIN-WALLED BEAMS: TECHNICAL APPLICATIONS AND MODELING STRATEGIES	3
2.1	CFS members	4
2.1.1	Production process	4
2.1.2	Applications	5
2.2	Analysis of thin-walled beams	8
2.2.1	The GBT theory	9
2.2.2	Finite Strip and constrained Finite Strip Methods	11
2.2.3	Constrained FEM	13
2.2.4	Beam models based on 3D elasticity reduction by generalized eigenvalue analysis	14
2.2.5	Carrera Unified Formulation	15
3	THE LINEAR GBT	17
3.1	Kinematics	18
3.2	Cross-section deformation modes	20
3.3	Generalized stresses	22
3.4	Cross-section stiffness matrix	22
3.5	The mixed-stress GBT linear finite element	27
4	GBT-BASED DESIGN OF FLEXIBLE ROOFING SYSTEMS	29
4.1	Verification of steel roofing systems	30
4.1.1	Structural modeling	33
4.1.2	Design parameters at SLS and ULS - Synthetic results	34
4.2	Some remarks	38
5	THE COROTATIONAL-BASED GBT: BUCKLING FE ANALYSIS	39
5.1	ICM for thin-walled beams	40
5.1.1	Quadratic generalized strains	42
5.1.2	Some remarks	42
5.2	Change of kinematic parameters	44
5.3	Essential flowchart to obtain a geometrically nonlinear finite element	48
5.4	Elastic energy of the linear finite element	48
5.5	Corotational observers over the finite element	49
5.5.1	Change of observer	50
5.5.2	Transformation approximation and geometric stiffness matrix	52
5.6	Numerical Tests	54
5.6.1	Rack-section beam	54
5.6.2	Trapezoidal-section beam	60

5.7	Conclusions	66
6	THE COROTATIONAL-BASED GBT: GEOMETRICALLY NON-LINEAR ANALYSES	67
6.1	Path-following analysis	68
6.1.1	Rotator approximation	68
6.1.2	Energy variations	69
6.1.3	Iterative solution scheme	70
6.2	Numerical Examples	72
6.2.1	Stocky rack-section beam subjected to distortional load	72
6.2.2	Rack-section beam subjected to shear force	80
6.2.3	Z-section beam subjected to distortion	89
7	CONCLUSIONS	99
A	DETAILS OF THE LINEAR GBT	103
A.1	Submatrices of the cross-section stiffness matrix	103
A.2	General form for the cross-section stiffness matrix	104
A.3	Modal decomposition	105
A.4	Self-equilibrated interpolations for generalized stresses	106
B	SELECTED EXAMPLES FOR GA AND TA APPROACHES	109
C	SECOND ORDER STRAINS IN TERMS OF GBT MODES	117
D	ROTATOR APPROXIMATION	119
	BIBLIOGRAPHY	121

LIST OF FIGURES

Figure 2.1	scheme of cold-formed machine production line	5
Figure 2.2	CFS section developed by specific manufacturers, image from [61].	6
Figure 2.3	Typical usage of CFS for framing and decking in industrial and residential buildings	6
Figure 2.4	Excerpt from [25], examples of distortional buckling modes.	7
Figure 2.5	Example of FSM discretization for a lipped channel section, image from [62]	11
Figure 2.6	FSM and cFSM signature curves example for a member under axial force, image from [62]	12
Figure 2.7	Examples of cFEM results for the study and identification of members with holes, from [3]	13
Figure 2.8	Higher order deformation modes can be obtained for general cross-section shapes from the FEM analysis of the 2D problem	14
Figure 2.9	Table from [14], highlighting the hierarchical enrichment made possible by CUF theory for 1D formulations	15
Figure 3.1	Thin-walled cross-section with 5 walls and 6 natural nodes. The local, right handed reference system associated to wall 2 is showed	18
Figure 3.2	Cross-section stiffness matrix for a cross-section with 5 walls. The coupling in the natural space is evident in the top image. The bottom part shows the stiffness matrix in the modal space.	24
Figure 3.3	Fundamental flexural modes for a C-shaped cross-section	25
Figure 3.4	Local flexural modes and in-plane wall-extensions.	26
Figure 4.1	Modeling laterally braced purlins rotationally restrained by sheeting, from [25].	31
Figure 4.2	Roof model restraints, image from [10].	32
Figure 4.3	Verification procedures at ULS for (a) TA and (b) GA.	33
Figure 4.4	Ratio r_1 according to TA and GA approaches	35
Figure 4.5	Ratio r_2 according to TA and GA approaches	36

Figure 4.6	Distribution of fibre stress ratio r_2 across all 100 examples	37
Figure 5.1	C-shaped cross-section: GBT deformation modes in the modal space	46
Figure 5.2	C-shaped cross-section: GBT deformation of fig. 5.1 after the change of kinematic parameters	47
Figure 5.3	Definition of the cross-section panel over the e -th finite element.	50
Figure 5.4	corotational observer onto the deformed configuration.	51
Figure 5.5	Rack-section beam under compression: geometry boundary conditions and loads	54
Figure 5.6	rack-section beam: included in-plane GBT modes	55
Figure 5.7	Rack-section beam, buckling modes 1 – 2, deformed shapes and cumulative contribution to y -displacement of natural node 1 (see fig. 5.5).	56
Figure 5.8	Rack-section beam, buckling modes 3 – 4, deformed shapes and cumulative contribution to y -displacement of natural node 1 (see fig. 5.5).	57
Figure 5.9	Rack-section beam, buckling modes 5 – 6, deformed shapes and cumulative contribution to y -displacement of natural node 1 (see fig. 5.5).	58
Figure 5.10	Rack-section beam: cumulative GBT modal contribution to buckling modes at $z/L = 1/4$	59
Figure 5.11	trapezoidal-section beam under compression: geometry boundary conditions and loads	60
Figure 5.12	trapezoidal-section beam: included in-plane GBT modes	61
Figure 5.13	Trapezoidal-section beam, buckling modes 1 – 2, deformed shapes and cumulative contribution to y -displacement of natural node 1 (see fig. 5.11).	62
Figure 5.14	Trapezoidal-section beam, buckling modes 3 – 4, deformed shapes and cumulative contribution to y -displacement of natural node 1 (see fig. 5.11).	63
Figure 5.15	Trapezoidal-section beam, buckling modes 3 – 4, deformed shapes and cumulative contribution to y -displacement of natural node 1 (see fig. 5.11).	64
Figure 5.16	Trapezoidal-section beam: cumulative GBT modal contribution to buckling modes at $z/L = 1/4$	65
Figure 6.1	Stocky rack-section beam subjected distortional load: geometry and load detail	73
Figure 6.2	Stocky rack-section beam subjected distortional load: deformed shapes	74

- Figure 6.3 Stocky rack-section beam subjected distortional load: equilibrium path for node 3 at $z/L = 1$ 75
- Figure 6.4 Stocky rack-section beam subjected distortional load: equilibrium path for node 6 at $z/L = 1$ 76
- Figure 6.5 Stocky rack-section beam subjected distortional load: equilibrium path for node 3 at $z/L = 1/2$ 77
- Figure 6.6 Stocky rack-section beam subjected distortional load: equilibrium path for node 6 at $z/L = 1/2$ 78
- Figure 6.7 Stocky rack-section beam subjected distortional load: cross-section at $z/L = 1$ 79
- Figure 6.8 Rack-section beam subjected shear forces: geometry and load detail 81
- Figure 6.9 Rack-section beam subjected to shear forces: deformed shapes 82
- Figure 6.10 Stocky rack-section beam subjected distortional load: equilibrium path for node 3 at $z/L = 1$ 83
- Figure 6.11 Stocky rack-section beam subjected distortional load: equilibrium path for node 6 at $z/L = 1$ 84
- Figure 6.12 Stocky rack-section beam subjected distortional load: equilibrium path for node 3 at $z/L = 1/4$ 85
- Figure 6.13 Stocky rack-section beam subjected distortional load: equilibrium path for node 6 at $z/L = 1/4$ 86
- Figure 6.14 Rack-section beam subjected to shear forces: cross-section at $z/L = 1/4$ 87
- Figure 6.15 Rack-section beam subjected to shear forces: cross-section at $z/L = 1$ 88
- Figure 6.16 Z-section beam subjected cross-section distortion: geometry and load detail 89
- Figure 6.17 Z-section beam (distortional load), 3D plot 90
- Figure 6.18 Stocky rack-section beam subjected distortional load: equilibrium path for node 2 at $z/L = 1$ 91
- Figure 6.19 Stocky rack-section beam subjected distortional load: equilibrium path for node 3 at $z/L = 1$ 92
- Figure 6.20 Stocky rack-section beam subjected distortional load: equilibrium path for node 2 at $z/L = 1/2$ 93

Figure 6.21	Stocky rack-section beam subjected distortional load: equilibrium path for node 3 at $z/L = 1/2$	94
Figure 6.22	Stocky rack-section beam subjected distortional load: equilibrium path for node 5 at $z = 312mm$	95
Figure 6.23	Z-section beam subjected to distortion: cross-section at $z/L = 1$	96
Figure 6.24	Z-section beam (distortional load), cross-section plot 2	97
Figure B.1	Sketch of Z-sections analyzed and relevant elastic restraints: on the left hand side shear restraint and lateral one, on the right hand side shear and rotational restraints.	109

ACRONYMS

FE Finite Element

ICM Implicit Corotational Method

CUF Carrera Unified Formulation

DSM Direct Strength Method

FSM Finite Strip Method

cFSM constrained FSM

cFEM constrained FEM

FEM Finite Element Method

AISI American Iron and Steel Institute

CFS Cold Formed Steel

ECCS European Convention for Constructural Steelwork

EC3 Eurocode 3

TA Traditional approach

GA GBT-based approach

GBT Generalized Beam Theory

ETM Effective Thickness Method

EWM Effective Width Method

ULS Ultimate Limit States

SLS Serviceability Limit States

RM Roof Model

CR Corotational



INTRODUCTION

Throughout history a lot of efforts have been made to improve the characteristics of structures and structural systems. During ancient and classical times one of the main challenges was on how to build larger and daring structures with the available materials and technologies. This certainly is still today one of the most exciting topic in engineering, especially considering what has been achieved by human intuition when formal modeling of structures was unfeasible or difficult: from the Pyramids, to the Italian Renaissance to early railway bridges during the Industrial Revolution.

Even if deeply connected to huge structures, the research for structural efficiency and lightness in engineering is not limited to them. Industrialized production of goods has changed the way we live, and the performances are not measured only on the basis of mechanical characteristics.

Ease of fabrication, transportation, assembly, along with environmental compatibility are key factors requested to implement a modern structural system. An answer to these concerns may be provided by structures made of thin-walled beams.

Thin-walled beams are slender structural bodies that possess a length L_b considerably greater than the cross-section characteristic dimension, h . The cross-section is in turn characterized by an extremely reduced thickness t . Just for sake of example, if the ratio L_b/h may range from 5 to 20, the h/t ratio may vary from 50 to 150. Designing structures made of very slender elements strongly improves structural efficiency, but their safety has to be guaranteed by a proper modeling and calculation.

Large-scale applications of thin-walled beams begun after World War II in the North America, where many of the main manufacturers and associations were born. As often happened throughout history, starting from the Galileo's theories about the mechanics of the beams, the engineering applications anticipated the full theoretical understanding of beams structures. This is especially true for thin-walled beams which can encompass a 3D complex kinematics and whose behavior may be not faithfully represented by classical beam theories.

A correct and clear prediction of structural behavior under all design conditions is probably one of the most desirable objective to be achieved to further extend the applications of thin-walled beams: to this extent, great effort has been spent in the last fifty years, including

both theoretical contributions and technical provisions. Nonetheless a gap among theory and practice is still evident to the design engineer.

Geometrical nonlinearity and sensitivity to imperfections are among the hardest problems still to be comprehensively addressed. The aim of this work is to offer a contribution in this field by formulating the geometrically nonlinear version of an the enriched beam theory named Generalized Beam Theory (GBT). The GBT peculiarity is to be able to consistently account for cross-section distortion along with the more “classical” kinematics of axial displacement, bending and torsional rotation in a comprehensive fashion. In particular, here, the geometrically nonlinear formulation is developed based on the Corotational (CR) approach. Some calculation examples, including numerical test and design studies, are provided in this very spirit: to show the potential of the proposed approach and to provide hints for more extensive applications.

The thesis structures reflects the presented objectives. Chapter 2 is devoted to the contextualization of this work into the very vast literature available. It is focused on the features of cold-formed steel beams, the most popular class of thin-walled beams. The manufacturing process is addressed, along with a perspective view on the analysis of thin-walled beams.

Chapter 3 introduces a state-of-the-art version of the linear GBT. The implementation of a linear beam finite element based on the Hellinger-Reissner potential is illustrated, including the contribution of fundamental and higher-order GBT modes.

Chapter 4 presents an extended study on cold-formed steel roofing system, emphasizing the differences in the verification approach whenever using semi-empirical formulae to address geometric nonlinearity and a simplified geometrically nonlinear GBT. The possibility of using GBT in design constitutes further motivation for the development of a geometrically exact version of the beam theory.

In Chapter 5 geometrically nonlinear GBT is formulated and the results in the framework of buckling analyses are discussed. The geometrically nonlinear model is recovered reusing the model available in the linear context. This generalization to the nonlinear context is obtained exploiting the corotational based method called Implicit Corotational Method (ICM).

The full derivation, starting from the linear strain energy is carried out, and the results of linearized buckling analyses with the new formulation are showed. The results show how a very good accuracy can be achieved for two meaningful problems, especially when compared to richer shell models.

Chapter 6, extends the ICM-based GBT to path-following analyses to prove how the limited kinematics introduced in the beam model can describe with good approximation some three-dimensional phenomena involving cross-section distortion.

THIN-WALLED BEAMS: TECHNICAL APPLICATIONS AND MODELING STRATEGIES

The aim of the following chapter is to contextualize this thesis into the extremely vast world of researches and applications of thin-walled structures. Thin-walled beams are largely used whenever an optimal strength-to-weight ratio is necessary. The most common thin-walled load bearing structures in civil engineering are made of cold-formed steel, but their analysis and design requires suitable tools and methods: an essential introduction is proposed to provide framework to the presentation of the [GBT](#), a higher order beam theory incorporating genuine folded plate concepts.

2.1 CFS MEMBERS

Light gauge metal steel, steel studs, lightweight framing collect what we can group under the more precise name Cold Formed Steel (CFS) members. CFS are thin-walled structural elements, characterized by the cold-working production process, being for this reason very thin with respect to their hot rolled counterpart.

CFS elements in civil engineering structures appeared in the late years of 1800 in Great Britain and the United States, but there was no wide diffusion up to the 1940s.

As a matter of fact, in 1939 the American Iron and Steel Institute (AISI) sponsored George Winter's research at Cornell University, who edited, seven years later, the first edition of the "Specifications for the Design of Cold-formed Steel Structural Members".

The massive adoption of CFS in Europe has been slower, but in the 1970s large scale applications appeared. In the early 1980s the European Convention for Constructural Steelwork (ECCS) published the "Good practices in steel cladding and roofing".

Since then, the adoption of CFS elements has greatly expanded all over the world: structural efficiency, process optimization and re-usability are among the success factors of this technology enabled by the contemporary evolution and research in design and calculation methods.

2.1.1 *Production process*

The very first step in the process that brings commercial CFS structural elements onto the market is the production of raw steel and its transformation into a "coil". Iron ore and steel scrap are mixed in a furnace, the melt is then poured into slabs that are subsequently reduced to thinner strips ("hot band").

The hot band is then reduced again into thinner and thinner sheets and a very thin, protective zinc coating is added by galvanization. The final product is the rolled coil, from whose a wide range of structural elements can be formed by cold-working processes.

Commonly used cold-working processes are press braking and roll forming, the former consist in working a planar sheet by an hydraulic press and is suitable for small scale production or relatively thick sheets. The latter is a continuous process taking potentially full advantage of many process optimization.

By using automated roll former machines, producers are nowadays able to deliver pre-cut, pre-punched and custom sized steel elements directly from CAD drawings.

The finished product is then ready to be sold on the mass market, either to distribution centers or directly to contractors and builders.

Another interesting option is the possibility of transport roll-forming machine to assist the construction directly on the site thus totally avoiding warehouse logistic.

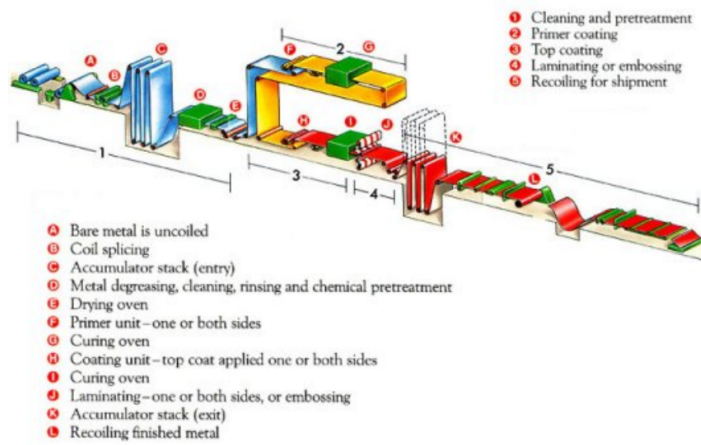


Figure 2.1: scheme of cold-formed machine production line

2.1.2 Applications

CFS members may be used as isolated members, nonetheless, due to their thinness, the highest structural optimization is often achieved when using complete structural systems. Hence framing, decking and roofings are commonly made of CFS members interacting with cladding or sheeting providing restraints. Standardized members are widely available and often worked directly on the construction site.

2.1.2.1 Members

Commonly used cross-sections are C, Z and their variations for isolated members and hat sections for decking panels. Variations are mainly composed or stiffened C and, to lesser extent, Z sections, in highly optimized fashion, like Sigma sections in racks. A number of independent manufacturers have developed custom production processes to provide stiffening enhancements, specific coatings or improved thermal, as showed in figure 2.2. Due to manufacturing constraints CFS beam thickness range from 0,5mm for uprights and dry walls to 8mm of larger beams.

2.1.2.2 Industrial and industrialized buildings

Industrial and industrialized buildings may be entirely made with CFS elements. Usage of thin-beams is especially devoted to secondary members, such purlins and girts, roof supports and walls. Prefabricated assemblies, such as trusses, are more common in low-rise, resi-

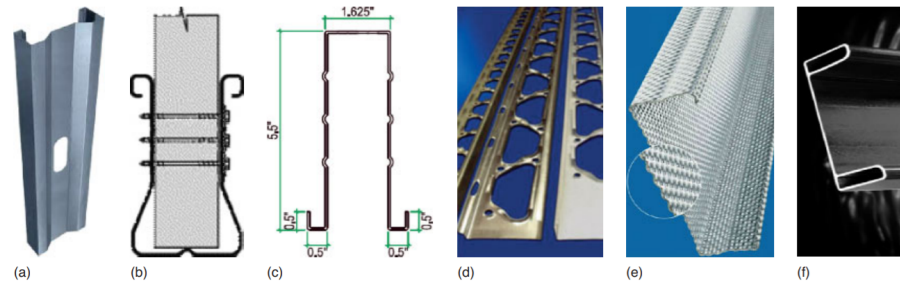
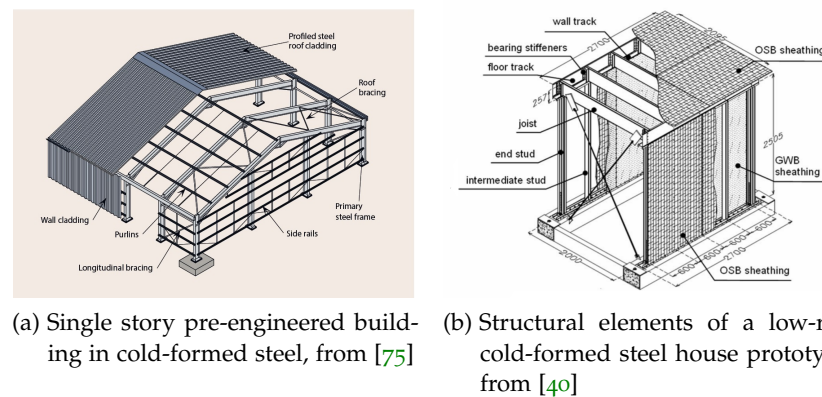


Figure 2.2: CFS section developed by specific manufacturers, image from [61].

dential buildings. Figure 2.3 shows two typical arrangements of CFS members.



(a) Single story pre-engineered building in cold-formed steel, from [75]

(b) Structural elements of a low-rise cold-formed steel house prototype, from [40]

Figure 2.3: Typical usage of CFS for framing and decking in industrial and residential buildings

2.1.2.3 Some problems in practical applications

Roll forming process typically produces CFS with open cross-sections. Z and C-shaped beams are the most widespread, but other ones like hat sections, sigma etc. are used in particular context or from manufacturers wanting to further optimizing strength characteristics.

Current approach to the verification of steel beams relies on the assumption rigid cross-section, implicitly defining a two-level model where local stability issues, are checked at the cross-section level and global stability is checked at the member level. For this reason, interaction is partially hidden or disregarded in the majority of approaches. Stability of members subjected to the interaction mechanisms among global and local phenomena is an active research field (for instance, the method of the Erosion of Critical Buckling Load", see [23, 24]).

Moreover, major design codes, such as Eurocode 3 (EC3) and American Iron and Steel Institute (AISI), identify an intermediate type of

stability issue for open section members, named “distortional”. Distortional behaviors are characterized by change in shape of the cross-section, as depicted in fig. 2.4. Distortional buckling has been historically of particular interest to designers since it may directly affect global member stability: a detailed history has been published by Schafer and Hancock [64], including the main steps for each decade, while an essential summary is provided in table 2.1.

Researches on thin-walled beams behavior, design methods and structural theories are advancing rapidly (see, e.g., recent reviews [38, 61, 63]), and some references for the designers, merging academic and designer’s expertise can be found in are [30, 78, 81] and [54] .

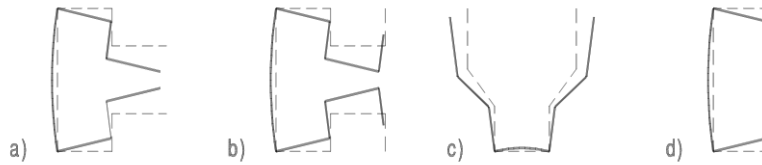


Figure 5.4: Examples of distortional buckling modes

(6) The effects of distortional buckling should be allowed for in cases such as those indicated in figures 5.4(a), (b) and (c). In these cases the effects of distortional buckling should be determined performing linear (see 5.5.1(7)) or non-linear buckling analysis (see EN 1993-1-5) using numerical methods or column stub tests.

Figure 2.4: Excerpt from [25], examples of distortional buckling modes.

period	researches on distortional buckling and applications in design
pre-1960	testing began at Cornell University in the early years of 1940's, "effective width" method based on Von Karman's formula for buckling of plates and experimental correction of Winter [77] for design at ULS. Elastic plate buckling solution provided a practical method for calculating stability of connected plates was available [46]. Local stiffener buckling (i.e. distortional behavior) was noticed in columns [18], but only qualitative provisions were given
1960s	Sharp developed an early a theoretical treatment of distortional buckling for lipped C beams and hat cross sections [68]
1970s	Isolated edge stiffeners were tested by replacing the web with a known support boundary condition [39]. Expressions developed in this period [21] are still the basis for the current specification on distortional buckling in the AISI codes.
1980s	First studies on highly optimized rack-sections by accounting for distortional buckling[37]. A method suitable for hand calculation and more refined with respect to Sharp's one, was proposed [41].
1990s	Eurocode 3, part 1-3, provided a method for predicting distortional buckling in members with simple cross-sections [26].

Table 2.1: essential the evolution of distortional buckling in design codes

2.2 ANALYSIS OF THIN-WALLED BEAMS

By now, beam theories have been a formidable tool for civil engineers and designer in general to assess the global behavior of physical structures. In this paragraph an overview of classical and more recent beam theories is presented, all within the assumption of linearized kinematics and infinitesimal strains in linear elasticity. Second order models, nowadays fundamental in design of slender structures, are easily derivable by the linearized kinematics and used in many software implementation all around the world. The basic theories, however have a long history to tell.

The assumption of the classic Euler-Bernoulli beam theory requires (i) rigid cross-cross and that (ii) the cross-section keeps perpendicular to the deformed beam axis. Generalized displacements are one trans-

lation per spatial direction and one rotation per cross-section direction. Corresponding generalized forces are axial force, and bending moments. Torsion deformations for many practical problems are negligible or can be faced by St. Venant homogeneous torsion for some cross-section shapes. The original beam theory addressing nonuniform torsion is the Vlasov's one [76], in which the generalized deformation warping is coupled to a new generalized stress called bimoment. Torsional rigidity is proportional to t^3 , hence torsional stiffness may be quite low in thin-walled beams. Moreover, for manufacturing constraints (see 2.1.1), often cross-section are not symmetrical, hence applied loads initiates rotation because shear center is typically outside of the cross-section.

However, the Vlasov beam model maintains the basic hypotheses of the cross-section being rigid in its own plane and of null shear deformability. Regarding the second of these, the work of Capurso [12, 13] extended the model of Vlasov to include shear deformation over the cross-section mid-line by generalizing the description of warping. More recently, other researchers have revolved around the inclusion of shear deformability on Vlasov like beam models. However, beam models based on the kinematics of Vlasov fail to take into account the effects of cross-section distortion and local in-plane deformation of the walls. Some approaches or beam theories allowing to overcome this limitation are briefly described in the following.

2.2.1 *The GBT theory*

The **GBT** is a beam theory with enriched kinematics. Its distinguishing feature it is the ability to consistently include higher order generalized displacements on top of classical beam ones.

In its very first formulation, due to Schardt [65], the generalized displacements were thought to allow in-plane cross-section distortion and the relevant out of plane displacements associated, i.e. the warping ones. It is perhaps worth to notice that Schardt himself was inspired in its work by the Vlasov's one and when referring to the newborn beam theory he also used the term "Faltwerke", German for "folded structures".

The subsequent book of Schardt [67] is still today a reference for **GBT** researchers all around the world, even if somewhat inaccessible to non-german speakers. An overview of publications from 1966 to 2001 can be found on the website <http://www.vtb.info/>, which is controlled by the Christof Schardt, the son of Richard.

Later on, Schardt and its group, published [66] their work in English, nonetheless the diffusion of **GBT** among the english-speaking community is probably due to Davies and coworkers, who applied the theory in a finite difference numerical implementation: their first

[19] and second order [20] analysis of cold-formed steel beams made the approach popular. Subsequently a lot of researchers have been researching on the GBT theory and its applications. Only a brief history is reported here, with no claim of completeness.

During the 2000s, Simão and da Silva[73] investigated the buckling behavior of open and closed members by making use of the GBT theory. Simão also explored applications of the GBT analysis to commercial cold-formed beams [72].

Another Portuguese group, led by Dinar Camotim, has been one of the most active in the last ten years in the development of the GBT. Camotim, started the Lisbon school, whose researchers have substantially contributed to the success of the theory: with Nuno Silvestre, a GBT analytical formula for the computation of distortional buckling loads of C,Z and rack sections were derived [70] and the first version of a geometrically nonlinear GBT for imperfect columns was proposed [69]. More recently, the research has been focused on deformation mode determination, review of kinematic assumptions and improved introduction of shear deformability as in the works by [11, 22, 71]. Intense researches have also been spent on geometrically nonlinear models accounting for cross-section distortion, including GBT ones, with elastic and elastoplastic material [33–35]. Moreover, a new approach to the calculation of cross-section deformation modes was proposed, in order to consistently deal with arbitrary cross-section shapes by Gonçalves et al. [36] and Bebiano et al. [7]. Moreover, the software package named GBTUL boosts the ability of other researchers to test the numerical implementation of the theory, its second version has been recently presented in [8].

Notwithstanding the impressive effort spent by the above-mentioned groups, GBT researches and applications have been pursued all around the world. Recent researches include a dynamic approach to cross-section analysis, as in [58] and analytical approaches for pre-buckling and buckling analyses as in [74]. Moreover, the solution of the semi-discretized problem has been addressed in [4].

Finally, interesting contributions on the development of a GBT-based numerical model for cold-formed roofing systems are [10, 48], while a GBT with shear deformation was introduced in [50]. A discussion on the relationship of the shear-deformable GBT with classical and non-classical beam theories is developed in [51] and effective procedure for the 3D stress-state recovery in [49]. Very recently, an high-performance flexibility-based GBT finite element inspired by the semi-analytical solutions of the beam differential equations has been proposed in [52].

2.2.2 Finite Strip and constrained Finite Strip Methods

The Finite Strip Method (FSM) was proposed in the late 1960s in the seminal paper of Cheung [16], being originally motivated by the ability of performing dimensional reduction of 3D problems for the implementation on “small and medium sized computers”. Since dimensionality reduction exhibits a series of engineering advantages besides computational effort, the method has been surviving throughout the years and found many applications in structural mechanics [17].

In the FSM a thin-walled structure is discretized onto a set of strips whose longitudinal interpolation is performed on the full support (i.e. the member axis) and not by subdividing the body in the classical FEM fashion. The advantages is hence dependent on the proper choice of shape function for the strip.

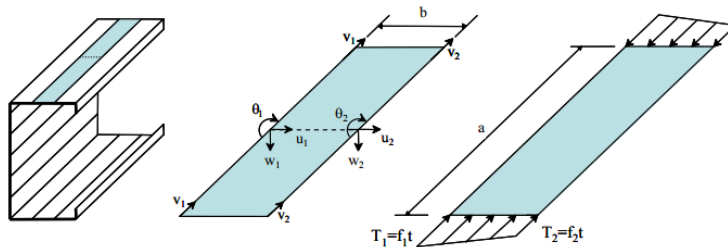


Figure 2.5: Example of FSM discretization for a lipped channel section, image from [62]

An interesting side-effect is that, in case of buckling analysis, results can be expressed as a function of the strip-length parameter. Plotting the critical load as function of the length parameter draws the so-called signature curve. The implementation of constraints for the solution, e.g. by enforcing null in-plane shear, or identifying transverse flexure led to the development of the constrained FSM (cFSM) method and signature curves, which are useful to classify buckling modes in design applications.

The development of the concept of “signature curve”, the interpretative power of its constrained version, the constrained FSM (cFSM), the availability of the software CUFSM (Li and Schafer [42]) and the development of the Direct Strength Method (DSM) for design made this approach very popular in North America.

The advances in this research area are quite rapid, nonetheless some developments are still work in progress, like the extension to general cross-section shapes, and the generalization to members with non-standard support and loading conditions. Particularly, this latter task may not be trivial, since it is deeply connected with the very basic assumption of the method. A comprehensive review of the method, including other developments not treated here, like the introduction

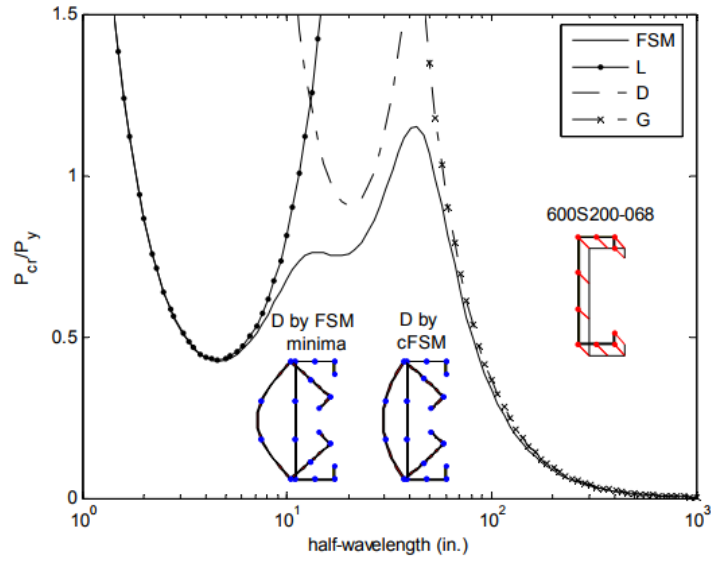


Figure 2.6: **FSM** and **cFSM** signature curves example for a member under axial force, image from [62]

of shear modes, structural optimization and identification of modes in nonlinear analysis may be found in [43].

2.2.3 Constrained FEM

Constrained FEM **cFEM** idea basically derives from the restraining method applied to **FSM** to enable modal identification. The displacement field of a standard, properly formulated, shell element, as the one proposed by Ádány [1], can be constrained to any modal deformation space, thus enabling the introduction of the amplitude functions governing the remaining degrees of freedom. The approach may lead to similar results but is conceptually different with respect to the **GBT** one: **GBT** introduces just the desired kinematics, whereas the definition of a proper restraining technique is the core of the **cFEM**.

Developments **cFEM** finite elements are very recent [2, 3]. Nonetheless, it potentially provides full modal decomposition and satisfy mechanical criteria needed for design. Being based on general purpose **FEM** possible applications are extremely vast. Moreover the relationship among beam theories and **cFEM** are yet to be explored, but constitute an interesting research area.

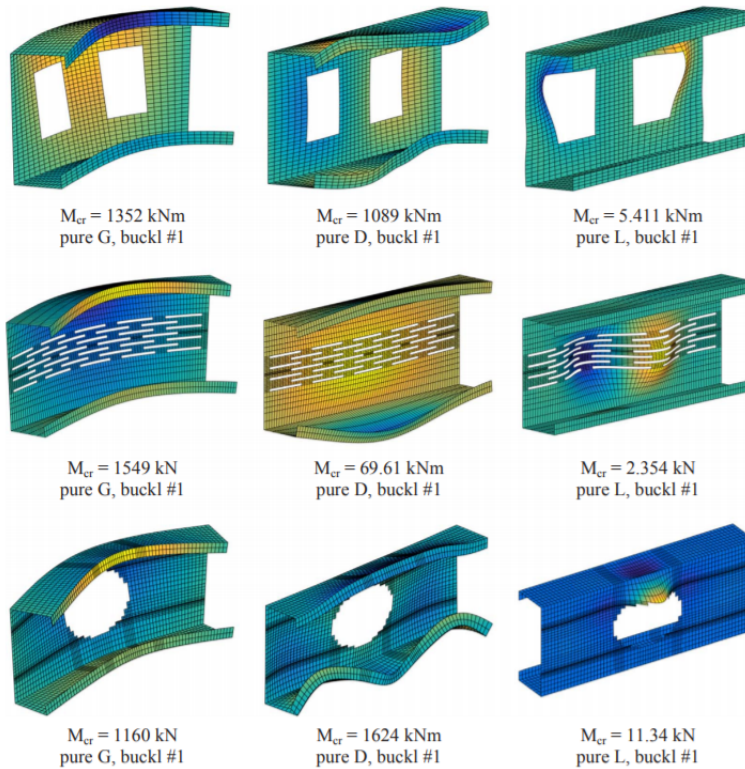


Figure 2.7: Examples of **cFEM** results for the study and identification of members with holes, from [3]

2.2.4 Beam models based on 3D elasticity reduction by generalized eigenvalue analysis

General approaches to the analysis of thin-walled beams have been explored by directly separating the 3D elasticity problem into a 2D [FEM](#) eigenvalue problem and the determination of eigenvectors amplitudes along a one-dimensional domain. The axial solution can be based on analytical functions or interpolated via the [FEM](#).

In this context, a 1D model has been recently presented by Genoese et al. [32], together with a finite element implementation based on the Hellinger-Reissner principle. The model does extend the St. Venant solution with higher order deformation modes. The advantage of using a semi-analytical solution for higher modes, which is in exponential form, consists in being able to assess a-priori the importance of different eigenvectors.

The approach has proven to be effective in buckling analyses [31], and it has been extensively compared to the [GBT](#) formulation in this context by Garcea et al. [29]. With respect to the [GBT](#), no simplifications are made on the in-plane behavior of the cross-section, therefore the applications to any cross-sectional shape is straightforward, avoiding some [GBT](#) complexities in the analysis of the cross-section.

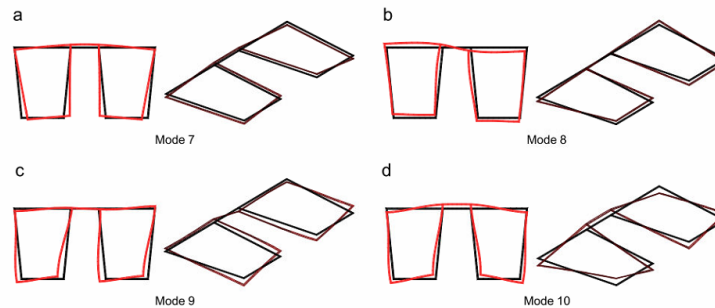


Figure 2.8: Higher order deformation modes can be obtained for general cross-section shapes from the [FEM](#) analysis of the 2D problem

2.2.5 Carrera Unified Formulation

The Carrera Unified Formulation (CUF) is a general FEM formulation for the approximation of structural mechanics problems. The interesting point, central to the formulation, is that the governing equations can be arranged according to the so-called Fundamental Nucleus, leading to the automatic formulation of several structural models (see fig. 2.9). Interesting applications have been performed and a recent review of the method may be found in Carrera et al. [15]. Finally, a geometrically nonlinear formulation has been recently proposed by Pagani and Carrera [56].

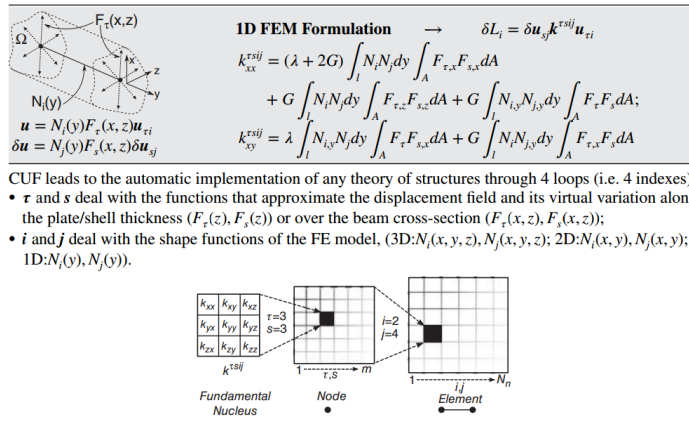


Figure 2.9: Table from [14], highlighting the hierarchical enrichment made possible by CUF theory for 1D formulations

THE LINEAR GBT

This Chapter introduces the linear Generalized Beam Theory (GBT) as originally proposed by Schardt [67] and subsequently improved by other researchers [50, 51] to include shear deformation in a consistent way with respect to classical and non-classical beam theories. The formulation of the relevant linear finite element [52], based on the Hellinger-Reissner variational principle, is then illustrated.

3.1 KINEMATICS

The basic idea of the GBT models is to decompose the three-dimensional displacement field $\mathbf{u}[s, n, z]$ into two conceptually different parts:

- a set of functions defined over the cross-section known in the literature as “GBT modes”, providing a cross-sectional discretization,
- amplitude functions, called generalized parameters, defined over the beam axis.

With this in mind, for the generic wall of the cross-section, the assumed displacement field is written, with respect to the local reference system, (see figure 3.1) as [50, 51]:

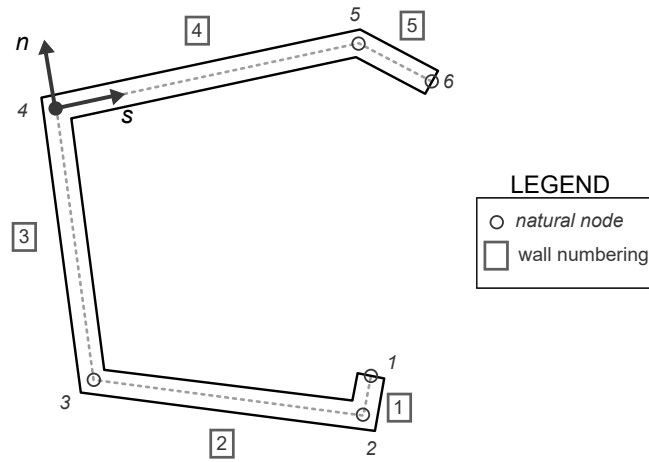


Figure 3.1: Thin-walled cross-section with 5 walls and 6 natural nodes. The local, right handed reference system associated to wall 2 is showed

$$\mathbf{u}[n, s, z] = \mathbf{N}[n, s] \delta[z],$$

$$\mathbf{u}[n, s, z] = \begin{bmatrix} u_n \\ u_s \\ u_z \end{bmatrix}, \quad \mathbf{N}[n, s] = \begin{bmatrix} \boldsymbol{\psi}[s] & \mathbf{0} \\ \boldsymbol{\zeta}[s, n] & \mathbf{0} \\ \mathbf{0} & \boldsymbol{\theta}[s, n] \end{bmatrix}, \quad \delta[z] = \begin{bmatrix} v[z] \\ w[z] \end{bmatrix}, \quad (3.1)$$

where u_n, u_s are the displacements orthogonal and parallel to the wall mid-line and u_z the one in the direction of the beam axis. The matrix \mathbf{N} collects the cross-section deformation modes $\boldsymbol{\psi}, \boldsymbol{\zeta}, \boldsymbol{\theta}$, dependent on local coordinates s, n . The aforementioned functions are written as:

$$\boldsymbol{\zeta}[n, s] = \boldsymbol{\mu}[s] - n \partial_s \boldsymbol{\psi}[s], \quad \boldsymbol{\theta}[n, s] = \boldsymbol{\varphi}[s] - n \boldsymbol{\psi}[s], \quad (3.2)$$

where ∂_s denotes the derivative with respect to the s coordinate.

The linear strain field is then computed from eqs. 3.1 and 3.2 through the point-wise compatibility equations, and the terms deriving from the bending part (i.e. depending on n) and those generated by the one associated to the membrane one are separated, and denoted, respectively, by the superscripts (M) , (B) ,

$$\begin{aligned}\varepsilon_{l,ss}[n, s, z] &= \varepsilon_{ss}^{(M)}[s, z] + \varepsilon_{ss}^{(B)}[n, s, z], \\ \varepsilon_{l,zz}[n, s, z] &= \varepsilon_{zz}^{(M)}[s, z] + \varepsilon_{zz}^{(B)}[n, s, z], \\ \varepsilon_{l,zs}[n, s, z] &= \varepsilon_{zs}^{(M)}[s, z] + \varepsilon_{zs}^{(B)}[n, s, z], \\ \varepsilon_{l,zn}[s, z] &= \varepsilon_{zn}^{(M)}[s, z],\end{aligned}\tag{3.3}$$

where:

$$\begin{aligned}\varepsilon_{ss}^{(M)} &= \partial_s \mu v, \\ \varepsilon_{ss}^{(B)} &= -n \partial_{ss} \psi v, \\ \varepsilon_{sz}^{(M)} &= \frac{1}{4} ((\partial_s \varphi + \mu) (\partial_z v + w) + (\mu - \partial_s \varphi) (\partial_z v - w)), \\ \varepsilon_{sz}^{(B)} &= \frac{1}{2} (-n \partial_s \psi) (\partial_z v + w), \\ \varepsilon_{zz}^{(M)} &= \varphi \partial_z w, \\ \varepsilon_{zz}^{(B)} &= -n \psi \partial_z w, \\ \varepsilon_{nz}^{(M)} &= \frac{1}{2} \psi (\partial_z v - w),\end{aligned}\tag{3.4}$$

and ∂_z denotes derivative with respect to the z coordinate.

By adopting Voigt notation, and representing only the non-null linear strains in the vector $\boldsymbol{\varepsilon} = [\varepsilon_{ss}, \varepsilon_{zz}, 2\varepsilon_{zs}, 2\varepsilon_{nz}]^T$, the strains can be rewritten as follows:

$$\begin{aligned}\boldsymbol{\varepsilon} &= \boldsymbol{\varepsilon}^{(M)} + \boldsymbol{\varepsilon}^{(B)}, \\ \boldsymbol{\varepsilon}^{(M)} &= \mathbf{b}^{(M)}[s, n] \mathbf{e}[z], \quad \boldsymbol{\varepsilon}^{(B)} = \mathbf{b}^{(B)}[s, n] \mathbf{e}[z],\end{aligned}\tag{3.5}$$

where

$$\begin{aligned}\mathbf{b}^{(M)} &= \begin{bmatrix} \partial_s \mu & 0 & 0 & 0 \\ 0 & \varphi & 0 & 0 \\ 0 & 0 & \partial_s \varphi + \mu & \frac{1}{2}(\mu - \partial_s \varphi) \\ 0 & 0 & 0 & \psi \end{bmatrix}, \\ \mathbf{b}^{(B)} &= \begin{bmatrix} -n \partial_{ss} \psi & 0 & 0 & 0 \\ 0 & -n \psi & 0 & 0 \\ 0 & 0 & -2n \partial_s \psi & 0 \\ 0 & 0 & 0 & 0 \end{bmatrix},\end{aligned}\tag{3.6}$$

The vector $e[z]$ collects the generalized deformations of the beam model, which can be expressed in terms of generalized displacements as:

$$e^T = \left[v^T \quad (\partial_z w)^T \quad \frac{1}{2}(\partial_z v + w)^T \quad (\partial_z v - w)^T \right].$$

Additionally, the compatibility operator D of the beam model may be highlighted by recasting the above relationship in a suitable fashion so that:

$$e = D \begin{bmatrix} v \\ w \end{bmatrix}.$$

In particular, when considering m GBT modes, the operator D is defined as:

$$D = I_m \otimes \mathcal{L}, \quad \mathcal{L} = \begin{bmatrix} 1 & 0 \\ 0 & \partial_z \\ \frac{1}{2}\partial_z & \frac{1}{2} \\ \partial_z & -1 \end{bmatrix}, \quad (3.7)$$

where \otimes denotes the Kronecker product and I_m the m -order identity matrix.

The strain field derived from the assumed kinematics leads to the full recovery of classical shear deformable beam theories, as discussed in detail in reference [51].

3.2 CROSS-SECTION DEFORMATION MODES

Deformation modes are associated to nodes on the cross-section, which can be either natural nodes (the vertices of the cross-section mid-line) or internal nodes (intermediate points along the wall mid-line).

Deformation modes associated to natural nodes are subdivided into fundamental flexural modes and transverse extension modes; those associated to the internal nodes are subdivided into local flexural modes, local transverse extension modes and nonlinear warping modes. Fundamental flexural modes are the same as those of the classical GBT proposed by Schardt [67]: one fundamental flexural mode can be defined for each natural node by assuming, along the section mid-line, a piece-wise linear function φ , $\mu = \partial_s \varphi$ and cubic ψ . In particular, functions ψ are determined by enforcing compatibility among the walls subjected to cylindrical bending. However, it is worth noting that, in contrast to the classical GBT, in the present formulation fundamental modes engender non-null engineering shearing strains and, in particular, have piece-wise constant (i.e. constant on each wall) $\varepsilon_{zs}^{(M)}$ along the section mid-line and constant ε_{zn} over the wall thickness. Only in-plane behavior is assumed for local flexural

modes, considering the associated warping effect negligible. Hence, cross-section modes μ, ψ, φ will be assumed null, cubic and null, respectively. Transverse extension modes are characterized by linear function μ and make it possible to account for cross-section distortion stemming from non-null transverse membrane strain $\varepsilon_{ss}^{(M)}$. Finally, local flexural modes, local transverse extension modes and nonlinear warping modes, based on nodes internal to the walls, could be added in order to enrich, respectively, the local bending behavior, the local transverse extension behavior and the warping description.

For a C-shaped cross-section with stiffening lips, the fundamental flexural modes in the modal base are depicted in figure 3.3, while local flexural and transverse extension in the modal base can be seen in figure 3.4.

3.3 GENERALIZED STRESSES

Generalized stresses s are defined from the following work equivalence condition, as work-conjugates to the generalized deformations e :

$$s^T e = \int_A \sigma^T \varepsilon dA, \quad (3.8)$$

where $\sigma[s] = [\sigma_{ss}, \sigma_{zz}, \tau_{zs}, \tau_{zn}]^T$ and A is the cross-section area. Assuming

$$s^T = \begin{bmatrix} S^T & M^T & T^T & V^T \end{bmatrix},$$

the following expressions for the components of s are obtained for flexural modes:

$$\begin{aligned} S &= \int_A (-n \partial_{ss} \psi^T + \partial_s \mu^T) \sigma_{ss} dA, \\ M &= \int_A (\varphi^T - n \psi^T) \sigma_{zz} dA, \\ T &= \int_A (-2n \partial_s \psi^T + \mu^T + \partial_s \varphi^T) \tau_{sz} dA, \\ V &= \int_A \left(\frac{1}{2} (\mu^T - \partial_s \varphi^T) \tau_{zs} + \psi^T \tau_{zn} \right) dA. \end{aligned} \quad (3.9)$$

The static equilibrium equation is imposed in the homogeneous form on the beam domain as by resorting to the operator \mathcal{L}^* , which is the differential operator adjont to the compatibility one \mathcal{L} , eq. 3.7, taking the form:

$$D^* s = 0, \quad D^* = I_m \otimes \mathcal{L}^*. \quad (3.10)$$

3.4 CROSS-SECTION STIFFNESS MATRIX

Under the hypothesis of linear elastic material, in the GBT the three-dimensional constitutive equations are usually assumed in the following form:

$$\sigma = \sigma_l^{(M)} + \sigma^{(B)}, \quad \sigma^{(M)} = \mathbf{C}^{(M)} \varepsilon^{(M)}, \quad \sigma^{(B)} = \mathbf{C}^{(B)} \varepsilon_l^{(B)} \quad (3.11)$$

where

$$\mathbf{C}^{(M)} = \begin{bmatrix} E & 0 & 0 & 0 \\ 0 & E & 0 & 0 \\ 0 & 0 & G & 0 \\ 0 & 0 & 0 & G \end{bmatrix}, \quad \mathbf{C}^{(B)} = \begin{bmatrix} \bar{E} & \nu \bar{E} & 0 & 0 \\ \nu \bar{E} & \bar{E} & 0 & 0 \\ 0 & 0 & G & 0 \\ 0 & 0 & 0 & G \end{bmatrix}, \quad (3.12)$$

coefficient and $\bar{E} = E/(1 - \nu^2)$. The cross-section stiffness matrix of the beam, i.e. the constitutive relationship among the generalized stresses and deformation, is defined as:

$$\mathbf{C} = \int_A (\mathbf{b}^{(M)} + \mathbf{b}^{(B)})^T (\mathbf{C}^{(M)} \mathbf{b}^{(M)} + \mathbf{C}^{(B)} \mathbf{b}^{(B)}) dA, \quad (3.13)$$

that leads to:

$$\mathbf{C} = \begin{bmatrix} \mathbf{C}_S & \mathbf{C}_{SM} & \mathbf{0} & \mathbf{0} \\ \mathbf{C}_{SM}^T & \mathbf{C}_M & \mathbf{0} & \mathbf{0} \\ \mathbf{0} & \mathbf{0} & \mathbf{C}_T & \mathbf{C}_{TV} \\ \mathbf{0} & \mathbf{0} & \mathbf{C}_{TV}^T & \mathbf{C}_V \end{bmatrix}, \quad (3.14)$$

with the expressions of the submatrices given in Appendix A.1.

The submatrices appearing into the cross-section stiffness matrix \mathbf{C} are full, so determining high coupling among the generalized deformation parameters, as showed pictorially in figure 3.2 and in detail in section A.2 of the Appendix. Moreover, the mechanical meaning of the generalized parameters is not obvious.

The peculiar process in the GBT is the modal transformation that allows to gain partial uncoupling among the generalized deformation parameters and to clarify their mechanical meaning. The new base is called “modal base”. The interested reader may refer to Appendix A.3 and to de Miranda et al. [51] for further details on modal decomposition.

Hereinafter all the quantities are to be intended as expressed in the modal base.

As it can be noted, the classical generalized deformations of a Vlasov beam are recovered, such as axial extension (mode 1), major an minor axis bending (mode 2 and 3) and twisting rotation about the shear center (mode 4). Modes 5-8 are typical GBT higher-order flexural deformations involving section distortion. Modes 9-13 are cross-sectional distortional modes due to wall extension. Modes 1-6, i.e. fundamental flexural, are depicted in 3.3 for a C-shaped cross-section, while higher order modes 7-13 in fig. 3.4.

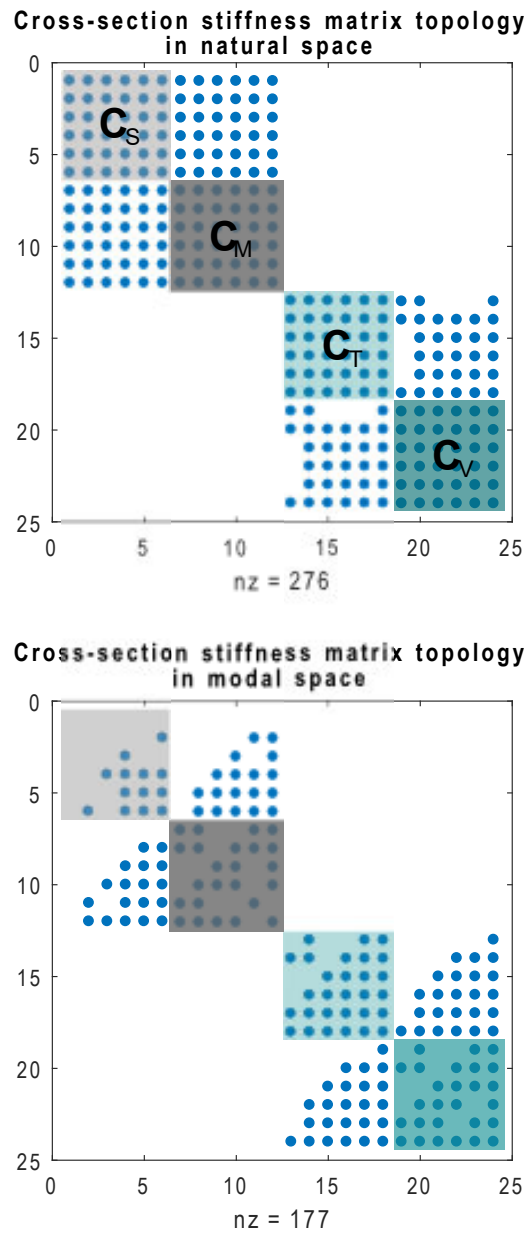


Figure 3.2: Cross-section stiffness matrix for a cross-section with 5 walls. The coupling in the natural space is evident in the top image. The bottom part shows the stiffness matrix in the modal space.

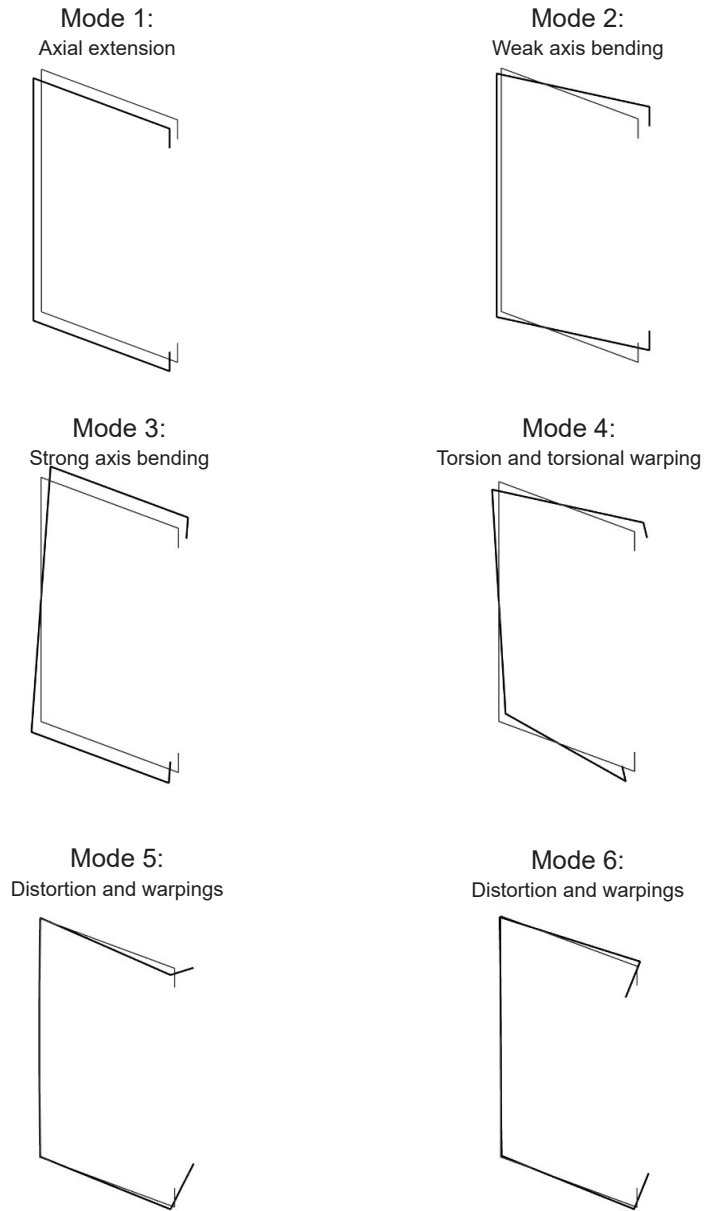


Figure 3.3: Fundamental flexural modes for a C-shaped cross-section

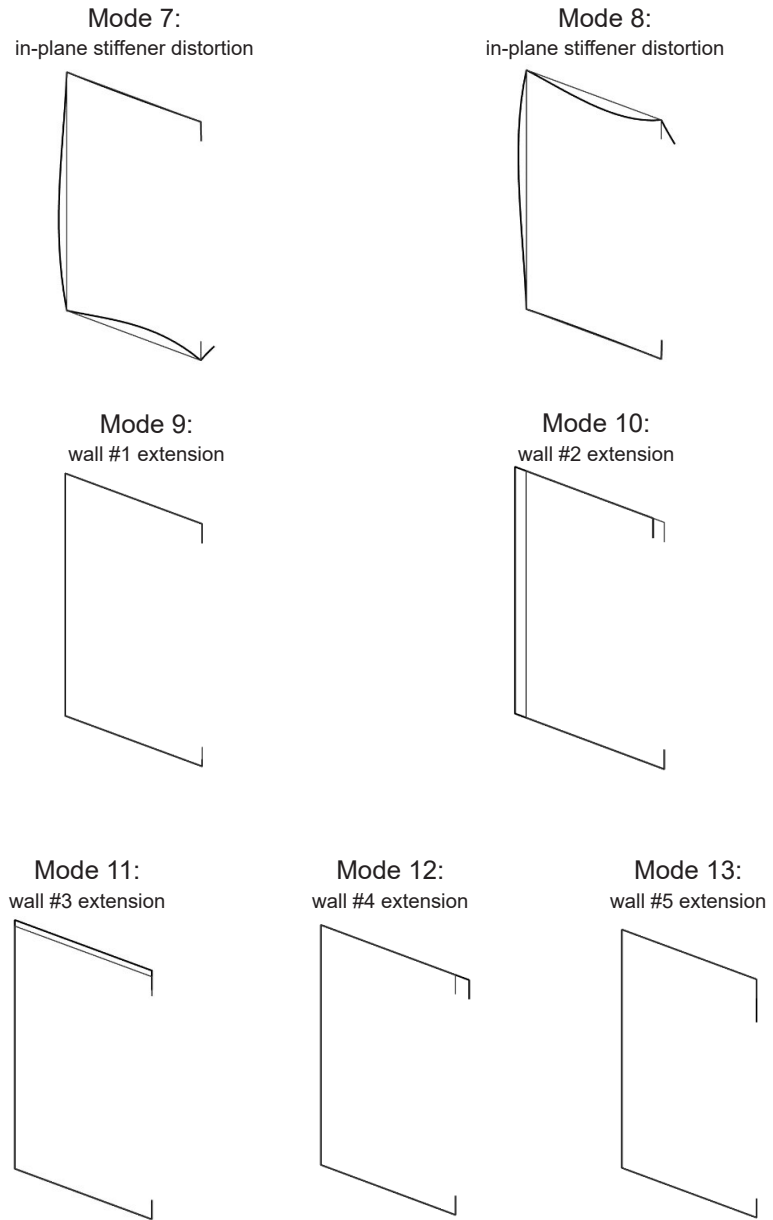


Figure 3.4: Local flexural modes and in-plane wall-extensions.

3.5 THE MIXED-STRESS GBT LINEAR FINITE ELEMENT

The mixed-stress GBT linear finite element [52], is based on the Hellinger-Reissner mixed energy functional, that can be written, for a 3D body of volume V , as a function of its displacement and stress fields $\mathbf{u}, \boldsymbol{\sigma}$:

$$\Phi[\boldsymbol{\sigma}, \mathbf{u}] = \int_V \boldsymbol{\sigma}^T \boldsymbol{\varepsilon}[\mathbf{u}] dV - \frac{1}{2} \int_V \boldsymbol{\sigma}^T \mathbf{C}^{-1} \boldsymbol{\sigma} dV, \quad (3.15)$$

being \mathbf{C} the linear elastic stiffness matrix. More specifically, for a prismatic beam body, the integration is firstly performed on the cross-section A and subsequently over the z axis:

$$\Phi[\boldsymbol{\sigma}, \mathbf{u}] = \int_z \int_A \boldsymbol{\sigma}^T \boldsymbol{\varepsilon}[\mathbf{u}] dA dz - \frac{1}{2} \int_z \int_A \boldsymbol{\sigma}^T \mathbf{C}^{-1} \boldsymbol{\sigma} dA dz,$$

which, introducing the generalized parameters $\boldsymbol{\delta}, \mathbf{s}$, turns into:

$$\Phi[\mathbf{s}, \boldsymbol{\delta}] = \int_z \mathbf{s}^T \mathbf{e}[\boldsymbol{\delta}] dz - \frac{1}{2} \int_z \mathbf{s}^T \mathbf{C}^{-1} \mathbf{s} dz.$$

In order to develop the finite element formulation, the beam domain, i.e. the z axis, is partitioned into non-overlapping elements of length L . Notice that all quantities hereinafter defined are intrinsically local to the element and stress field has no continuity requirements between the elements, while displacements continuity among elements is ensured in the assembly phase.

On the generic element, the following representation is assumed for the generalized stresses:

$$\mathbf{s}[z] = \mathbf{P}[z] \boldsymbol{\beta},$$

being \mathbf{P} the stress approximation matrix and $\boldsymbol{\beta}$ the vector of the unknown stress parameters, local to each element. In particular, here, motivated by the very good results obtained in [52], stress modes collected in \mathbf{P} are assumed to be self-equilibrated, i.e. to satisfy a-priori the equilibrium equations in homogeneous form. To account for the presence of body forces, a particular solution of the equilibrium equations may be added to the final stress approximation, as usually done in hybrid stress models [57]. To lighten the text, the expression of \mathbf{P} is given in Appendix A.4

The interpolation of the generalized displacements associated to the generic mode m , $\delta^m[z]$ is of linked type (see for instance [55]) and can be written as:

$$\delta^m[z] = \begin{bmatrix} v^m[z] \\ w^m[z] \end{bmatrix} = N^m \mathbf{q}^m, \quad \mathbf{q}^m = \begin{bmatrix} q_{v1}^m \\ q_{w1}^m \\ q_{v2}^m \\ q_{w2}^m \end{bmatrix},$$

$$N^m[z] = \begin{bmatrix} N_v^m \\ N_w^m \end{bmatrix} = \begin{bmatrix} 1 - \frac{z}{L} & \frac{1}{2}(z - \frac{z^2}{L}) & \frac{z}{L} & \frac{1}{2}(\frac{z^2}{L} - z) \\ 0 & 1 - \frac{z}{L} & 0 & \frac{z}{L} \end{bmatrix}, \quad (3.16)$$

where \mathbf{q}^m collects the nodal values of the displacements due to the relevant mode. For later convenience it is here worth noticing that whenever interpolating all the modes, the relationship 3.16 can be expanded accounting for all the modes:

$$\underbrace{\begin{bmatrix} \delta^1[z] \\ \vdots \\ \delta^m[z] \\ \vdots \\ \delta^M[z] \end{bmatrix}}_{\delta[z]} = \underbrace{\begin{bmatrix} N^m[z] & \cdots & 0 & \cdots & 0 \\ \vdots & \ddots & \vdots & \cdots & \vdots \\ 0 & \cdots & N^m[z] & \cdots & 0 \\ \vdots & \cdots & \vdots & \ddots & \cdots \\ 0 & \cdots & 0 & \cdots & N^m[z] \end{bmatrix}}_{N_{\delta[z]}} \underbrace{\begin{bmatrix} \mathbf{q}^1 \\ \vdots \\ \mathbf{q}^m[z] \\ \vdots \\ \mathbf{q}^M[z] \end{bmatrix}}_{\mathbf{q}}. \quad (3.17)$$

The energy of the linear GBT finite element in mixed format, can hence be rewritten in terms of the discrete parameters $\boldsymbol{\beta}, \mathbf{q}$ as follows:

$$\Phi_e[\boldsymbol{\beta}, \mathbf{q}] = \boldsymbol{\beta}^T \left(\int_L \mathbf{P}^T \mathbf{D} N_{\delta} dz \right) \mathbf{q} - \frac{1}{2} \boldsymbol{\beta}^T \left(\int_L \mathbf{P}^T \mathbf{C}^{-1} \mathbf{P} dz \right) \boldsymbol{\beta}, \quad (3.18)$$

that leads to:

$$\Phi_e[\boldsymbol{\beta}, \mathbf{q}] = \boldsymbol{\beta}^T \mathbf{G} \mathbf{q} - \frac{1}{2} \boldsymbol{\beta}^T \mathbf{H} \boldsymbol{\beta}. \quad (3.19)$$

Using standard arguments, the finite element stiffness matrix reads:

$$\mathbf{K} = \mathbf{G}^T \mathbf{C}^{-1} \mathbf{G}.$$

"Successful design is not the achievement of perfection but the minimization and accommodation of imperfection."

— Henry Petroski

Roofing systems are often made by cold-formed, thin-walled purlins, such as Z-shaped ones. These purlins usually span several bays and are submitted to various loadings (snow, wind, dead loads due to equipment, etc.). Purlins are stabilized by the roof sheeting, which provides, depending on the roof type, some degree of restraint: shear restraint due to roof diaphragm effect, rotational restraint due to bending rigidity of the panels, and lateral restraint.

With the aim of showing the importance the applicability of [GBT](#) to the design of real structures, a numerical study is performed to validate two performance based verification approaches for flexible roofing systems in the framework of Eurocode 3 ([EC3](#)).

This chapter addresses the validation of two possible performance-based verification procedures for cold-formed roofing system. The first one, here named Traditional approach ([TA](#)) defines the kinematic of the beam according to a Vlasov model and leaves the effect of cross-section distortion to a separate procedure, based on the Effective Thickness Method ([ETM](#)). The second one, named GBT-based approach ([GA](#)), includes cross-section distortion in the kinematics of the beam theory and does not reduce cross-sectional properties according to a specialized stiffener model.

The proposed validation is aimed at assessing the necessity of a [GBT](#)-based approach to take into account cross-section distortion. The results provide further motivations for the development of a geometrically nonlinear [GBT](#).

4.1 VERIFICATION OF STEEL ROOFING SYSTEMS

Light roofing systems are today a popular construction technology. Particularly, Cold Formed Steel (CFS) sheeting are usually a cost-efficient alternative to heavier concrete-based technologies and are faster to erect. One of the driving factor contributing to the success of CFS roofings is the evolution of construction technology which switched from hook-bolts fastening to faster, more efficient self-drilling fastenings. This makes the construction system faster and simpler to assemble and allows for an effective collaboration among the roof panels and the steel purlins.

The typology of structural system is codified by the Eurocode [25] but, despite its simple physical configuration, the physical modeling of the system is not simple. Prescriptive approaches based on simplified or semi-empirical models are often used in the design practice. The mechanical behavior of roofing systems is generally rather complicated and difficult to be described by simplified models, since design criteria have to include provisions both for gravity loading and for uplift loading, usually applied at the middle of the top flange. If, on one hand, both conditions may physically trigger a distortion of the cross-section, it is especially evident in the latter case, for which an equivalent-spring model suitable for direct calculation of bottom-flange displacement can be included (see the bottom left part of figure 4.1).

A vast amount of literature is devoted to the mechanical, technical and normative aspects of such systems including full and simplified 3D shell FE modeling [44, 45], buckling analyses [5, 79], and experimental testing [80].

The Roof Model (RM) approach [10] is based on a beam model interacting with continuous elastic restraints, which represent the action of the supported panels. These elastic restraints can be of three types, according to the stiffness of the panel:

- Rotational Restraints: rotational spring to torsional rotation about the beam axis;
- Lateral Restraints: a set of independent Winkler's spring that resist with elastic forces in the direction parallel to the cross-section flanges;
- Shear Restraints: rotational springs applied onto the top of the web, restraining the web-to-flange junction rotation about the beam axis, i.e. the roof does not exhibit significant stiffness in the direction parallel to the flanges, but prevent the movement of the top flange.

The aforementioned restraints were introduced in EC3 in order to improve the design of such systems, and have to be experimentally derived both for the RM approach and for the prescriptive EC3 one.

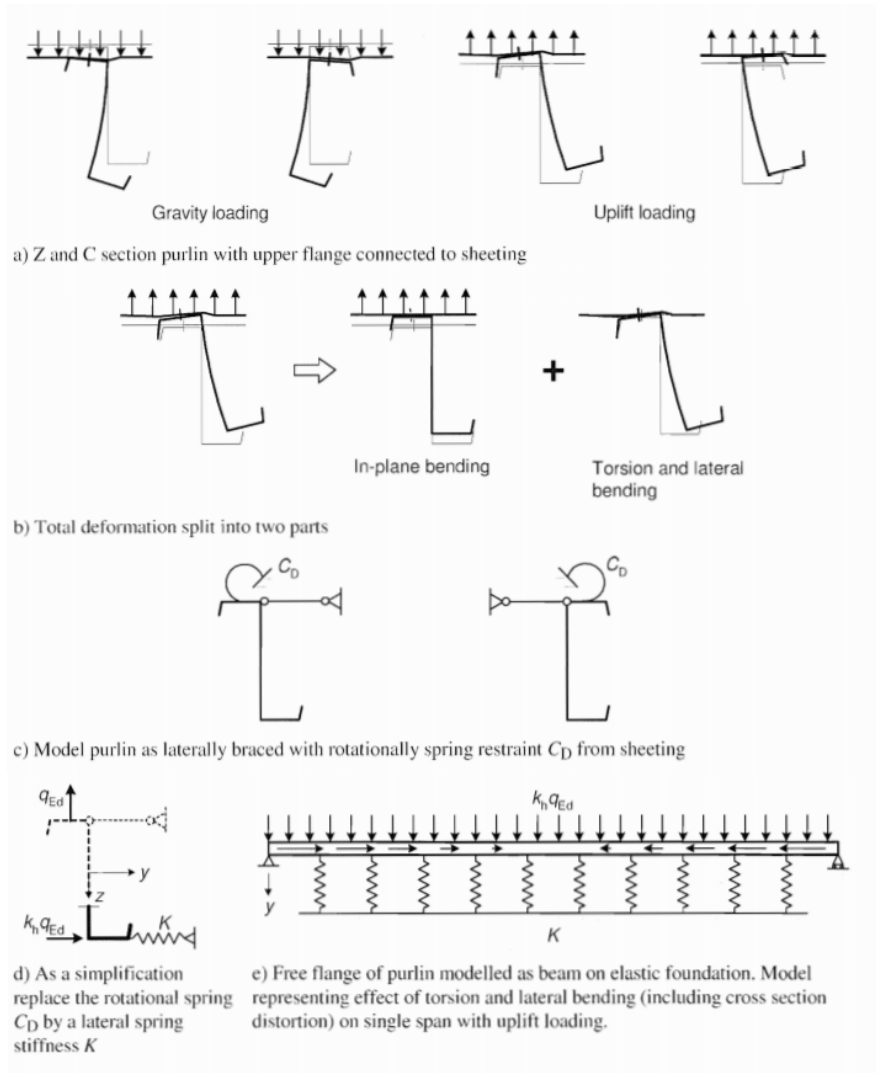


Figure 4.1: Modeling laterally braced purlins rotationally restrained by sheeting, from [25].

The Eurocode “calculation method” explicitly allows for the use of a second order analysis to check for the distortional behavior of the purlin as restrained by the sheeting. For a clear explanation is worth reporting some of the clauses of the paragraph 10.1.2 of EC3 [25]:

(1) Unless a second order analysis is carried out, the method given in [...] should be used to allow for the tendency of the free flange to move laterally (thus inducing additional stresses) by treating it as a beam subjected to lateral load

[...]

(5) A numerical analysis using the rotational spring stiffness C_D obtained from 10.1.5.2 may also be used if lateral restraint is not supplied or if its effectiveness cannot be proved. When the numerical analysis is carried out, it

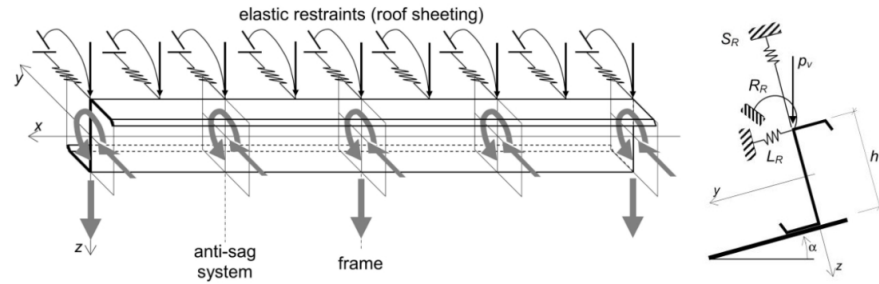


Figure 4.2: Roof model restraints, image from [10].

should take into account the bending in two directions, torsional St Venant stiffness and warping stiffness about the imposed rotation axis.

(6) If a second order analysis is carried out, effective sections and stiffness, due to local buckling, should be taken into account

In this framework, the numerical **RM** approach allows for an easy generalization of the method for a vast range of geometrical dimensions, load and restraint conditions, since it presents the following advantages:

- It is not required to check a-priori the stiffness of the roofing system, i.e. no limitation is virtually provided once elastic restraints are experimentally characterized,
- the beam model employed can be used to obtain the full 3D displacement field, simplifying the physical modeling and ensuring faster checks,
- the stress check can be performed directly, this is true both for the fiber stress and the Von Mises check.

With this in mind, two approaches to possible approaches to apply the **RM** are compared in the following:

- The Traditional approach (**TA**) that consists in modeling the purlin as a Vlasov beam with elastic restraints. The Vlasov beam model cannot include cross-section distortion phenomena, so the effective section is to be reduced for the effect of local and distortional buckling (by using both Effective Width Method (**EWM**) and the Effective Thickness Method (**ETM**)).
- The GBT-based approach (**GA**) that includes cross-section distortion into the beam model by using the **GBT**. Still, the verification is carried out onto the effective cross-sectional properties reduced for the effect of local buckling only, according to the **EWM**, as requested by **EC3**.

In both beam the approaches second-order effects are included. The verification procedure for fibre stress at Ultimate Limit States (ULS) is synthesized in figure 4.3 for both the two approaches.

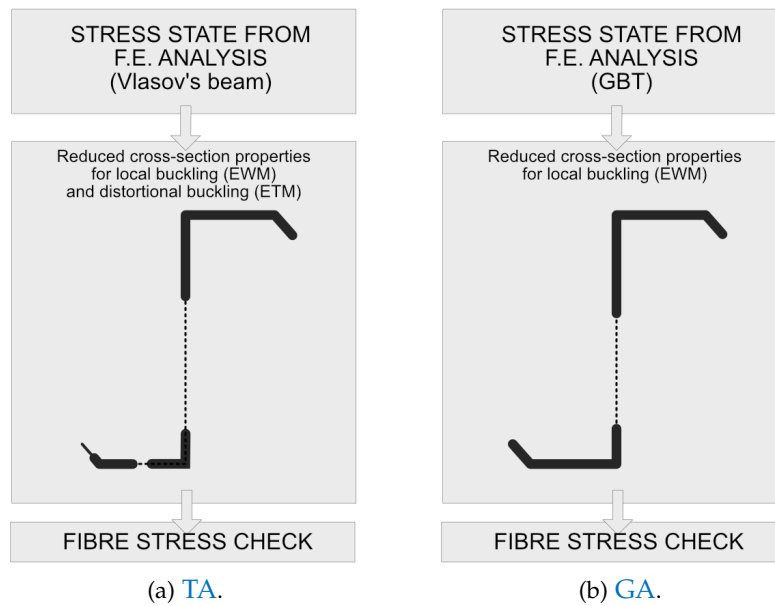


Figure 4.3: Verification procedures at ULS for (a) TA and (b) GA.

4.1.1 Structural modeling

In the following, some design examples are analyzed using both the TA and GA. For each design example, a continuous beam on multiple intermediate supports is analyzed. In correspondence with the supporting systems, the cross-section is reinforced by a sleeve. From the modeling point of view this is taken into account by supposing that the strengthening length is formed by a cross-section twice as thick with respect to the cross-section of the beam. This strengthening area will be hereinafter referred to as “overlap”.

Intermediate anti-sag bars may be present to prevent lateral displacements. The present study focuses on analyzing a range of 15 different Z-shaped cross-sections restrained by continuous elastic restraints. The intensity of the load, number of roof spans and magnitude of restraints are chosen parametrically in a range of typical design values to provide a comprehensive overview of many design conditions. 100 design examples have been verified.

4.1.2 Design parameters at SLS and ULS - Synthetic results

In order to compare the results of the two approaches over the ensemble of roofing systems analyzed, two synthetic design parameters and their variation are analyzed. The first one, suitable for Serviceability Limit States (SLS) conditions, is the ratio of the maximum shear center displacement δ_{sc} that occurs onto the structure during the most severe SLS load combination, over the length of the relevant span L_{span} , including overlapping lengths, and can hence be written as:

$$r_1 = \left(\frac{\delta_{sc}}{L_{span}} \right)_{SLS}$$

Clearly the choice of this parameter includes the effect of cross-section distortion only at the stiffness level, but it has been retained more faithful and compliant to the usual design practice, where higher-order beam models are not usually employed and checking the whole three-dimensional displacement field is an unnecessary burden. Overall results in terms of r_1 for all 100 structures analyzed are reported in figure 4.4.

The second design parameter, suitable for the Ultimate Limit States (ULS) analysis of the beams, is the fiber stress ratio of the most severe ULS combination:

$$r_2 = \left(\frac{\sigma_{zz}}{f_{yd}} \right)_{ULS'} \quad (4.1)$$

where f_{yd} is the design yield stress. Normalization over f_{yd} is performed to provide an homogeneous measure of the stress state across different steel grades, since cold-formed purlins may be rolled from coils with quite different yield strengths. The above defined ratio r_2 is strongly affected by the calculation hypotheses adopted.

As regards the fibre stress σ_{zz} , for both approaches one may write:

$$\sigma_{zz} = \frac{N_{Ed}}{A_{eff}} + \frac{M_{y,Ed}}{W_{eff,y}} + \frac{M_{z,Ed}}{W_{eff,z}} + \frac{M_{\omega}\omega}{I_{\omega,eff}} + \sigma_{higher}$$

The first four terms on the right hand side refer to the contributions of fibre stresses deriving from the relevant generalized stresses of the Vlasov beam model (normal stress N_{Ed} , bending moments $M_{y,Ed}$, $M_{z,Ed}$, bimoment M_{ω}), calculated according to the effective cross-sectional quantities (effective area A_{eff} , effective section moduli $W_{eff,y}$ and $W_{eff,z}$, effective torsion warping constant $I_{\omega,eff}$). According to the hypotheses adopted, the effective quantities are referred to cross-section reduced for local buckling only in the GA approach, while the TA one includes a thickness reduction of the stiffener to account for increased stress intensity due to the cross-section distortion effect. The term σ_{higher} refers to the contribution of higher order generalized stresses deriving from the cross-section distortion in the GBT analysis (for TA approach $\sigma_{higher} = 0$).

Results in terms of fiber stresses ratio r_2 are reported for GA and TA in detail in figure 4.5 and their distributions are compared in figure 4.6. A further comparison of the distributions of r_2 for TA and GA is given in figure 4.6. Finally, boards collecting the results of some selected example are presented in Appendix B.

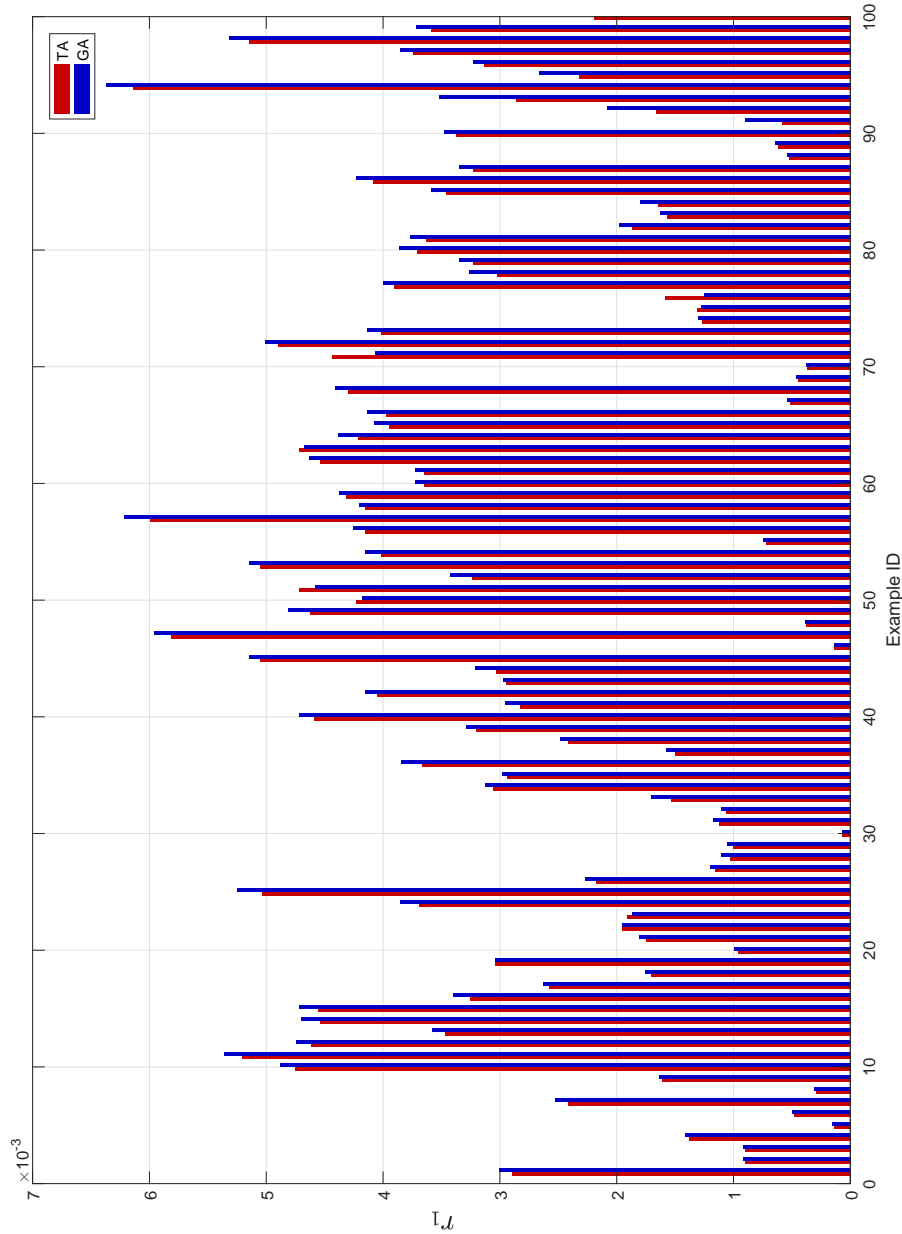


Figure 4.4: Ratio r_1 according to TA and GA approaches

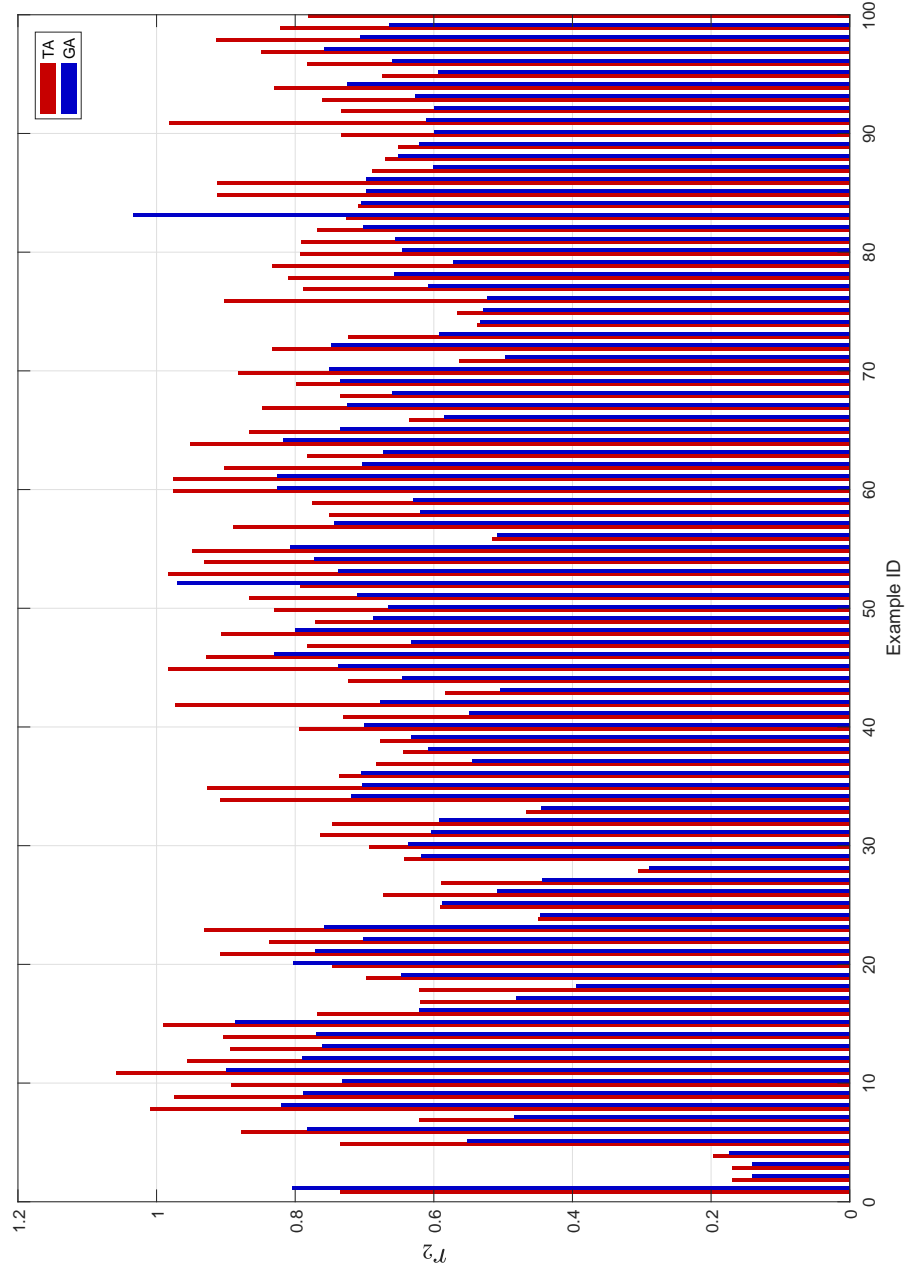


Figure 4.5: Ratio r_2 according to TA and GA approaches

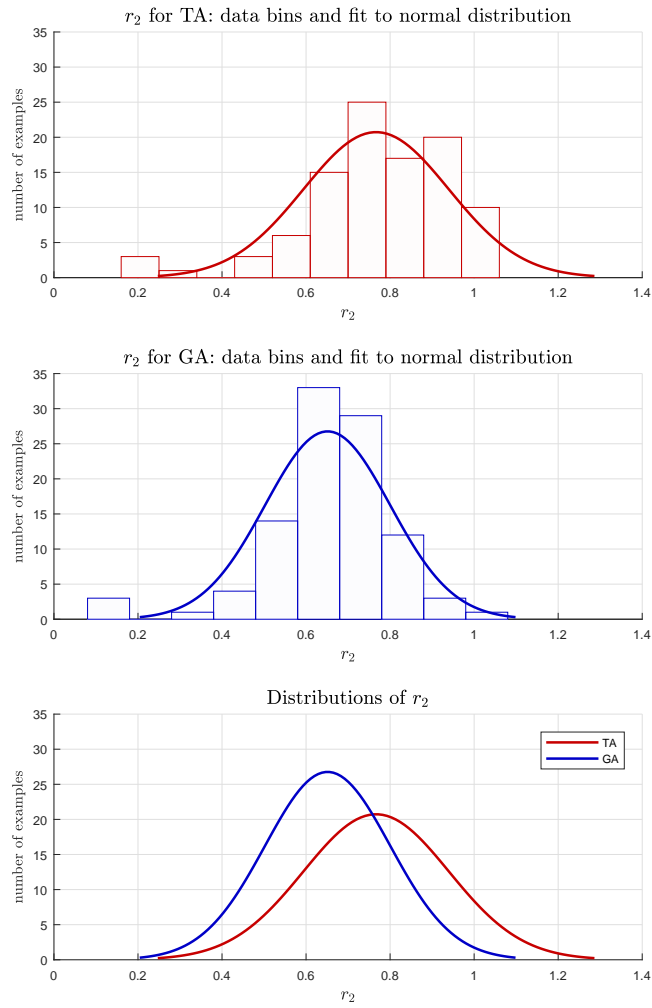


Figure 4.6: Distribution of fibre stress ratio r_2 across all 100 examples

4.2 SOME REMARKS

The idea behind both the **TA** and the **GA** approach is to provide a performance based verification method for the verification of cold-formed steel purlins in the framework of **EC3**, providing a complete Roof Model (**RM**) for the design of steel roofings.

With respect to cross-section distortion behavior, the **GA** approach is virtually exact when computing the cross-section displacement (at least with respect to the chosen discretization), while the **TA** approach does not include cross-sectional kinematics, relying on the reduction of cross-sectional characteristics due to local and stiffener buckling.

The two approaches were compared showing different results for r_1 and r_2 design parameters, to be considered at **SLS** and **ULS** respectively. For the former, minor differences are found, at least in relative value. Nonetheless it is to be highlighted that the displacement of the shear-center tends to hide the additional kinematics introduced in the **GA**.

Conversely, the design parameter r_2 , which is closely related to the maximum fiber stress (see 4.1), is directly affected by both the structural model and the stress check hypothesis 4.3.

The results over the number of examples tested show a tendency of the **TA** method to predict on average a higher state of stress (in more than 80% of the examples), but failing to predict an intense stress-state due to section distortion in a limited number of cases (5%). Being based on a parametric study focusing on distortional phenomena only, these results do not allow to draw a definitive conclusion on the verification procedures of cold formed steel roofings, but strongly motivates the adoption of higher order beam models in performance-based methods

The development of a performance-based method in the framework of **EC3** may lead to a better prediction of local stress states, allowing for a further optimization of flexible systems.

THE COROTATIONAL-BASED GBT: BUCKLING FE ANALYSIS

Corotational (CR) methods allow for a convenient extension of linear models to geometrically nonlinear ones. However, because of the higher order generalized displacements, the application of CR strategies to higher order beam theories is not straightforward.

This Chapter shows how to obtain the geometrically nonlinear GBT finite element from the relevant linear one by using the Implicit Corotational Method (ICM). The key idea is referring to the GBT nature as folded plate model, associating multiple CR observers to a single GBT finite element. The results of buckling analyses for beams with complex cross-section geometries are presented and comparisons with finite element shell models are made.

The content of this Chapter is based on the paper 'A corotational based geometrically nonlinear Generalized Beam Theory: buckling FE analysis', referenced at [53], published on International Journal of Solids and Structures on August, 2017

5.1 ICM FOR THIN-WALLED BEAMS

Absolute notation will be used in this only, to introduce the basics of the Implicit Corotational Method (ICM). The ICM can be defined as a tool to obtain geometrically exact nonlinear models from the corresponding linear ones [28]. ICM-based structural elements, such as beams and shells, have shown excellent performance by providing a consistent way of dealing with finite rotations and displacements [27].

The strain energy of a three-dimensional body may be written, in terms of Biot stress/strain [9], as:

$$\Phi[\mathbf{T}, \mathbf{u}] = \int_V \mathbf{T} \cdot \mathbf{E}[\mathbf{u}] dV - \frac{1}{2} \int_V \mathbf{T} \mathbf{C}^{-1} \mathbf{T} dV, \quad (5.1)$$

where \mathbf{T} and $\mathbf{E}[\mathbf{u}]$ are the Biot stress and strain tensors, respectively, \mathbf{u} the three-dimensional displacement field, \mathbf{C} the linear elastic stiffness tensor, and V the body volume.

Let us introduce a corotational description of motion, and denote with \mathbf{Q} the point-wise rotation of the CR observer. Moreover, denote with \mathbf{R} the rotational tensor associated to the polar decomposition of the deformation gradient $\mathbf{F} = \mathbf{I} + \nabla \mathbf{u}$, being \mathbf{I} the identity tensor and $\nabla \mathbf{u}$ the displacement gradient. In case of $\mathbf{Q} = \mathbf{R}$, the Biot strain with respect to the CR observer is the linear strain tensor:

$$\mathbf{E} = \boldsymbol{\varepsilon}, \quad (5.2)$$

being $\boldsymbol{\varepsilon} = \frac{1}{2}(\nabla \mathbf{u}^T + \nabla \mathbf{u})$ the linear strain tensor. Otherwise, whenever $\mathbf{Q} \approx \mathbf{R}$, the Biot strain is well approximated by the sum of the linear strain tensor and the tensor $\boldsymbol{\rho}$, quadratic in the displacement gradient:

$$\mathbf{E} \approx \boldsymbol{\varepsilon} + \boldsymbol{\rho}, \quad \boldsymbol{\rho} = \frac{1}{2}(\boldsymbol{\varepsilon} \boldsymbol{\omega} - \boldsymbol{\omega} \boldsymbol{\varepsilon} - \boldsymbol{\omega} \boldsymbol{\omega}), \quad (5.3)$$

where $\boldsymbol{\omega} = \frac{1}{2}(\nabla \mathbf{u}^T - \nabla \mathbf{u})$. As can be easily seen, the goal of the method is to select \mathbf{Q} such that $\boldsymbol{\omega}$ is almost negligible and, hence, the Biot strain tensor is almost equal to the linear strain tensor. Moreover, as extensively discussed in [28], it can be assumed that \mathbf{T} and \mathbf{E} are related by the same constitutive law of the linear theory. Therefore, when $\mathbf{Q} \approx \mathbf{R}$, both the kinematic and constitutive equations coming from the linear theory correspond to those of the nonlinear problem expressed in terms of Biot tensors, at least with the assumption of small strains.

Consider now a beam structural model and denote by z the beam axis abscissa, by A the beam cross-section, and by $\mathbf{s}[z]$ and $\boldsymbol{\delta}$ the vectors of the generalized stresses and generalized displacements, respectively. The recovery of the nonlinear beam model using the ICM is based on the following hypotheses:

$$\nabla \mathbf{u} \equiv \nabla \mathbf{u}_l[\boldsymbol{\delta}[z]] = \boldsymbol{\varepsilon}_l[\boldsymbol{\delta}[z]] + \boldsymbol{\omega}_l[\boldsymbol{\delta}[z]], \quad \mathbf{T} \equiv \boldsymbol{\sigma}_l[\mathbf{s}[z]] \quad (5.4)$$

with ∇u_l the displacement gradient associated to a linearized kinematics, ε_l and ω_l its symmetric and skew-symmetric parts respectively, and σ_l the standard linear stress tensor. Substituting eq. 5.4 into eq. 5.1, with the Biot strain E defined by eq. 5.3 and performing the integration on the beam cross-section, yields the following expression for the strain energy of the nonlinear beam model:

$$\Phi[\mathbf{s}, \delta] = \int_z \mathbf{s}^T (e[\delta] + \mathbf{h}[\delta]) dz - \frac{1}{2} \int_z \mathbf{s}^T \mathbf{C}^{-1} \mathbf{s} dz, \quad (5.5)$$

where

$$\mathbf{s}^T (e[\delta] + [\delta]) = \int_A \sigma_l[\mathbf{s}] \cdot (\varepsilon_l[\delta] + \rho_l[\delta]) dA, \quad (5.6)$$

and

$$\mathbf{s}^T \mathbf{C}^{-1} \mathbf{s} = \int_A \sigma_l[\mathbf{s}] \cdot \mathbf{C}^{-1} \sigma_l[\mathbf{s}] dA,$$

being ρ_l defined in terms of ε_l and ω_l according to eq. 5.3. In the above equations, $e + \mathbf{h}$ denotes the generalized deformation of the beam model (sum of e , linear function of the displacement gradient and \mathbf{h} , quadratic function of the displacement gradient) and \mathbf{C} the cross-section stiffness matrix of the beam model.

The strain energy, eq. 5.5, is described in terms of the kinematic parameters δ referred to a CR observer. Assuming a CR frame for each cross-section, A , defined by a rotation $\mathbf{Q}[z]$, accounting for the transformation law between the CR observer and a fixed one, the strain energy of the structural model can be formally written as

$$\Phi[\mathbf{s}, \check{\delta}] = \int_z \mathbf{s}^T (e[\mathbf{g}[\check{\delta}]] + \mathbf{h}[\mathbf{g}[\check{\delta}]]) dz - \frac{1}{2} \int_z \mathbf{s}^T \mathbf{C}^{-1} \mathbf{s} dz, \quad (5.7)$$

where $\check{\delta}$ are the generalized displacements evaluated into the fixed frame, while

$$\delta = \mathbf{g}[\check{\delta}] \quad (5.8)$$

denotes the transformation law between the generalized displacements in the two reference frames.

To complete the model, the definition of the rotation \mathbf{Q} has to be specified. As already mentioned, the goal of the method is to have $\mathbf{Q} = \mathbf{R}$. With this in mind, a typical choice could be that of a rotation \mathbf{Q} such that the average, over the whole cross-section, of the skew-symmetric part of the linear displacement gradient is null, that is

$$\frac{1}{A} \int_A \omega_l[\mathbf{g}[\check{\delta}]] dA = \mathbf{0}. \quad (5.9)$$

Alternatively, the beam cross-section can be partitioned into parts A_i and, for each part A_i , a CR frame defined by a rotation $\mathbf{Q}_i[z]$ can be assumed.

For example, in a thin-walled beam, A_i can be the cross-section of the single wall or of part of it. Analogously to the previous case, a convenient choice for \mathbf{Q}_i could be that of a rotation such that the average, over A_i , of the skew-symmetric part of the linear displacement gradient is null:

$$\frac{1}{A_i} \int_{A_i} \omega_l [\mathbf{g}_i[\check{\delta}]] dA = \mathbf{0}, \quad (5.10)$$

denoting with

$$\delta = \mathbf{g}_i[\check{\delta}] \quad (5.11)$$

the transformation law between the generalized displacements of the i -th CR frame and the fixed one. In this case, the strain energy of the structural model can be written as in eq. 5.7 by replacing \mathbf{g} with: \mathbf{g}_i :

$$\Phi[\mathbf{s}, \check{\delta}] = \sum_i \int_z \mathbf{s}^T (\mathbf{e}[\mathbf{g}_i[\check{\delta}]] + \mathbf{h}[\mathbf{g}_i[\check{\delta}]]) dz - \frac{1}{2} \int_z \mathbf{s}^T \mathbf{C}^{-1} \mathbf{s} dz, \quad (5.12)$$

where the sum is over the cross-section partitions and the integrand in the first integral can be defined analogously to eq. 5.7 when referring the integration to the relevant cross-section partition.

5.1.1 Quadratic generalized strains

To complete the geometrically nonlinear model according to the ICM, quadratic generalized strains \mathbf{h} , corresponding to the quadratic components of the Biot strain (eq. 5.3), must to be evaluated. As it can be verified, in GBT these strains can be written as:

$$\mathbf{h}[\delta] = \mathbf{C}^{-1} \int_A (\mathbf{b}^{(M)T} \mathbf{C}^{(M)} + \mathbf{b}^{(B)T} \mathbf{C}^{(B)}) \rho_l[\delta] dA.$$

The full expressions of the components of $\rho_l[\delta]$ are provided in Appendix C.

5.1.2 Some remarks

For a linear elastic beam model, the three-dimensional linear stress tensor $\sigma_l[\mathbf{s}]$ and the gradient of the linear three-dimensional displacement $\nabla \mathbf{u}_l[\delta]$ are available as linear functions of the generalized stresses \mathbf{s} and generalized displacements δ . The use of this information allows, to obtain the corresponding nonlinear beam model completely defined by the strain energy, eq. 5.7.

Moreover, note that the generalized deformation can be evaluated using a linear, \mathbf{e} , or a quadratic, $\mathbf{e} + \mathbf{h}$, expression, yielding different accuracy in the recovery of the polar decomposition rotation \mathbf{R} (see [28] for more details on the ICM and remarks on the recovered structural

models using this method). In other words, this leads to different approximations in the filtering of the local point-wise rotation with a different response of the model.

Finally, it is worth to remark that the use of single **CR** frame for each cross-section leads to a model which is geometrically exact with respect to the rigid body motion of the whole cross-section, and with a linear or a quadratic approximation with respect to the local motion (into the **CR**) if, respectively, e or $e + h$ are employed. On the other hand, the use of multiple **CR** frames, one for each part A_i of the cross-section, allows to obtain a geometrically exact model with respect to the rigid body motion of each part of the cross-section.

When generalized deformations are evaluated by linear expression and multiple corotational observers are placed on the cross-section, eq. 5.7, reads:

$$\Phi[s, \delta] = \sum_i \int_z s^T (e[g_i[\delta]]) dz - \frac{1}{2} \int_z s^T C^{-1} s dz.$$

In the following, only linear generalized strains e will be used for the **ICM**-based, geometrically nonlinear **GBT** finite element.

5.2 CHANGE OF KINEMATIC PARAMETERS

From now on, attention will be focused on the generic e -th one-dimensional, GBT mixed-stress finite element introduced in Section 3.5, in which \mathbf{q} is the vector collecting the generalized displacements at the end nodes of the element.

Based on the GBT kinematic hypotheses, the relationship of eq. 3.1 between generalized displacements $\delta[z]$ and three-dimensional ones $\mathbf{u}[s, n, z]$ holds and it is here recalled for convenience:

$$\mathbf{u}[n, s, z] = \mathbf{N}[n, s]\delta[z].$$

Moreover, considering a single GBT finite element, it is recalled from eq. 3.17, that:

$$\delta[z] = \mathbf{N}_\delta[z]\mathbf{q},$$

Parameters $\delta[z]$, as well as their finite element counterparts \mathbf{q} , are the kinematic parameters commonly used in the classical GBT literature and represent the amplitude of the cross-section deformation modes, which typically involve the displacement of more than one node, or more generally point, of the cross-section. Hence, parameters \mathbf{q} do not correspond to specific cross-section points displacements. For convenience, it is useful to rewrite them in terms of three-dimensional displacement components of specific cross-section points, hereinafter assumed as the generalized displacements of the GBT finite element and collected in the vector \mathbf{d} . For reader's convenience, a summary of the displacements nomenclature can be found in table 5.1.

Using the above equations, it is possible to write the relationship between \mathbf{q} and \mathbf{d} in the following form:

$$\mathbf{d} = \mathbf{A}\mathbf{q}, \quad (5.13)$$

where matrix \mathbf{A} collects the evaluations of $\mathbf{N}[n, s]$ in the chosen cross-section points. Clearly, the dimensions of matrix \mathbf{A} depend on the number of the selected cross-section points and on the number of the assumed cross-section deformation modes. As it can be easily verified, if all the classes of the modes are assumed (i.e. flexural, transverse extension and local flexural), then the matrix \mathbf{A} is square and non-singular, so that is it possible to write:

$$\mathbf{q} = \mathbf{A}^{-1}\mathbf{d}. \quad (5.14)$$

Conversely, if only some classes of deformation modes are assumed, there is always a non-singular minor of matrix \mathbf{A} with the same dimension of vector \mathbf{q} , so that it is possible to write a relationship analogous to eq. 5.14 between \mathbf{q} parameters and a part of the \mathbf{d} parame-

ters. Equation 5.14 allows to express q in terms of d and, hence, to reparametrize the beam kinematics as function of d .

The effect of a change of kinematic parameters is shown in figures 5.1 and 5.2, mapping 18 modal amplitudes q to the same number of cross-section point displacements d (cross-section points are assumed to coincide with cross-section natural nodes).

	GBT generalized displacements	3D displacement
Continuous field	$\delta[z]$	$u[n, s, z]$
Discrete parameters	q	d

Table 5.1: Nomenclature for continuous fields and discrete parameters

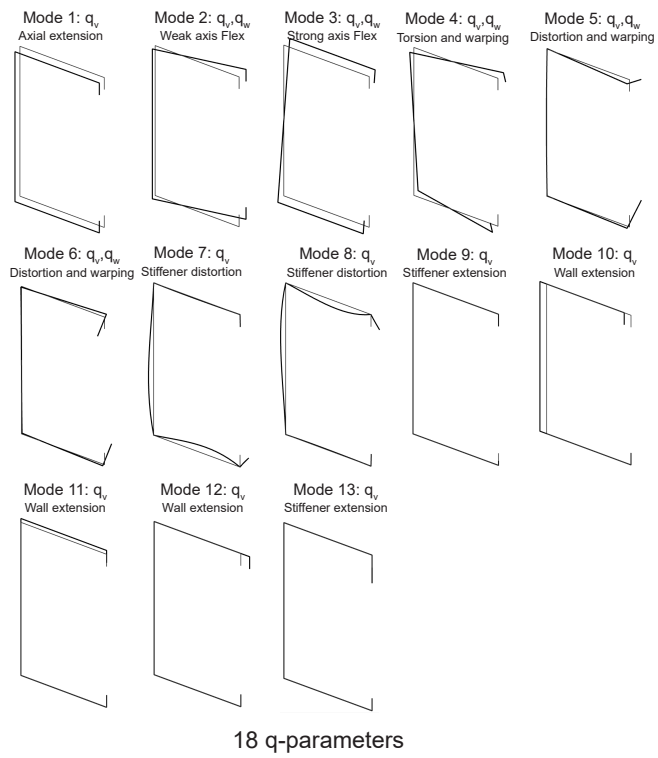


Figure 5.1: C-shaped cross-section: GBT deformation modes in the modal space

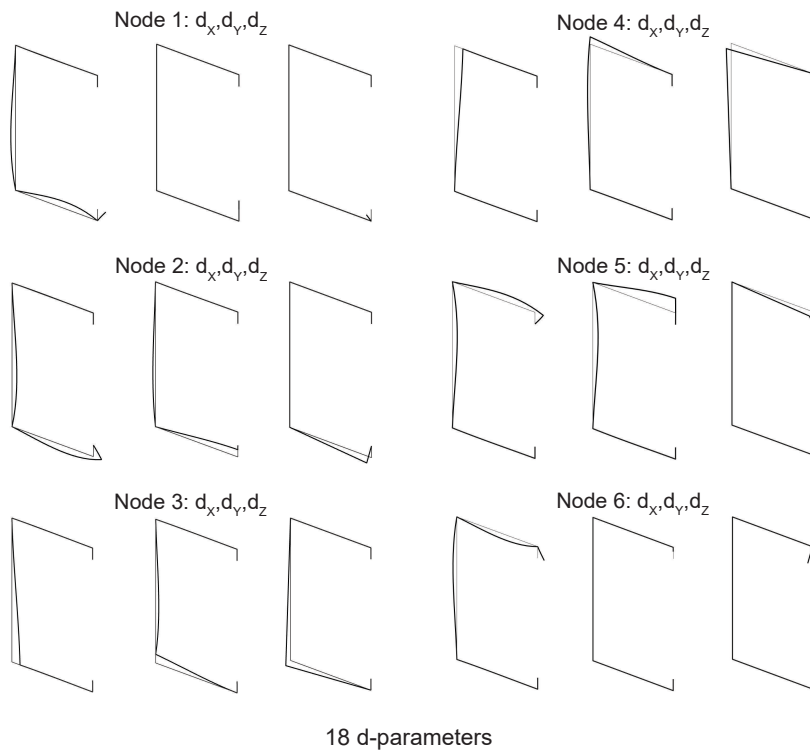


Figure 5.2: C-shaped cross-section: GBT deformation of fig. 5.1 after the change of kinematic parameters

5.3 ESSENTIAL FLOWCHART TO OBTAIN A GEOMETRICALLY NON-LINEAR FINITE ELEMENT

To underline the basic ingredients needed to formulate a geometrically nonlinear, ICM-based finite element, the main stages of the process are reported. For a thorough review, the interested reader may refer to the available literature [27, 28].

Three main steps might be identified in the implementation of nonlinear models starting from linear structural theories:

(A) DEFINITION OF THE COROTATIONAL OBSERVER A CR observer should be attached over the domain of the finite element.

(B) STRUCTURAL MODEL IN THE COROTATIONAL FRAME With respect to the corotational observer, the structural model is deemed to be valid. The strain energy is written with respect to the corotational frame by making use of the constitutive equations of the linear theory.

(C) CHANGE OF OBSERVER Strains are expressed as a function of the corotational displacements by introducing a nonlinear transformation. The adoption of a second order local structural model, as of equation 5.3 increases the accuracy and allows to recover a geometrically exact theory.

In the following Sections, the steps (b) and (c) are illustrated in detail.

5.4 ELASTIC ENERGY OF THE LINEAR FINITE ELEMENT

Let us recall the expression of the strain energy of the linear GBT finite element in mixed format derived in Section 3.5:

$$\Phi = \underbrace{\beta^T \left(\int_L P^T D N_\delta dz \right)}_{\Phi^m} q - \frac{1}{2} \underbrace{\beta^T \left(\int_L P^T C^{-1} P dz \right)}_{\Phi^c} \beta,$$

where subscripts (m) and (c) refers to the mixed term and to the complementary one. The focus will now be shifted on Φ^m , as being subjected to the transformation of the CR observers. When, as discussed in section 5.1, the cross-section is partitioned term into parts A_i , the term Φ^m can be written as:

$$\Phi^m = \sum_i \Phi_i^m,$$

where Φ_i^m can be obtained by resorting to the integration of over the relevant partition A_i of the cross-section:

$$\Phi_i^m = \beta^T \left(\int_L P^T (C^{-1})^T C_i D N_\delta dz \right) q, \quad (5.15)$$

where:

$$\mathbf{C}_i = \int_{A_i} (\mathbf{b}^{(M)} + \mathbf{b}^{(B)})^T (\mathbf{C}^{(M)} \mathbf{b}^{(M)} + \mathbf{C}^{(B)} \mathbf{b}^{(B)}) dA.$$

Equation 5.15 can then be recasted in terms of \mathbf{d} by making use of the introduced reparametrization 5.14:

$$\Phi_i^m = \boldsymbol{\beta}^T \left(\int_L \mathbf{P}^T (\mathbf{C}^{-1})^T \mathbf{C}_i \mathbf{D} \mathbf{N}_\delta dz \right) \mathbf{A}^{-1} \mathbf{d}.$$

Summarizing, it is possible rearrange the strain energy of the linear GBT finite element in eq. 3.19 by taking into account the contributions of different cross-section partitions, and expressing it in terms of parameters \mathbf{d} :

$$\Phi = \boldsymbol{\beta}^T \sum_i \mathbf{G}_i^d \mathbf{d} - \frac{1}{2} \boldsymbol{\beta}^T \mathbf{H} \boldsymbol{\beta}, \quad (5.16)$$

where

$$\mathbf{G}_i^d = \int_L \mathbf{P}^T \mathbf{H}^T \mathbf{C}_i \mathbf{D} \mathbf{N}_\delta dz \mathbf{A}^{-1},$$

and \mathbf{H} is the element flexibility matrix defined in Section 3.5.

5.5 COROTATIONAL OBSERVERS OVER THE FINITE ELEMENT

A corotational observer is a fictitious entity defined over some space subdomain whose aim is to provide an advantageous observation of the body which is attached to. In particular, it is dedicated to filter out the rigid body motion of the observed physical entity, providing geometrical transformations that relates the initial state of the body in the base (i.e. undeformed) configuration and its corotated one.

To apply this principle to the GBT finite element, consider figure 5.3, and focus the attention on the generic i -th panel $ABCD$. The reference system of the i -th panel is centered in its geometric center, O_i .

As the panel moves in space following the trajectories of the points A, B, C, D , a corotational system, that approximates the average rigid body motion of the panel, can be defined according to the 3D displacements of such points. Then, the corotational reference system is just to be intended as a convenient observer for the motion of the panel and of the finite element as a whole, as depicted in figure 5.4.

Let x_A, x_B, x_C, x_D be the positions of the points A, B, C, D in the base configuration with respect to a fixed reference system x, y, z , and

$$\check{\mathbf{d}}_i = \begin{bmatrix} \check{\mathbf{d}}_A & \check{\mathbf{d}}_B & \check{\mathbf{d}}_C & \check{\mathbf{d}}_D \end{bmatrix},$$

be the vector collecting their point displacements. The displacement of the origin of the corotational frame O_i is written as:

$$\check{\mathbf{d}}_{O_i} = \frac{1}{4} (\check{\mathbf{d}}_A + \check{\mathbf{d}}_B + \check{\mathbf{d}}_C + \check{\mathbf{d}}_D),$$

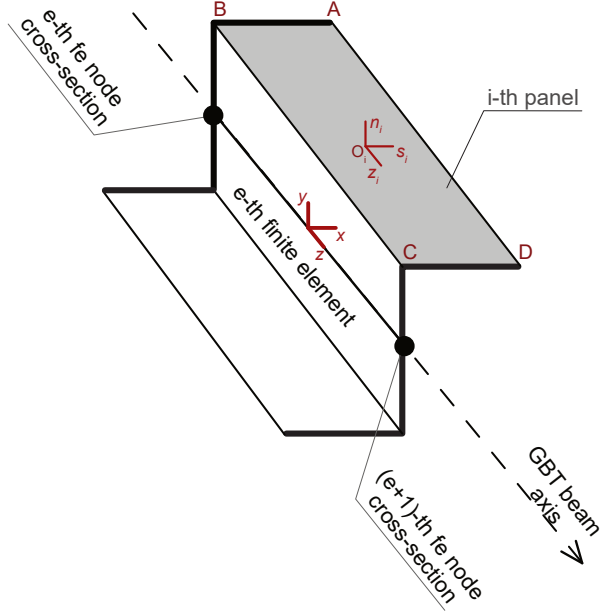


Figure 5.3: Definition of the cross-section panel over the e -th finite element.

and the orientation of the corotational observer is chosen according to the triad $\check{\mathbf{i}}_s, \check{\mathbf{i}}_n, \check{\mathbf{i}}_z$, which is built to be a right-handed orthogonal one:

$$\begin{aligned}
 \check{\mathbf{i}}_z &= \frac{\mathbf{v}_z}{\|\mathbf{v}_z\|}, & \mathbf{v}_z &= \frac{1}{2}(\mathbf{x}_C + \mathbf{x}_D + \check{\mathbf{d}}_C + \check{\mathbf{d}}_D) - \check{\mathbf{d}}_{O_i}, \\
 \check{\mathbf{i}}_n &= \frac{\mathbf{v}_n}{\|\mathbf{v}_n\|}, & \mathbf{v}_s &= \frac{1}{2}(\mathbf{x}_D + \mathbf{x}_A + \check{\mathbf{d}}_D + \check{\mathbf{d}}_A) - \check{\mathbf{d}}_{O_i}, \\
 \check{\mathbf{i}}_s &= \check{\mathbf{i}}_n \times \check{\mathbf{i}}_z, & \mathbf{v}_n &= \check{\mathbf{i}}_z \times \mathbf{v}_s.
 \end{aligned} \tag{5.17}$$

The full expression of the triad can be further simplified by taking into account that $L = \|\mathbf{x}_A + \mathbf{x}_D\|$ and $L_p = \|\mathbf{x}_C + \mathbf{x}_D\|$. Each panel defined over the finite element can be provided with such a reference system defined by its panel coordinates and (arbitrary) displacements. Panel coordinates can be obtained by change of kinematic parameters of GBT modes detailed in Section 5.2.

5.5.1 Change of observer

Once the i -th observer orientation has been defined, supported by the i -th panel partitioning the cross-section, it is characterized in terms of the rotation matrix \mathbf{Q}_i associated to the triad of eq. 5.17, and the translation vector $\check{\mathbf{d}}_{O_i}$. It is now possible to write the relationship ex-

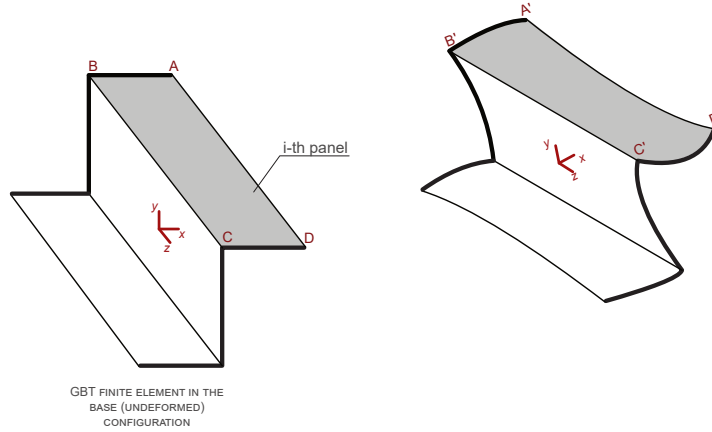


Figure 5.4: corotational observer onto the deformed configuration.

pressing the kinematic parameters \mathbf{d} of the beam with respect to the privileged reference frame. Consider a point N of the cross-section associated to one of the **GBT** finite element nodes and let x_N represents its position in the fixed reference frame x, y, z . Moreover, and denote with $\check{\mathbf{d}}_N$ and \mathbf{d}_N its displacements in the fixed and **CR** reference frames respectively.

The following geometrical transformation relates the displacements as observed by the fixed reference frame configuration and those observed by the corotational frame:

$$\mathbf{d}_N = \mathbf{g}_i[\check{\mathbf{d}}_N] = \mathbf{Q}_i^T[\check{\mathbf{d}}_i](\check{\mathbf{d}}_N + \mathbf{x}_N - \check{\mathbf{d}}_{O_i}) - \mathbf{x}_N. \quad (5.18)$$

5.5.1.1 Strain energy in the corotational frame

The nonlinear strain energy, accounting for arbitrary displacements of the the finite element $\check{\mathbf{d}}$ with respect to the base configuration, is easily written by considering its linear form onto the corotational systems. By taking into account the geometrical transformations of the **CR** observers placed on the finite element and summing the contributions on the cross-section partitions, the strain energy turns to be:

$$\Phi = \boldsymbol{\beta}^T \sum_i \mathbf{G}_i^d \mathbf{g}_i[\check{\mathbf{d}}] - \frac{1}{2} \boldsymbol{\beta}^T \mathbf{H} \boldsymbol{\beta}, \quad (5.19)$$

where $\mathbf{g}_i[\check{\mathbf{d}}]$ has to be intended as the application of the transformation of eq. 5.18 to all $\check{\mathbf{d}}_N$.

It is worth underlining that, because of the non-local nature of the displacement variables (as seen, e.g., in fig. 5.2), the single observer has to look at the whole deformed element, applying the relevant geometrical transformation to the whole set of parameters $\check{\mathbf{d}}$.

5.5.2 Transformation approximation and geometric stiffness matrix

In order to perform buckling analysis, the second variation of Φ must be carried out. Let the operator Ω , obtained by the variations of the strain energy of eq. 5.19 be written as:

$$\Omega[\boldsymbol{\beta}, \check{\boldsymbol{d}}] = \begin{bmatrix} -\boldsymbol{H} & \boldsymbol{L}[\check{\boldsymbol{d}}] \\ \boldsymbol{L}^T[\check{\boldsymbol{d}}] & \boldsymbol{M}[\boldsymbol{\beta}, \check{\boldsymbol{d}}] \end{bmatrix}. \quad (5.20)$$

The generic element a, b of the submatrices of Ω may be readily written by performing partial derivatives with respect to the relevant components of the vectors $\boldsymbol{\beta}, \check{\boldsymbol{d}}$, having n_β and $n_{\check{\boldsymbol{d}}}$ components respectively:

$$\begin{aligned} H_{ab} &= -\frac{\partial^2 \Phi}{\partial \beta_a \partial \beta_b}, & a = 1, \dots, n_\beta, & \quad b = 1, \dots, n_\beta, \\ M_{ab} &= \frac{\partial^2 \Phi}{\partial \check{d}_a \partial \check{d}_b}, & a = 1, \dots, n_{\check{\boldsymbol{d}}}, & \quad b = 1, \dots, n_{\check{\boldsymbol{d}}}, \\ L_{ab} &= \frac{\partial^2 \Phi}{\partial \beta_a \partial \check{d}_b}, & a = 1, \dots, n_\beta, & \quad b = 1, \dots, n_{\check{\boldsymbol{d}}}. \end{aligned}$$

For the purpose of linearized buckling analyses, the pre-buckling displacements \boldsymbol{d} are assumed to be null, hence \boldsymbol{L} is constant and not dependent on $\check{\boldsymbol{d}}$, being exactly the one of the linear case in eq. 3.19, $\boldsymbol{L} = \boldsymbol{G}$:

$$\Omega[\boldsymbol{\beta}, \check{\boldsymbol{d}}] = \begin{bmatrix} -\boldsymbol{H} & \boldsymbol{G} \\ \boldsymbol{G}^T & \boldsymbol{M}[\boldsymbol{\beta}, \check{\boldsymbol{d}}] \end{bmatrix}.$$

With respect to the linear case, the only additional term is hence the geometric stiffness matrix \boldsymbol{M} , ruled by the expression of the transformations \boldsymbol{g}_i .

5.5.2.1 A remark on the expansion of the corotational transformation

When willing to perform a linearized buckling analysis, only quadratic strain energy terms with respect to the displacements are usually included when obtaining \boldsymbol{M} . Hence, the corotational transformation of eq. 5.18 are expanded in Taylor series. To make the operation feasible, this task is performed by using a series expansion of order p of the rotator \boldsymbol{Q}_i , denoted as $\boldsymbol{Q}_{i,p}$.

For sake of completeness, the Taylor series expansions of the rotator \boldsymbol{Q}_i , with respect to the parameters $\check{\boldsymbol{d}}_i$ will be provided in the next Chapter, but notice that the first order one ($p = 1$) assumes a familiar form:

$$\mathbf{Q}_{i,1} = \mathbf{I} + \begin{bmatrix} 0 & \frac{1}{2} \frac{\check{d}_{Ay} + \check{d}_{Dy} - \check{d}_{By} - \check{d}_{Cy}}{L_p} & \frac{1}{2} \frac{\check{d}_{Cx} + \check{d}_{Dx} - \check{d}_{Ax} - \check{d}_{Bx}}{L} \\ -\frac{1}{2} \frac{\check{d}_{Ay} + \check{d}_{Dy} - \check{d}_{By} - \check{d}_{Cy}}{L_p} & 0 & \frac{1}{2} \frac{\check{d}_{Cy} + \check{d}_{Dy} - \check{d}_{Ay} - \check{d}_{By}}{L} \\ -\frac{1}{2} \frac{\check{d}_{Cx} + \check{d}_{Dx} - \check{d}_{Ax} - \check{d}_{Bx}}{L} & -\frac{1}{2} \frac{\check{d}_{Cy} + \check{d}_{Dy} - \check{d}_{Ay} - \check{d}_{By}}{L} & 0 \end{bmatrix}. \quad (5.21)$$

5.6 NUMERICAL TESTS

5.6.1 Rack-section beam

A simply supported rack-section beam subjected to uniform compression is considered (fig. 5.5). Warping and higher order modes are restrained at both ends, therefore rotations about the x -axis and y -axis are allowed on the supports and torsion is prevented. The kinematic of the GBT model includes the full set of fundamental cross-section deformation modes and two local flexural modes associated to the end nodes 1 and 15. The finite element mesh is set to 20 one-dimensional elements along the axis. The in-plane displacement field of cross-section deformation modes is included in fig. 5.6. Linear buckling analysis results are compared with those of a 3D shell model: buckling multipliers are collected in table 5.2 and corresponding modal shapes can be observed in figs. 5.7, 5.8 and 5.9. It is clear that the results are in good agreement both qualitatively and quantitatively and the relative error on buckling multiplier is less than 3%. Even if the first buckling load could have been predicted almost correctly without including section distortion, it is to be stressed that the first four buckling loads fall in quite a narrow range: this cannot be noted without accounting for cross-section distortion. Finally, in order to provide a better physical insight into the behavior of the structure, the cumulative contribution of GBT modes to the in-plane displacements are reported in fig. 5.10.

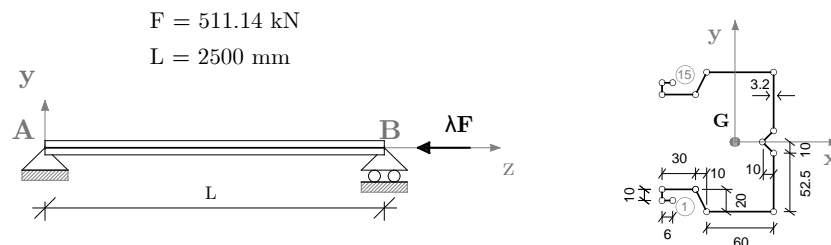


Figure 5.5: Rack-section beam under compression: geometry boundary conditions and loads

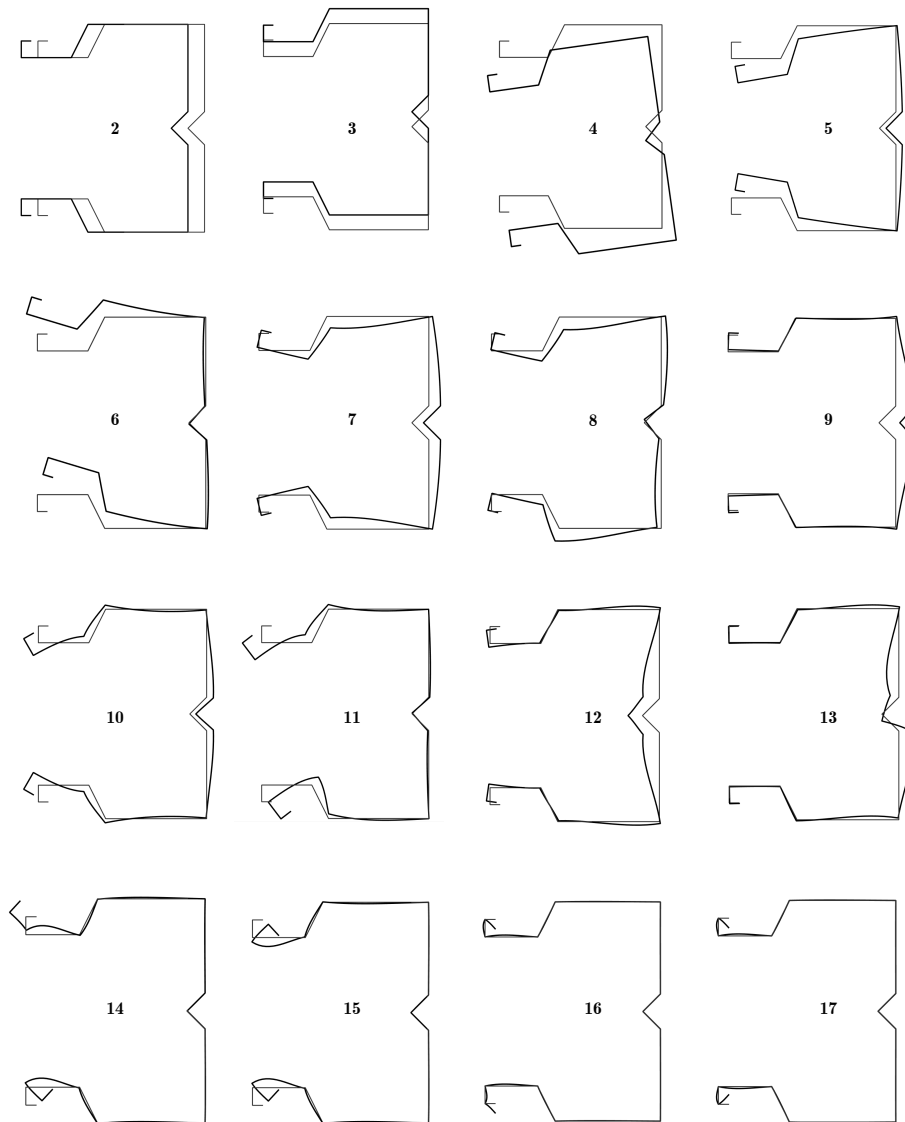


Figure 5.6: rack-section beam: included in-plane **GBT** modes

Buckling multiplier	GBT	3D SHELL	% Error
λ_1	1.000	0.993	0.74
λ_2	1.037	1.033	0.32
λ_3	1.066	1.048	1.70
λ_4	1.083	1.062	1.96
λ_5	1.363	1.329	2.50
λ_6	1.435	1.405	2.17

Table 5.2: Rack-section beam: first six buckling multipliers evaluated using GBT. Comparison with results obtained using 3D shell finite elements.

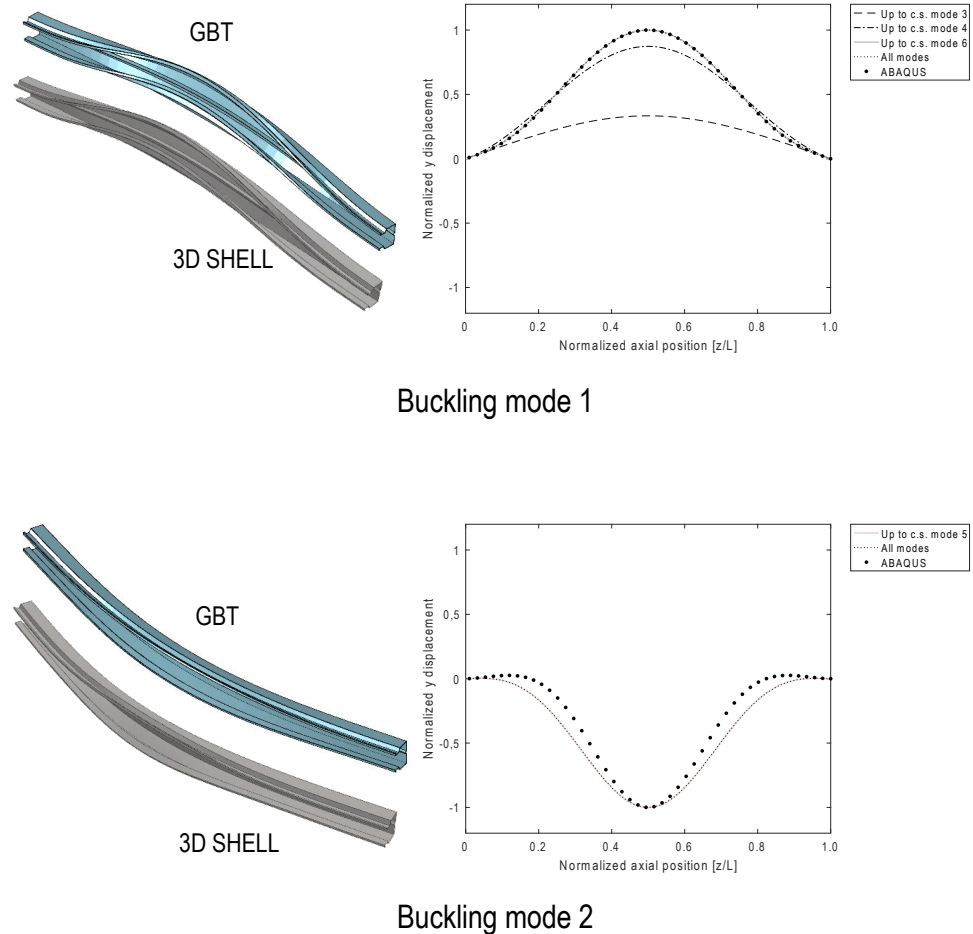
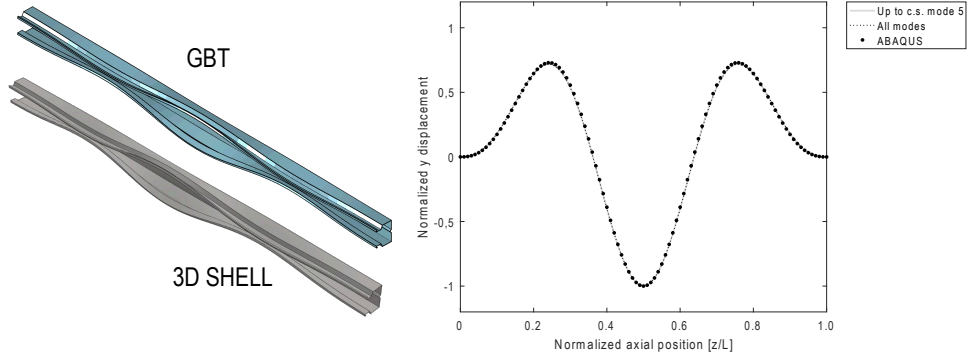
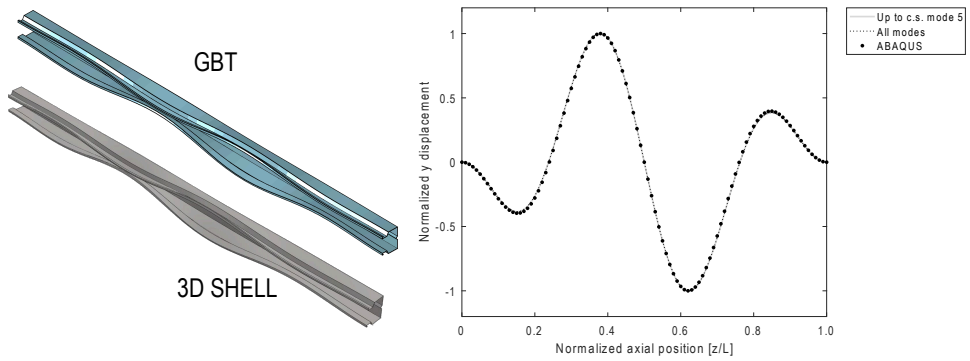


Figure 5.7: Rack-section beam, buckling modes 1 – 2, deformed shapes and cumulative contribution to y -displacement of natural node 1 (see fig. 5.5).

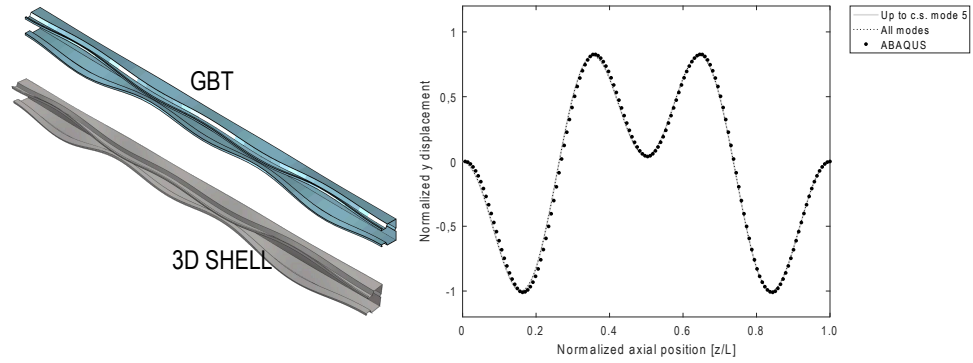


Buckling mode 3

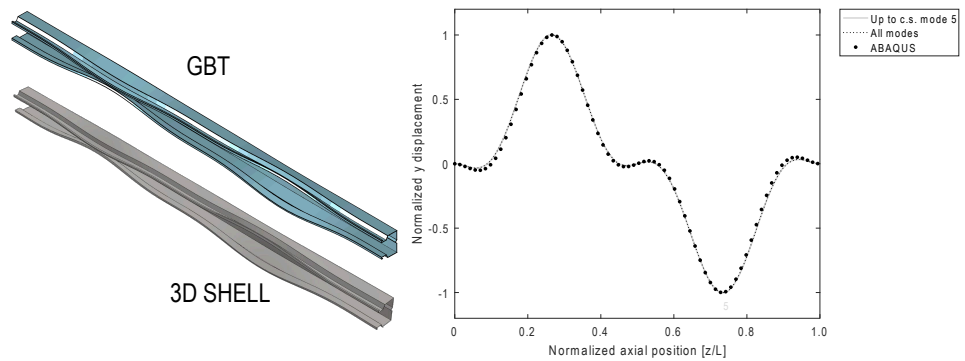


Buckling mode 4

Figure 5.8: Rack-section beam, buckling modes 3 – 4, deformed shapes and cumulative contribution to y -displacement of natural node 1 (see fig. 5.5).

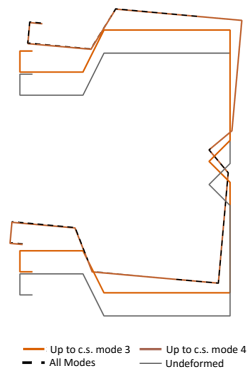


Buckling mode 5

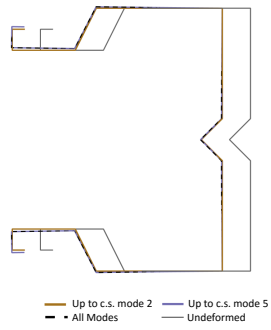


Buckling mode 6

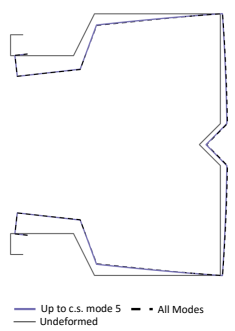
Figure 5.9: Rack-section beam, buckling modes 5 – 6, deformed shapes and cumulative contribution to y -displacement of natural node 1 (see fig. 5.5).



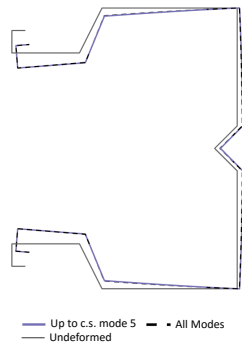
(a) Buckling mode 1



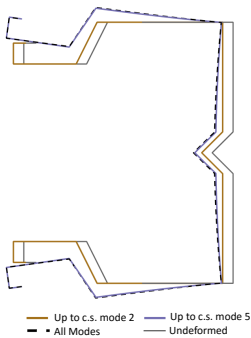
(b) Buckling mode 2



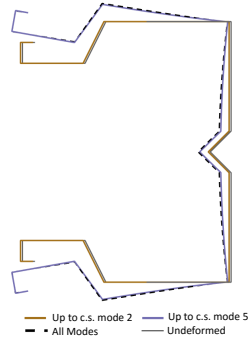
(c) Buckling mode 3



(d) Buckling mode 4



(e) Buckling mode 5



(f) Buckling mode 6

Figure 5.10: Rack-section beam: cumulative GBT modal contribution to buckling modes at $z/L = 1/4$

5.6.2 Trapezoidal-section beam

This example deals with the analysis of a trapezoidal section panel (fig. 5.11). Despite its common use as roofing panels, engineers are starting to use this kind of structural element as beams due to the low cost and ease of creating stiffer members by coupling them ([47]). The beam model is set to ideally reproduce a supported condition, with warping rotation about the major inertia axis and higher-order modes restrained at both ends. The GBT model includes the full set of fundamental cross-section deformation modes and two local flexural associated to the end nodes 1 and 14. The finite element mesh is set to 80 one-dimensional elements along the axis. The in-plane displacements of all cross-section deformation modes are shown in Fig. 10. As in the previous tests, a linear buckling analysis is carried out and results are compared with those of a 3D shell model: the buckling loads are collected in table 5.3 and the corresponding modal shapes are given in figs. 5.13, 5.14 and 5.15 respectively. It can be seen that, also in this case, the results are in good agreement both qualitatively and quantitatively: the GBT model makes the analysis of unorthodox cross-section shapes possible even by one-dimensional beam elements. Finally, the GBT modes contributions to the buckled shapes are shown in fig. 5.16.

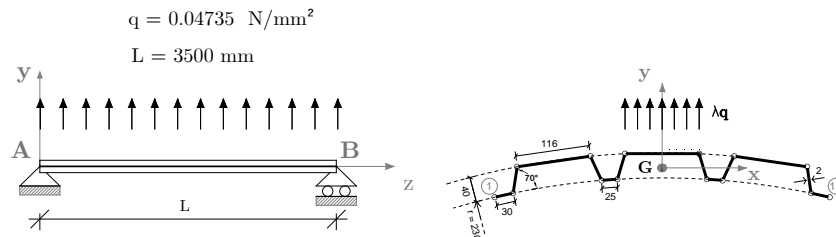


Figure 5.11: trapezoidal-section beam under compression: geometry boundary conditions and loads

Buckling multiplier	GBT	3D SHELL	% Error
λ_1	1.000	0.997	0.31
λ_2	1.008	1.000	0.87
λ_3	1.022	1.002	1.97
λ_4	1.033	1.009	2.36
λ_5	1.159	1.162	0.26
λ_6	1.165	1.165	0.75

Table 5.3: Trapezoidal-section beam: first six buckling multipliers evaluated using GBT. Comparison with results obtained using 3D shell finite elements.

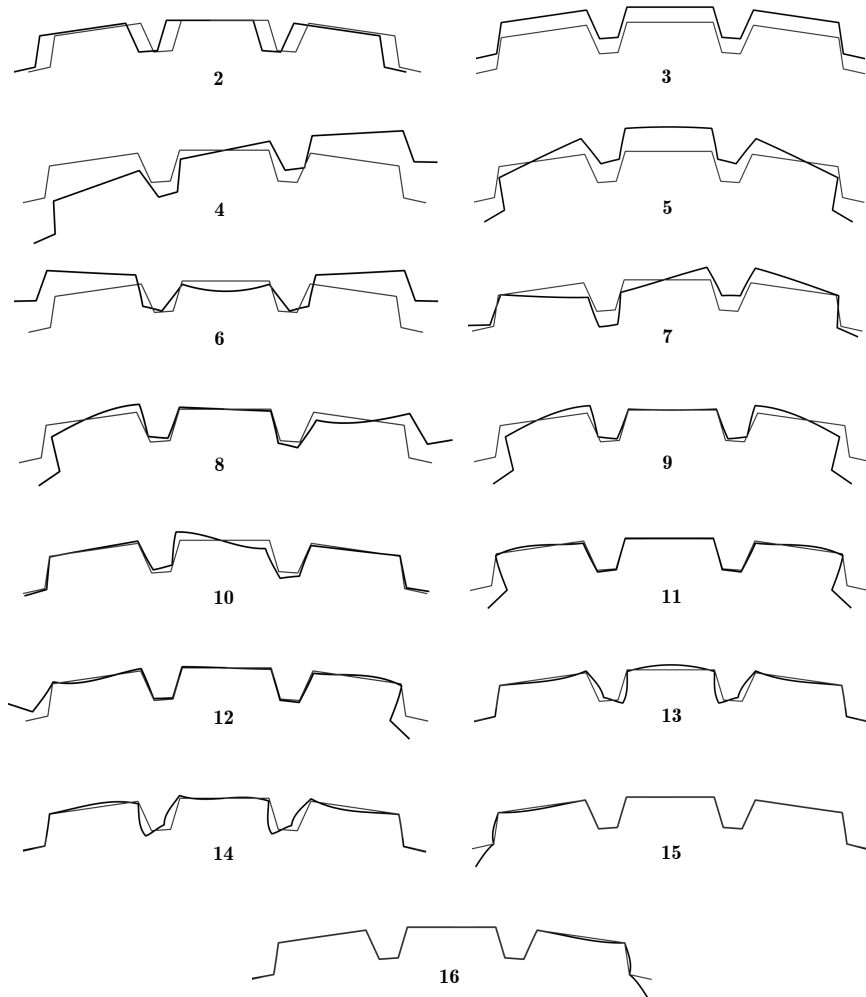
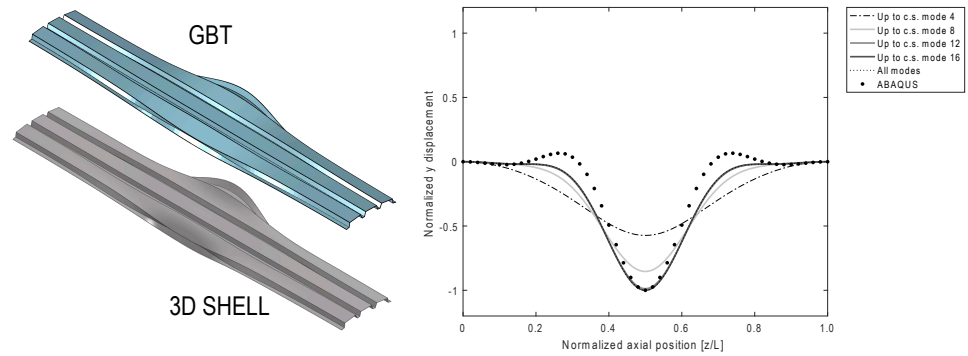
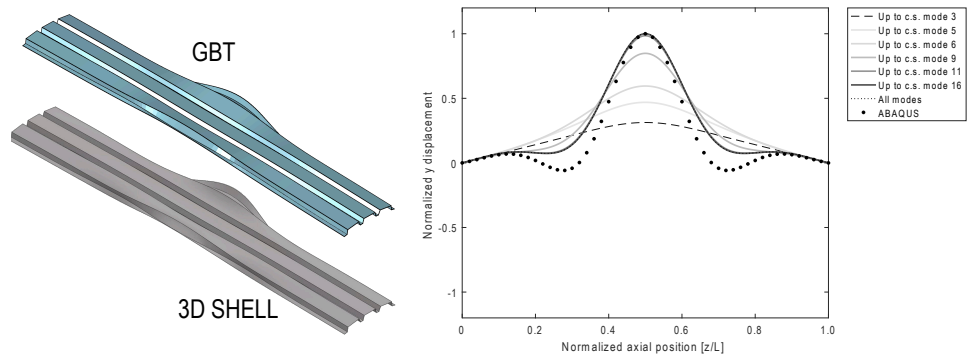


Figure 5.12: trapezoidal-section beam: included in-plane **GBT** modes

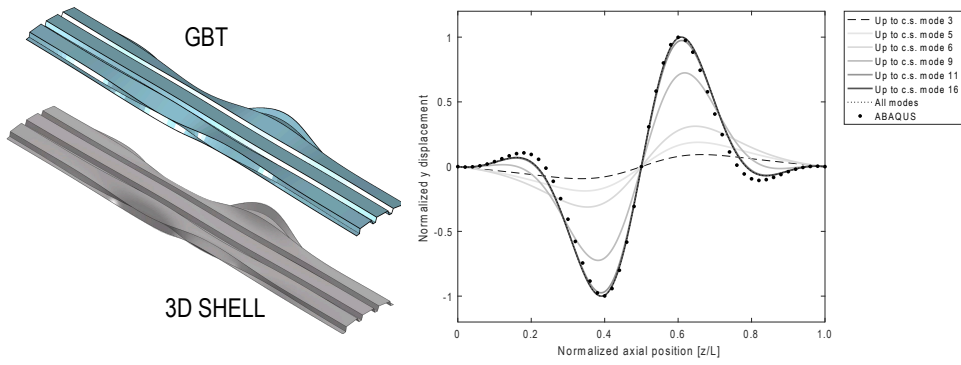


Buckling mode 1

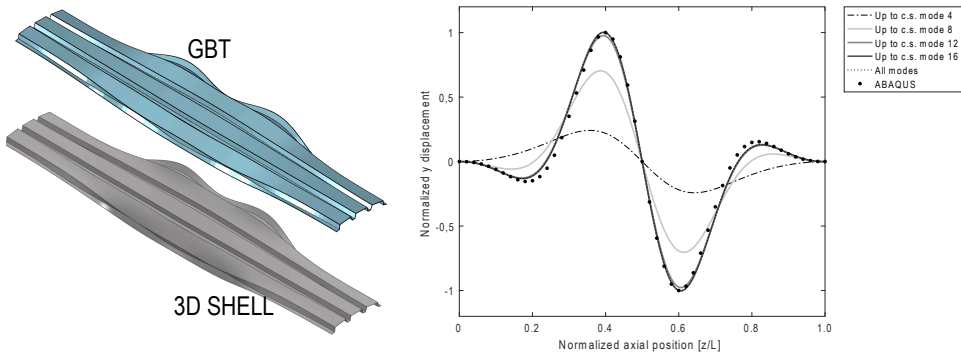


Buckling mode 2

Figure 5.13: Trapezoidal-section beam, buckling modes 1 – 2, deformed shapes and cumulative contribution to y -displacement of natural node 1 (see fig. 5.11).

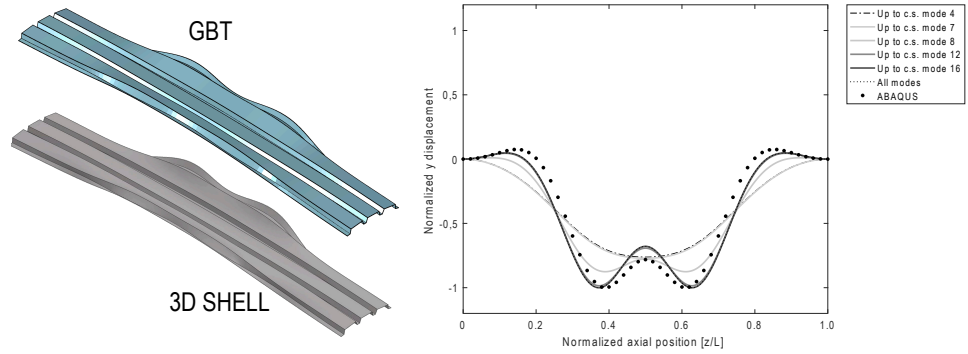


Buckling mode 3

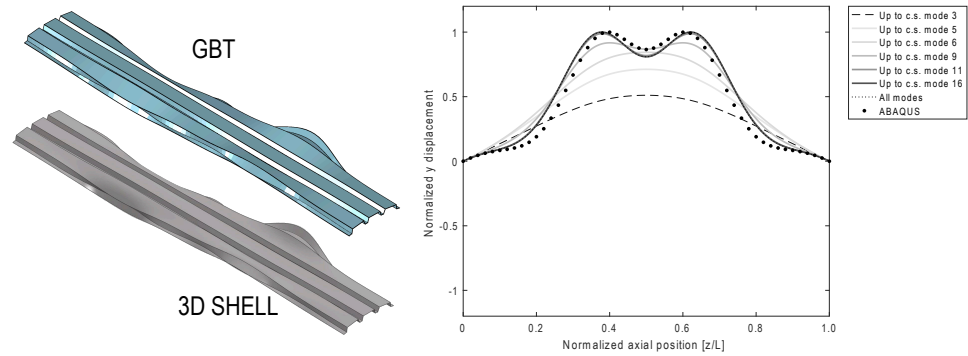


Buckling mode 4

Figure 5.14: Trapezoidal-section beam, buckling modes 3 – 4, deformed shapes and cumulative contribution to y -displacement of natural node 1 (see fig. 5.11).

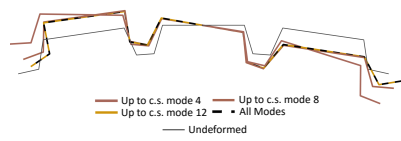


Buckling mode 5

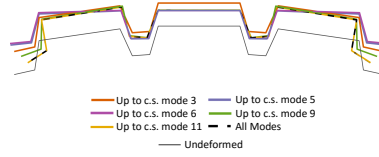


Buckling mode 6

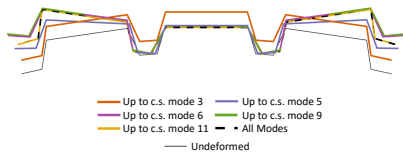
Figure 5.15: Trapezoidal-section beam, buckling modes 3 – 4, deformed shapes and cumulative contribution to y -displacement of natural node 1 (see fig. 5.11).



(a) Buckling mode 1



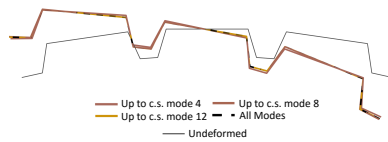
(b) Buckling mode 2



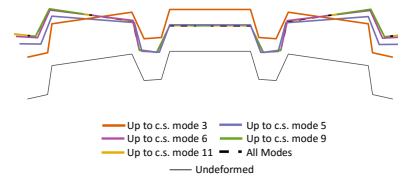
(c) Buckling mode 3



(d) Buckling mode 4



(e) Buckling mode 5



(f) Buckling mode 6

Figure 5.16: Trapezoidal-section beam: cumulative GBT modal contribution to buckling modes at $z/L = 1/4$

5.7 CONCLUSIONS

A geometrically nonlinear, GBT-based, finite element was presented. The main strength of the approach is the full recovery of the underlying linear theory by exploiting of the ICM features.

The nonlinear model accounts both for rigid body motions of the cross-section and for the relative motion of cross-section walls in the 3D space. Results of buckling analyses confirm the ability of the model to account for cross-section distortion, even when dealing with complex cross-section shapes. Results are accurate with respect to 3D shell finite elements, both in terms of buckling shapes and multipliers. The proposed element is able to cope with highly distortional behaviors typical of open thin-walled beams.

Lastly it is worth to underline that the procedure is generally applicable as long as a change of kinematic parameters in the form 5.13 and the relevant inverse relationship 5.14 is available. This not only uncovers the nature of GBT as a folded plate model, but also makes the approach potentially extendable to any thin-walled beam theory.

6

THE COROTATIONAL-BASED GBT: GEOMETRICALLY NONLINEAR ANALYSES

"Computational mathematics
is mainly based on two ideas:
Taylor series and linear
algebra."

— Lloyd N. Trefethen

This Chapter extends the approach adopted in the previous one to treat fully geometrically nonlinear problems, providing a path-following solution to **GBT** beams in large displacements and rotations. The solution is performed by adopting an arc-length scheme. The numerical results show the effectiveness of the approach, providing directions for further researches.

6.1 PATH-FOLLOWING ANALYSIS

Writing the strain energy in the corotational frame, as in eq. 5.19, allows to obtain the geometrically nonlinear model by using the geometrical transformation \mathbf{g}_i associated to the i -th panel. This Chapter includes some basic tools needed to implement the path-following analysis for the ICM-based, GBT finite element presented in Chapter 5, specifying with greater detail the strain energy variations and the relevant approximations.

6.1.1 Rotator approximation

The approximation of the rotators is of primary importance for the development of a geometrically nonlinear, corotational-based models. Finite 3D rotations can be described in matrix notation by a 3×3 orthogonal matrix \mathbf{Q}_i . As a matter of fact, the objective is to locally describe the rotation matrix \mathbf{Q}_i in terms of suitable variables to perform strain energy variations by usual directional derivatives. One possible way, as reported for instance in a similar context in [27], is to parametrize the rotator as a function of the rotation vector $\boldsymbol{\varphi}_i$ and its magnitude φ_i :

$$\boldsymbol{\varphi}_i = [\varphi_{i1}, \varphi_{i2}, \varphi_{i3}]^T, \quad \varphi_i = \|\boldsymbol{\varphi}_i\|.$$

By using Rodrigues' formula [60] the rotation matrix \mathbf{Q}_i can be expressed as:

$$\mathbf{Q}_i[\boldsymbol{\varphi}_i] = \mathbf{I} + \frac{\sin \varphi_i}{\varphi_i} \mathbf{W}_i[\boldsymbol{\varphi}_i] + \frac{(1 - \cos \varphi_i)}{\varphi_i^2} \mathbf{W}_i^2[\boldsymbol{\varphi}_i], \quad (6.1)$$

where \mathbf{W}_i is the spin matrix:

$$\mathbf{W}_i = \text{spin}[\boldsymbol{\varphi}_i] = \begin{bmatrix} 0 & -\varphi_{i3} & \varphi_{i2} \\ \varphi_{i3} & 0 & -\varphi_{i1} \\ -\varphi_{i2} & \varphi_{i1} & 0 \end{bmatrix}.$$

This representation is singularity free and includes just the minimal set of parameters, being bijective for $0 \leq \varphi_i < 2\pi$. Variations of \mathbf{Q}_i may then be expressed by variations of \mathbf{W}_i , but this can be not an easy task.

Alternatively, a non-minimal parametrization for \mathbf{Q}_i may be provided, i.e. to by exploiting the 12 panel displacements $\check{\mathbf{d}}_i$ to define the rotation matrix, as showed in eq. 5.17. The resulting expression, still highly nonlinear, can be the expressed by its p -th order Taylor expansion $\mathbf{Q}_{i,p}$ as follows:

$$\mathbf{Q}_{i,p}[\check{\mathbf{d}}] = \mathbf{I} + \mathbf{V}_{i,2} + \mathbf{V}_{i,2} + \dots + \mathbf{V}_{i,p} \quad (6.2)$$

where I is the identity matrix, the expansion of $V_{i,1}$ is given in the previous Chapter and that of V_2 in Appendix D.

6.1.2 Energy variations

First energy variation defines the equilibrium and compatibility equations of the geometrically nonlinear model, while the second one leads to the definition of the tangent operator needed for the iterative solution. Let the configuration parameters of a single GBT finite element be collected in the vector $\eta_r^T = [\beta_r, \check{d}_r]$, where the subscript r indicates the variation of the parameters.

The strain energy Φ of the finite element, as expressed in the corotational frame, is recalled here for convenience from eq. 5.19:

$$\begin{aligned}\Phi &= \sum_i \Phi_i^m + \Phi^c, \\ \Phi_i^m &= \beta^T G_i^d g_i[\check{d}], \\ \Phi^c &= -\frac{1}{2} \beta^T H \beta.\end{aligned}$$

Denoting with (n) the n -th Frèchet derivative, the variations of the strain energy become:

- 1st variation:

$$\begin{aligned}\Phi^{c(1)} &= -\beta_1^T H \beta, \\ \Phi_i^{m(1)} &= \beta_1^T G_i^d g_i[\check{d}] + \beta^T G_i^d g_i^{(1)}[\check{d}] \check{d}_1\end{aligned}\quad (6.3)$$

- 2nd variation:

$$\begin{aligned}\Phi^{c(2)} &= -\beta_1^T H \beta_2, \\ \Phi_i^{m(2)} &= \beta_1^T G_i^d g_i^{(2)}[\check{d}] \check{d}_2 + \beta_2^T G_i^d g_i^{(1)}[\check{d}] \check{d}_1 + \beta^T G_i^d g_i^{(2)}[\check{d}] \check{d}_1 \check{d}_2.\end{aligned}$$

APPROXIMATION FOR THE FIRST VARIATION Whenever performing the first energy variation in eq. 6.3, the function $g_i[\check{d}]$ is suitable to be directly evaluated, while its Frèchet derivatives may be approximated. In such case, the approximation of the rotator Q_i , eq. 6.2, is directly involved, with an approximation error related to the expansion order adopted. To limit the problem, the rotation of the CR frame is expressed as the product of a reference system $Q_{i,ref}$, evaluated in the equilibrium configuration, times the approximate rotator $Q_{i,inc}[\check{d}]$, which takes into account the additional rotations within the step:

$$Q_i = Q_{i,inc}[\check{d}] Q_{i,ref}$$

for a deeper discussion of the problem with respect to the local structural model adopted, the interested reader may refer to the available literature [27].

RECOVERY OF THE LINEAR MODEL The proposed scheme clearly recovers the linear model whenever one takes $\mathbf{Q}_i = \mathbf{I}$, by reducing the corotational transformations to the identity $\mathbf{d} = \check{\mathbf{d}}$ and thus the same exact variations of the linear model.

6.1.3 Iterative solution scheme

The equilibrium path is provided by the solution of the nonlinear equations, coming from the first variation of the strain energy. Path-following techniques aim at reconstructing the equilibrium path by using “small” incremental steps, relying on the local regularity of the solution.

In this context, Newton schemes make use of the load multiplier λ as continuation parameter, while arc-length schemes, as originally proposed by Riks in [59], parametrizes the nonlinear equations with respect the configuration variables $\boldsymbol{\eta}$ and the load multiplier λ , aiming at determining a sequence of equilibrium configurations $\{\boldsymbol{\eta}^k, \lambda^k\}$.

Path-following algorithms starts from equilibrium configurations $\{\boldsymbol{v}^k, \lambda^k\}$, perform a guess about the next equilibrium configuration $\{\boldsymbol{v}^{guess}, \lambda^{guess}\}$ and correct the guess to minimize the residual in the nonlinear equation, to terminate when the desired tolerance for the residual is achieved, reaching the next equilibrium configuration $\{\boldsymbol{\eta}^{k+1}, \lambda^{k+1}\}$.

Let $\lambda^k \mathbf{p}$ be the external applied load vector, an equilibrium configuration k satisfies exactly the relationship:

$$f[\boldsymbol{\eta}^k] - \lambda^k \mathbf{p} = \mathbf{0},$$

being $f[\boldsymbol{\eta}] = \Phi^{(1)}$. On the contrary, the guess will exhibit a residual, namely:

$$\mathbf{r}^{guess} = f[\boldsymbol{\eta}^{guess}] - \lambda^{guess} \mathbf{p}$$

The Riks method adopts ζ as control parameter, being defined by an additional relationship :

$$t[\boldsymbol{\eta}, \lambda] - \zeta^{k+1} = 0,$$

where t is a restraint surface that has to intersect the equilibrium path. Many choice may in principle be made for the restraint surface, one of the simplest one being the hyperplane:

$$\begin{aligned} \mathbf{n}_\eta^T (\boldsymbol{\eta} - \boldsymbol{\eta}^{guess}) + n_\lambda (\lambda - \lambda^{guess}) &= 0, \\ \mathbf{n}_\eta^T &= \mathbf{M} (\boldsymbol{\eta}^{guess} - \boldsymbol{\eta}^k), \quad n_\lambda = \mu (\lambda^{guess} - \lambda^k), \end{aligned}$$

with \mathbf{M}, μ suitable metric factors defining an inner product for $\{\boldsymbol{\eta}, \lambda\}$, a simple choice, used in the following, could be $\mathbf{M} = \mathbf{I}, \mu = 1$. The solution is found by iterative corrections $\{\Delta \boldsymbol{\eta}^{k,i}, \Delta \lambda^{k,i}\}$:

$$\begin{bmatrix} \Omega[\boldsymbol{\eta}^k] & \mathbf{p} \\ \mathbf{n}_v^T & n_\lambda \end{bmatrix} \begin{bmatrix} \Delta\boldsymbol{\eta}^{k,i} \\ \Delta\lambda^{k,i} \end{bmatrix} = \begin{bmatrix} \mathbf{r}^{k,i} \\ 0 \end{bmatrix}, \quad (6.4)$$

so that

$$\begin{aligned} \boldsymbol{\eta}^{k+1} &= \boldsymbol{\eta}^k + \sum_i \Delta\boldsymbol{\eta}^{k,i}, \\ \lambda^{k+1} &= \lambda^k + \sum_i \Delta\lambda^{k,i}. \end{aligned}$$

Path-following techniques require high-accuracy in the definition of the first energy variation, which actually defines the equilibrium path. Similar accuracy is not requested for the second variation of the energy which is used to define the linear system 6.4 as obtained in the last equilibrium configuration.

6.2 NUMERICAL EXAMPLES

A set of numerical examples is presented to show the performances of the proposed approach. Two open-section were tested, for which the proposed change of kinematic parameters introduced in section 5.2 applies. Fundamental flexural modes, local lip modes and wall-extension ones are used.

As anticipated in subsection 5.1.2, on the corotational frame the GBT model is considered to be linear. If, on one hand, this may limit the accuracy of results, on the other hand shows how the proposed approach can properly deal with some interesting problems with no other refinements. Results are also quantitatively compared to fully geometrically nonlinear analyses performed in the commercial software ADINA by employing the well known MITC4 finite element [6], with a very fine structured mesh.

For the all the presented numerical tests, the material is assumed to be steel, characterized by elastic modulus $E = 210000 \text{ MPa}$ and Poisson coefficient $\nu = 0.3$.

In the quantitative displacements plot, the displacement field as obtained by the nonlinear GBT model has been evaluated by using:

- linear strains only onto the corotational system
- a second-order approximation for the variation of the corotational relationship g_i that generates the nonlinear strains, eq. 5.18.

6.2.1 Stocky rack-section beam subjected to distortional load

Consider the short cantilever beam presented in figure 6.1. The structure presents an highly-stiffened rack-like cross-section (the same as in section 5.6.1). The beam is 600 mm long, with a distortional load applied at the free end. The objective of the test is to demonstrate how it is possible to deal with purely cross-section distortion phenomena in highly stiffened members. Cross-section deformation modes are 45 overall: the same of test of section 5.6.1 with the addition of wall-extension modes.

A mesh of 20 GBT finite elements is taken into consideration. Three-dimensional deformed shapes for increasing load multiplier are reported in figure 6.2, showing synthetically the structural behavior: the end cross-section flanges rotate symmetrically about the web-to-flange junctions leading to a dramatic change in shape of the initial structural configuration, while along the axis the same qualitative behavior occurs with a rapidly decreasing amplitude, as usual for distortional modes. Figures 6.3,6.4 show in detail the displacements of the free cross-section, as compared to the reference solution: y -displacements of the node 3 as well as all the components of displace-

ments of node 6 clearly highlight the nonlinear behavior. A good overall agreement with the reference solution can be noticed for node 3, while node 6 equilibrium curves show that some quantitatively minor phenomena cannot be addressed. Figures 6.56.6 show that the displacement amplitude decreases really fast far from the load application point. Finally, figure 6.7 shows the end cross-section deformed shapes until to incipient closure.

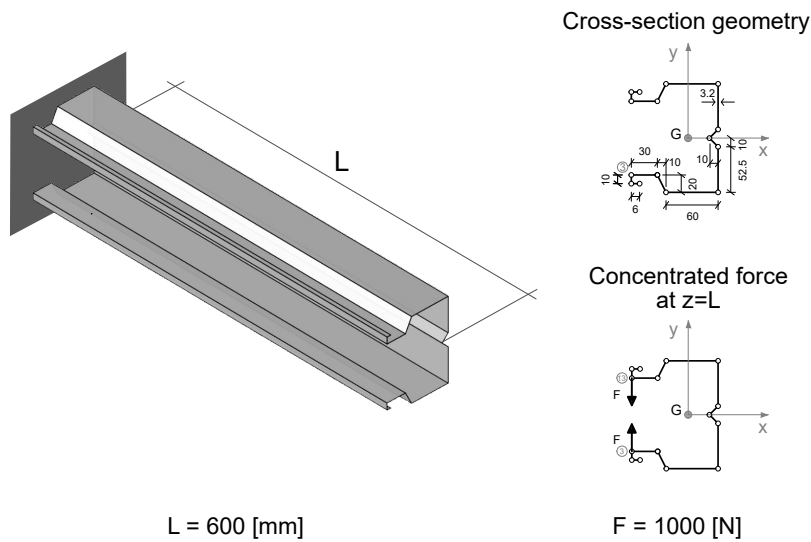


Figure 6.1: Stocky rack-section beam subjected distortional load: geometry and load detail

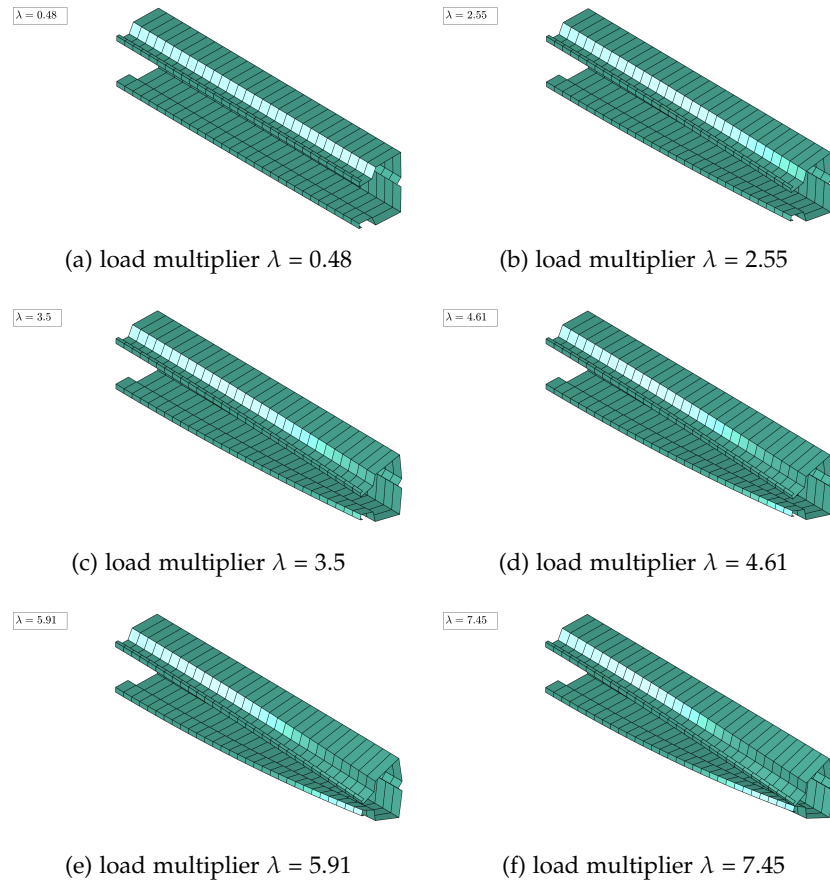


Figure 6.2: Stocky rack-section beam subjected distortional load: deformed shapes

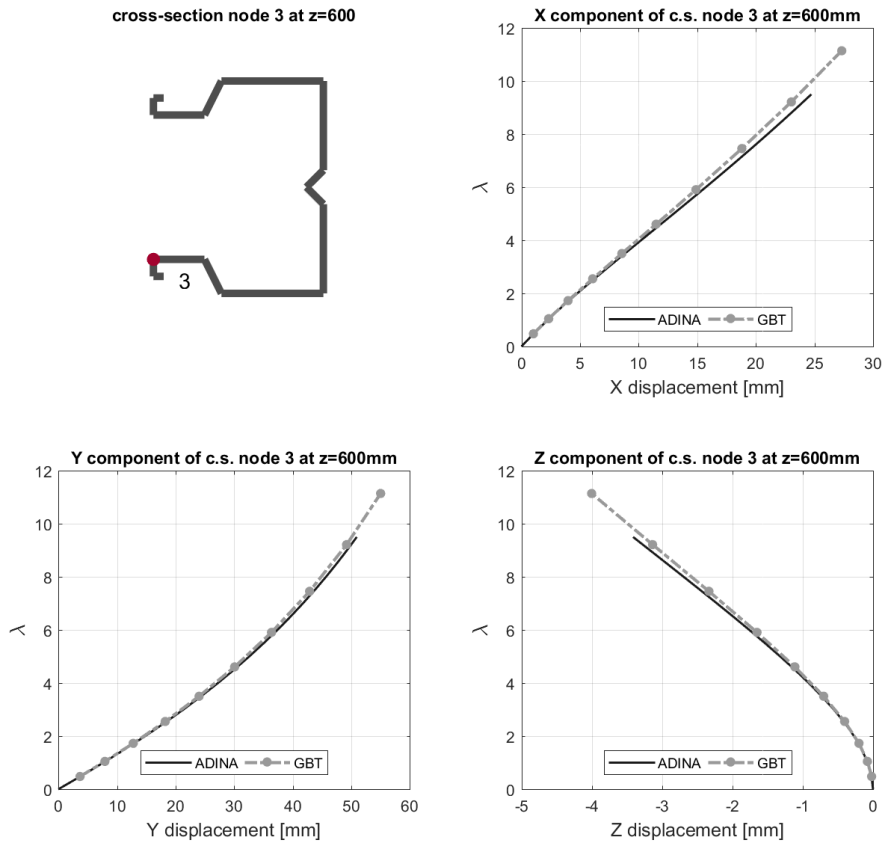


Figure 6.3: Stocky rack-section beam subjected distortional load: equilibrium path for node 3 at $z/L = 1$

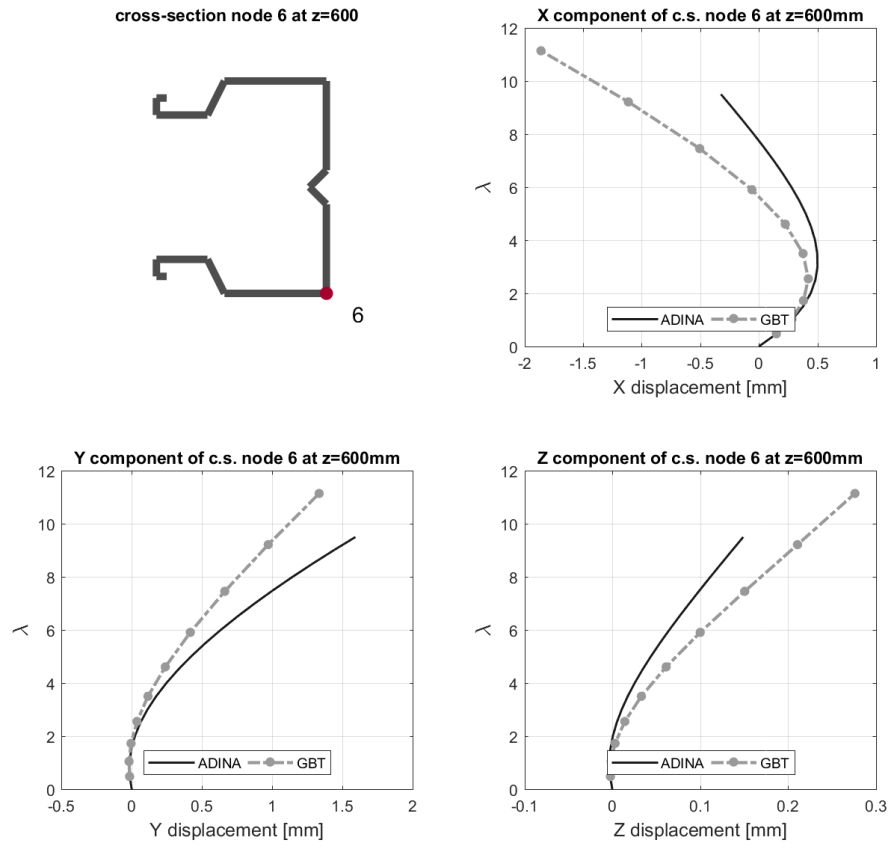


Figure 6.4: Stocky rack-section beam subjected distortional load: equilibrium path for node 6 at $z/L = 1$

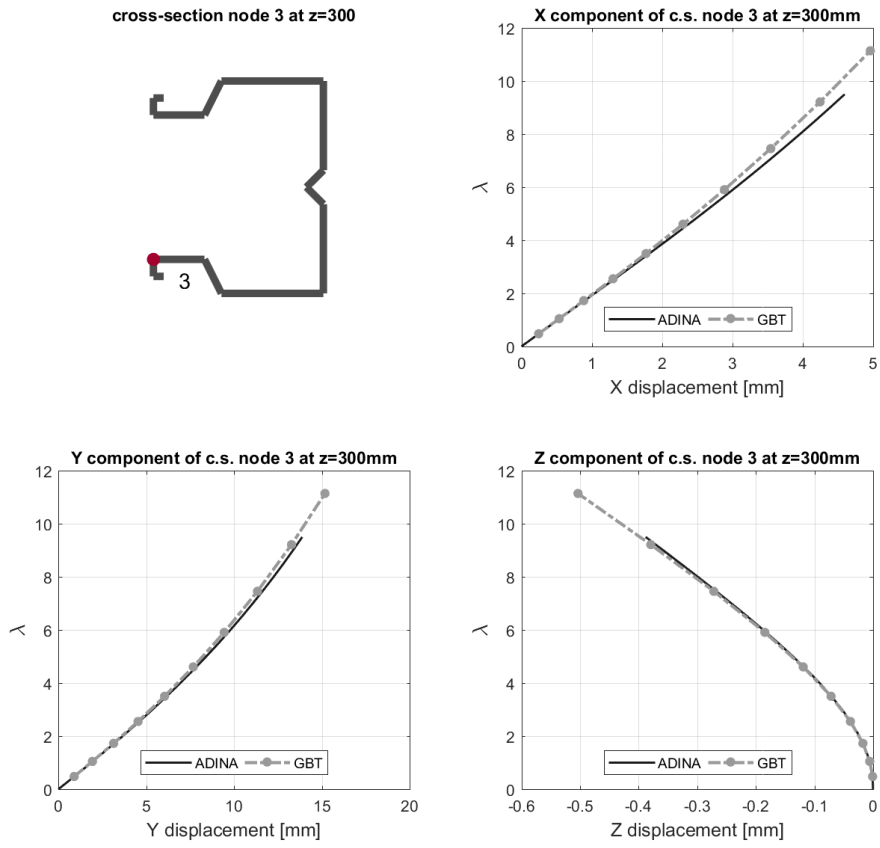
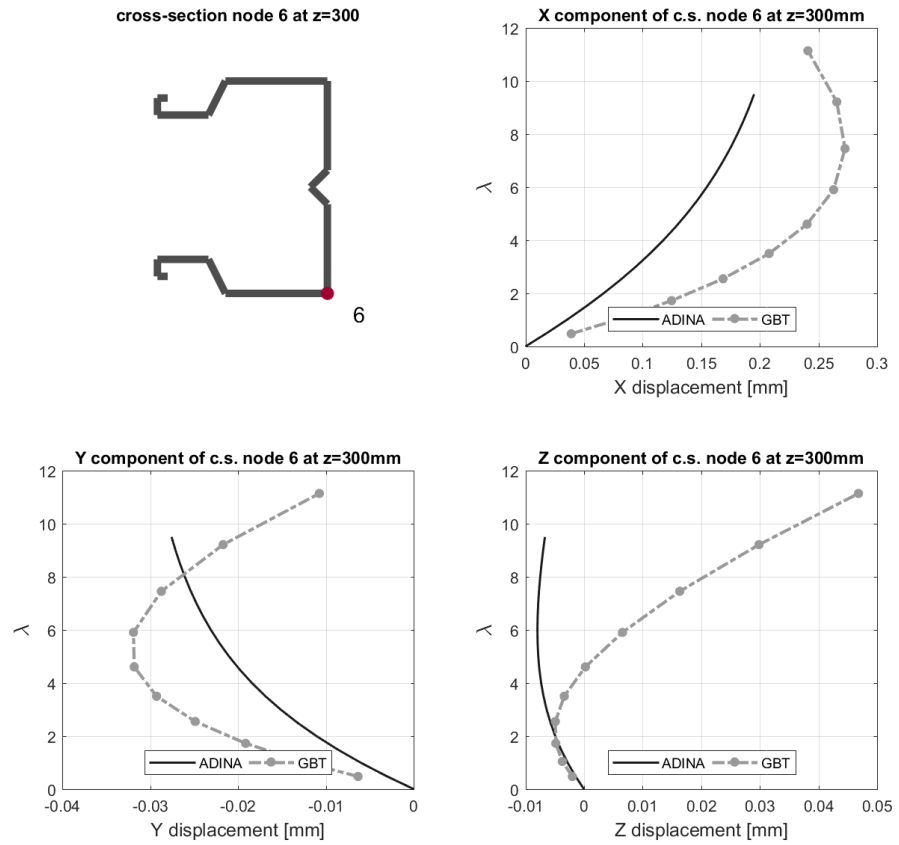


Figure 6.5: Stocky rack-section beam subjected distortional load: equilibrium path for node 3 at $z/L = 1/2$



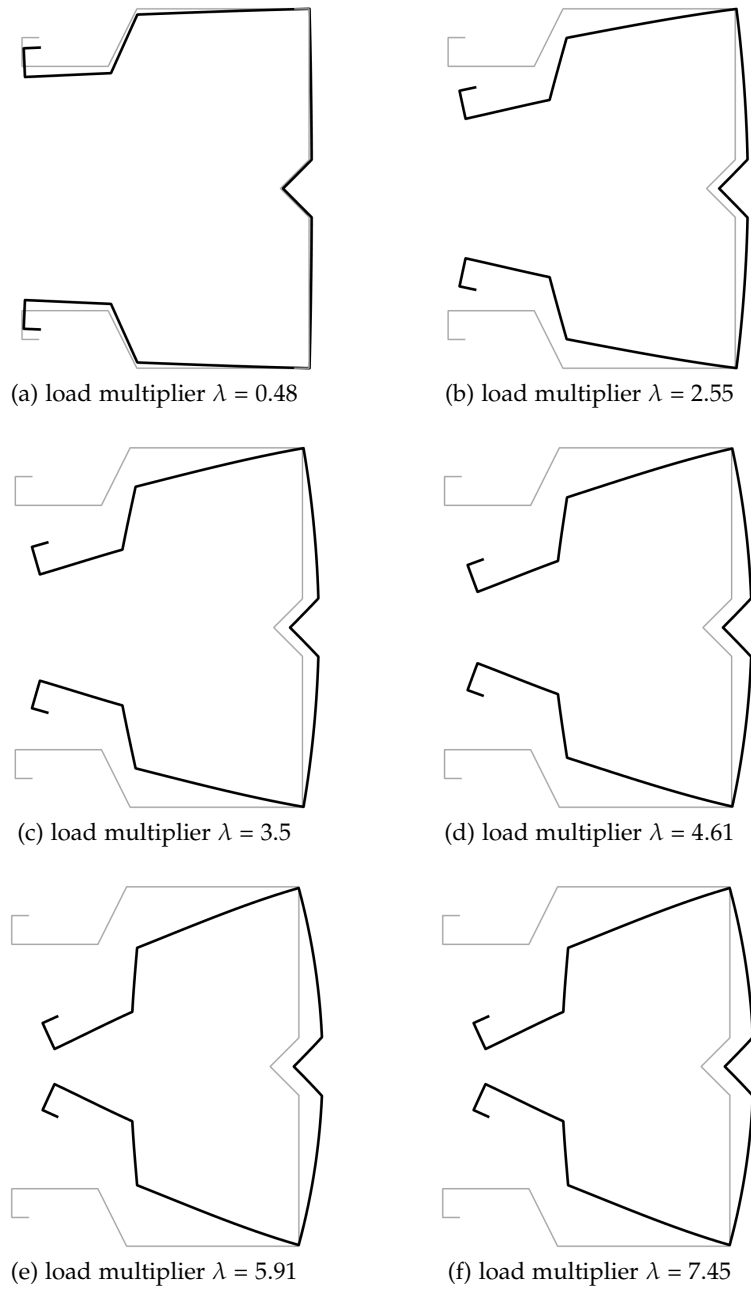


Figure 6.7: Stocky rack-section beam subjected distortional load: cross-section at $z/L = 1$

6.2.2 Rack-section beam subjected to shear force

In this test, a cantilever beam with a rack-section shape is analyzed, as in fig. 6.8. The test is designed in order to assess the ability of the model of capturing interaction between global beam deformation and distortional cross-section deformation. The beam is 2000mm long and the cross-section 2.3mm thick, with the same geometry of the previous test cross-section. The finite element mesh is made of 20 GBT finite elements. The same cross-section deformation modes of the previous test are assumed.

The load is applied at the free end and consists in two symmetrical forces, whose resultant is a shear load parallel to the cross-section weak axis. The external load, when acting on the linearized kinematics, would activate a global and a distortional mode.

The example shows that distortional behavior is not only amplified by geometrical nonlinearity and that, differently from the linear case, a highly distortional behavior is triggered close to the fixed end. The deformed shapes in fig. 6.9 show the loading sequence of the structure and relevant interactive phenomena. Figures 6.10 to 6.13 show the displacements of node 3 and 6 of the cross-sections at $z/L = 1$ and $z/L = 1/4$. The inspection of the x-displacement component of nodes 3 and 6 at the free end highlights a global loss of stiffness of the beam at $\lambda \approx 7$. Contemporarily, at $z/L = 1/4$, (figs. 6.12,6.13) node 3 suddenly snaps in towards the cross-section center. This occurs symmetrically and hence strongly reduces the stiffness of the cross-section. As it can be noticed, the agreement with respect to the reference solution is good. Finally, the deformed shapes of the cross-sections at $z/L = 1$ and $z/L = 1/4$ are reported in figs. 6.15,6.14.

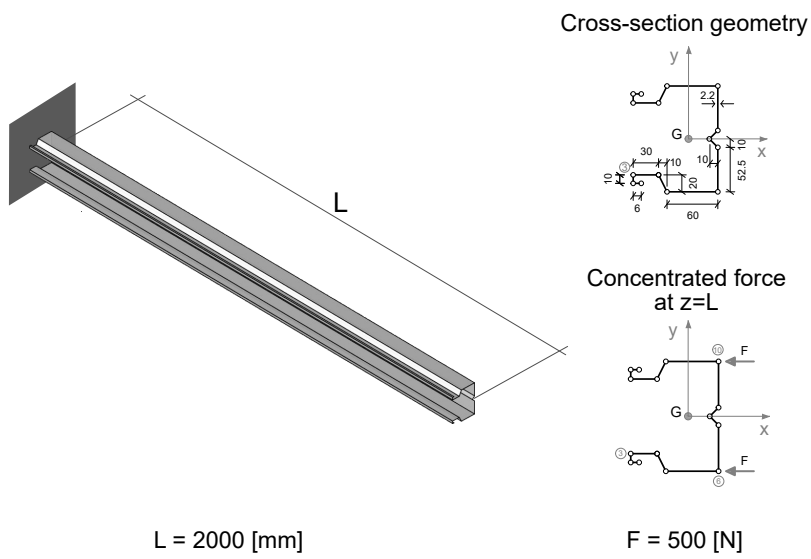


Figure 6.8: Rack-section beam subjected shear forces: geometry and load detail

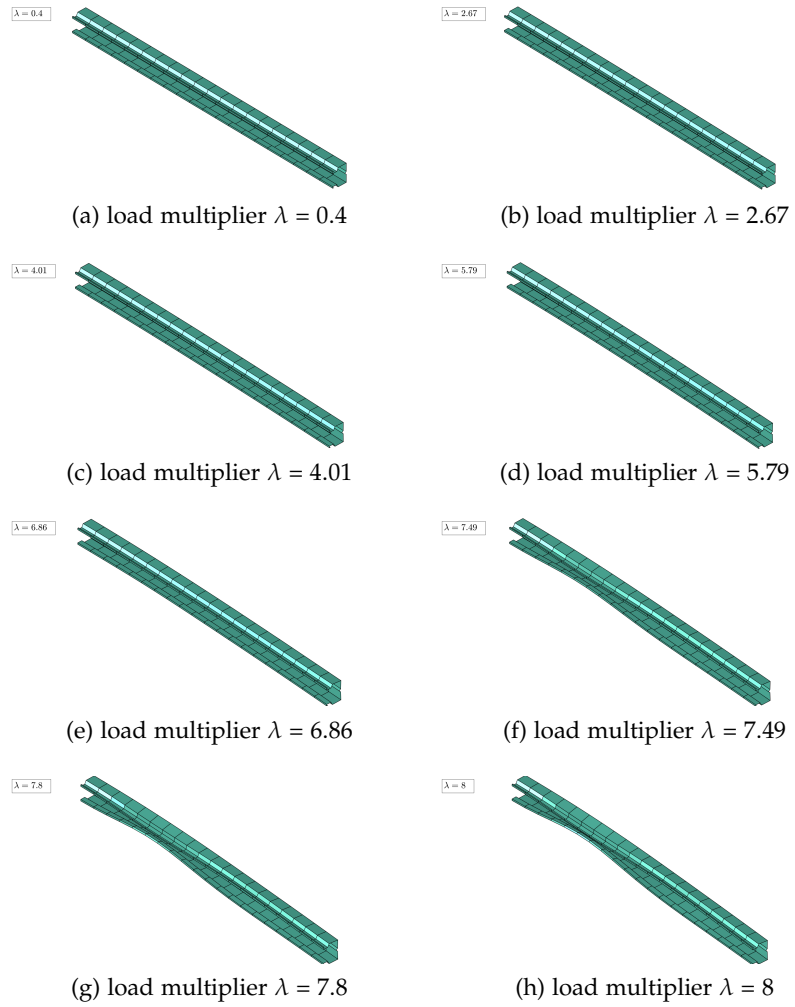


Figure 6.9: Rack-section beam subjected to shear forces: deformed shapes

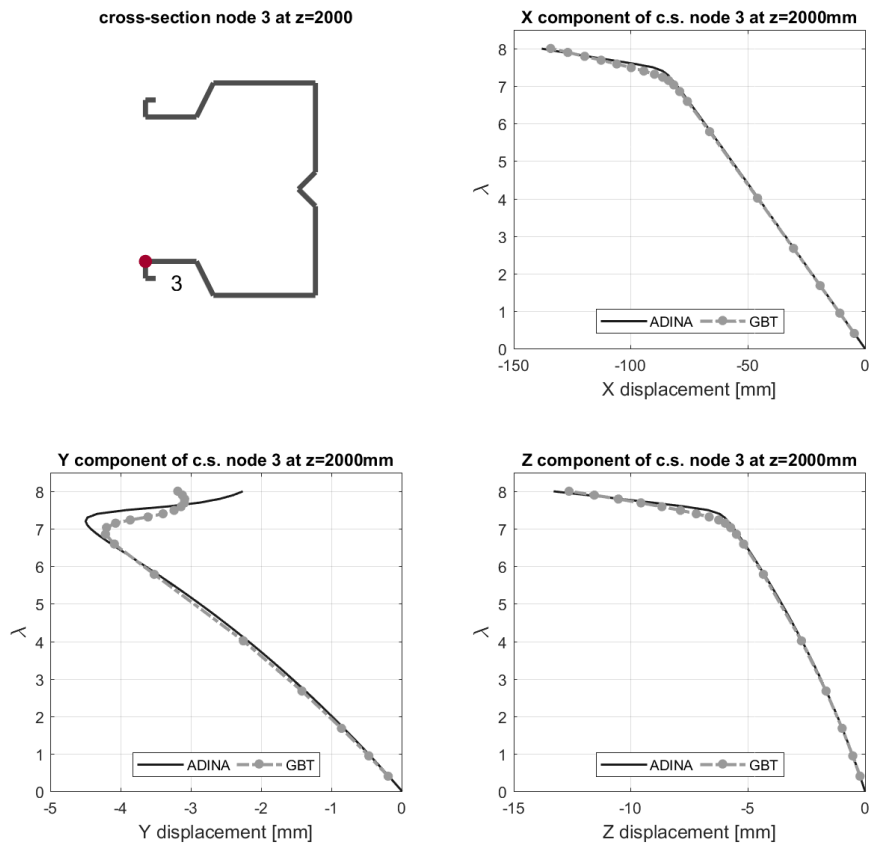


Figure 6.10: Stocky rack-section beam subjected distortional load: equilibrium path for node 3 at $z/L = 1$

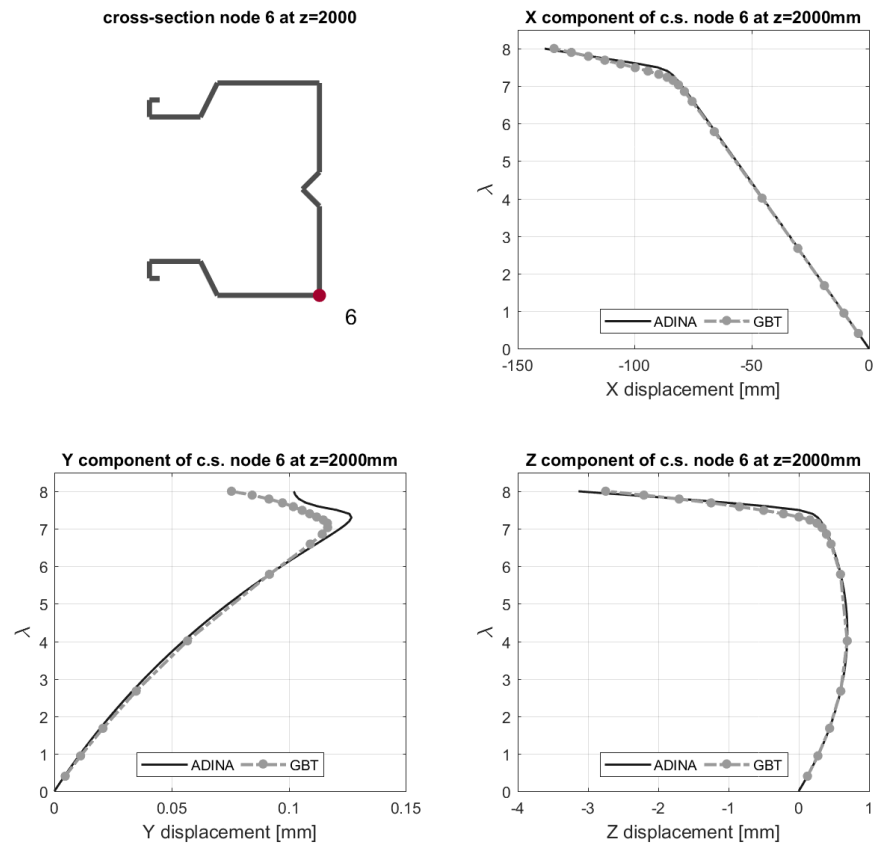


Figure 6.11: Stocky rack-section beam subjected distortional load: equilibrium path for node 6 at $z/L = 1$

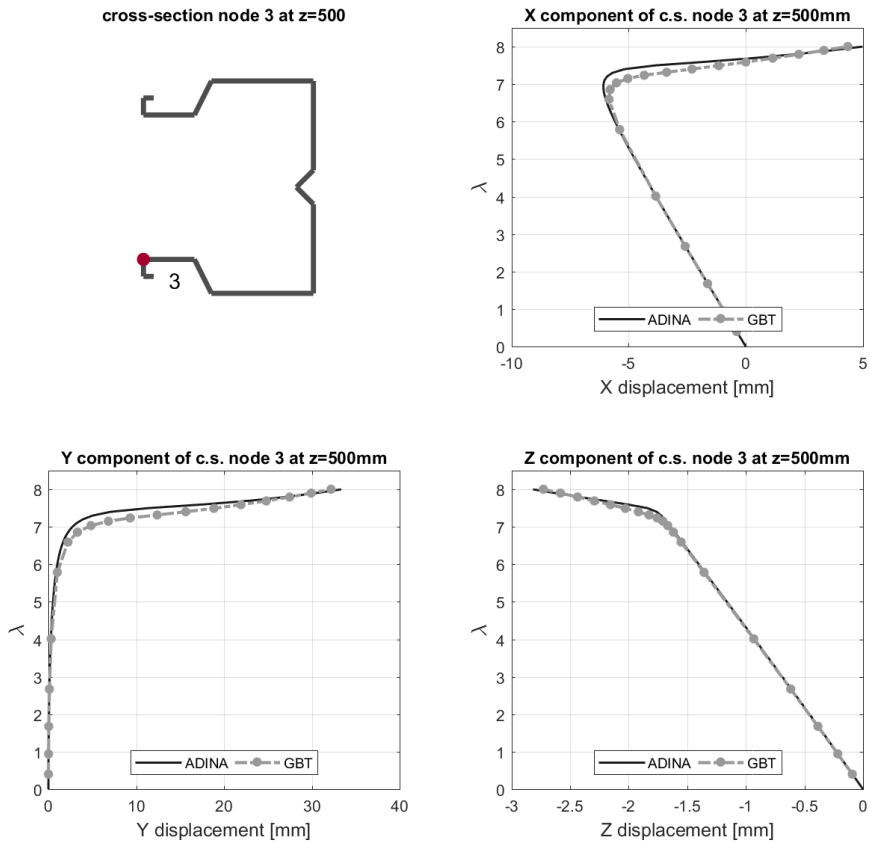


Figure 6.12: Stocky rack-section beam subjected distortional load: equilibrium path for node 3 at $z/L = 1/4$

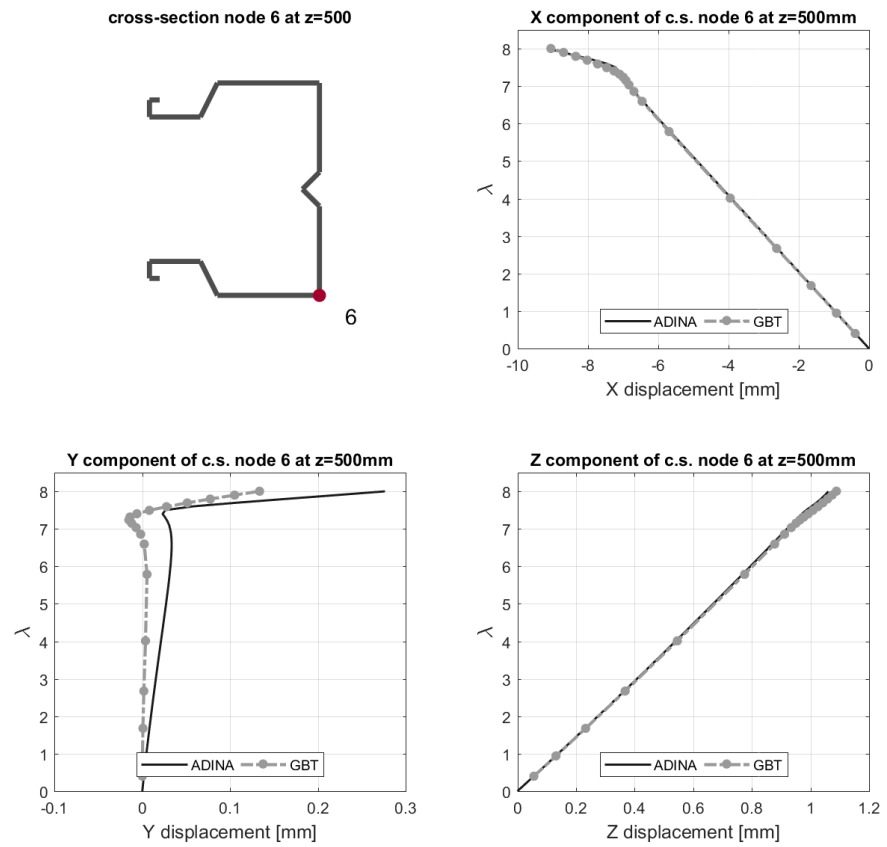


Figure 6.13: Stocky rack-section beam subjected distortional load: equilibrium path for node 6 at $z/L = 1/4$

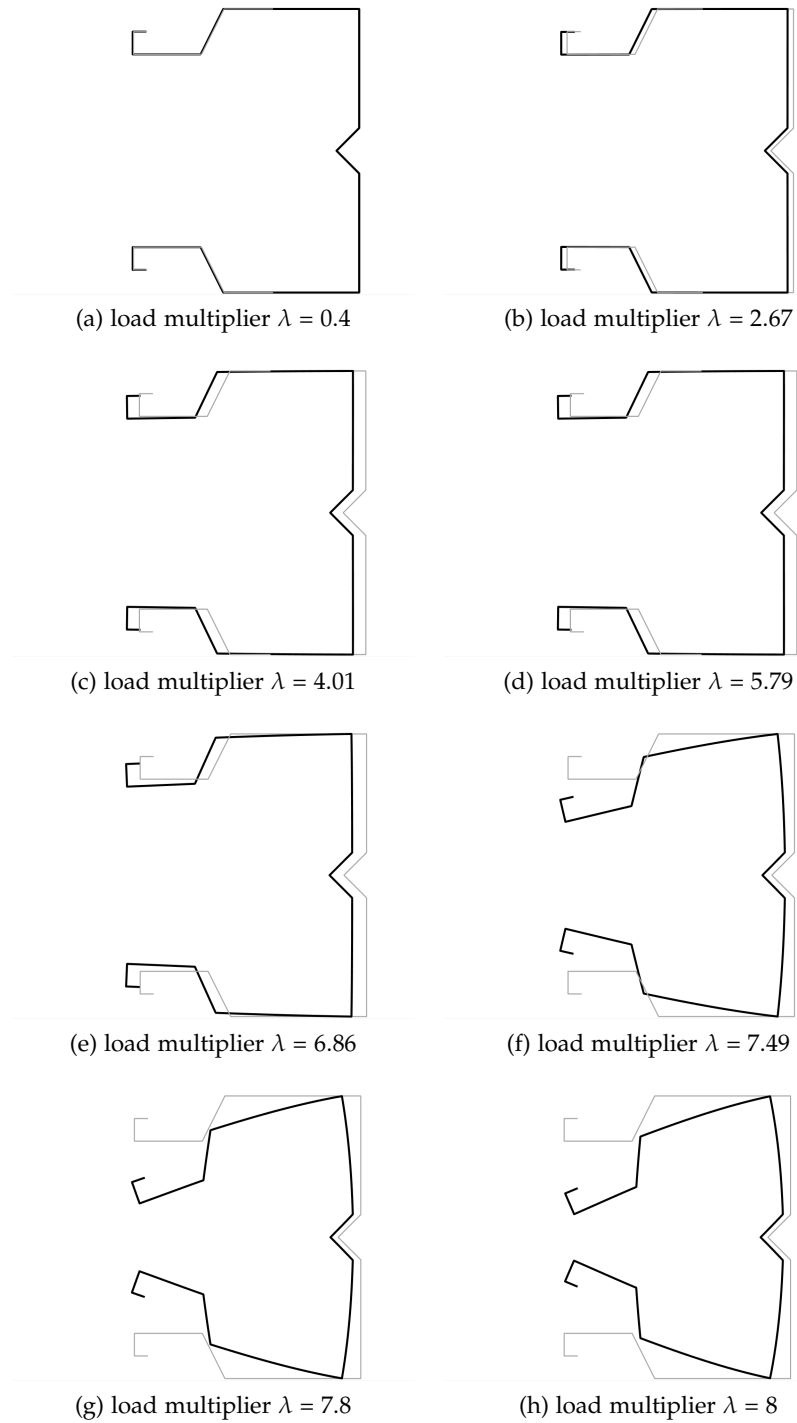


Figure 6.14: Rack-section beam subjected to shear forces: cross-section at $z/L = 1/4$

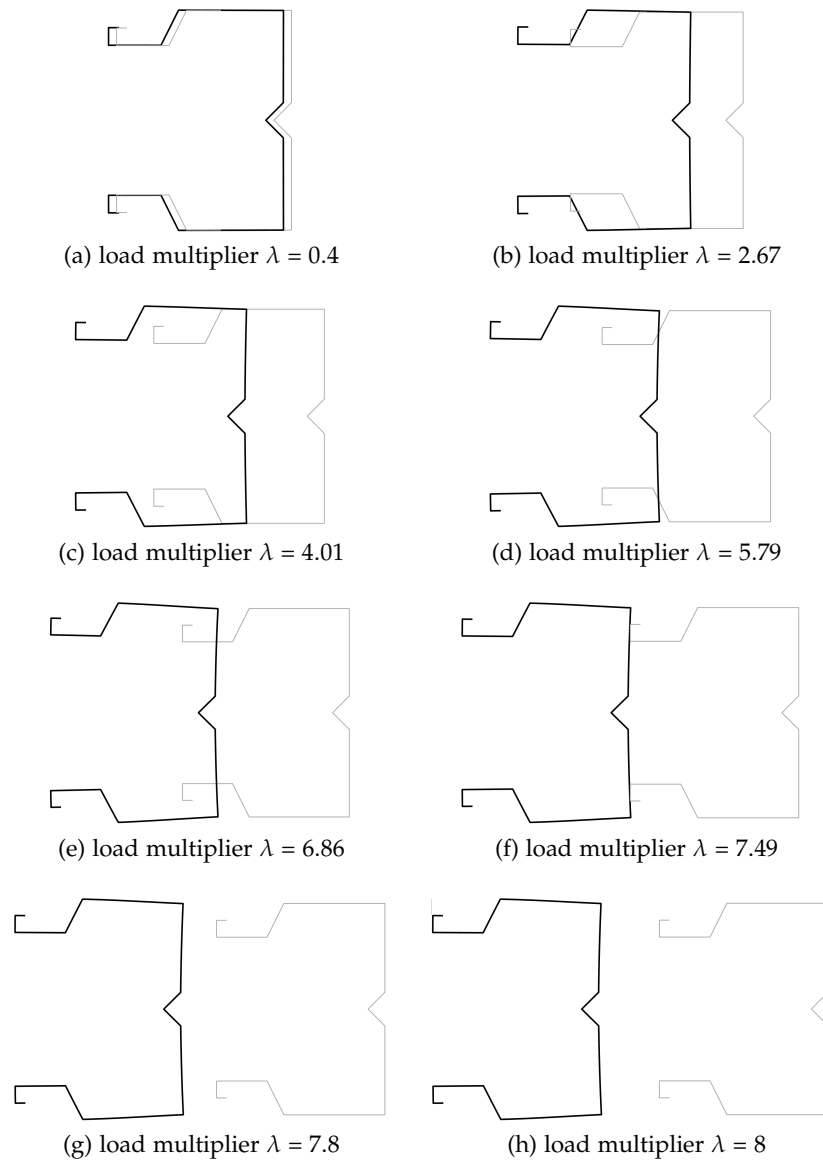


Figure 6.15: Rack-section beam subjected to shear forces: cross-section at $z/L = 1$

6.2.3 Z-section beam subjected to distortion

A long Z-section cantilever beam, subjected to a point load at the free cross-section is studied, see fig. 6.16. The beam is 5000mm long, and the load is applied on the mid of the lower flange, to mimic the application of the load passing through a screw and triggering both torsion and cross-section distortion. A mesh made of 50 finite elements is used.

The deformed shape of the beam is shown in fig. 6.16, presenting both distortional and global phenomena. Figures 6.18 to 6.21 show the displacement components of node 2 and 3 of the cross-section at $z/L = 1$ and $z/L = 1/2$, while the displacement components of node 5 close to the fixed end (at $z = 312\text{mm}$) are shown in fig. 6.22. Moreover, the deformed cross-sections at $z/L = 1$ and $z/L = 312\text{mm}$ are shown in figs. 6.23 and 6.24. As it can be noted, the sudden appearance of cross-section distortion close to the fixed end (see figs. 6.22 and 6.24) softens the global behavior of the structure, as it can be seen from the y-displacement of node 3 in fig. 6.19. In general, the equilibrium paths are reproduced with good accuracy, especially before the occurrence of the aforementioned distortional phenomenon.

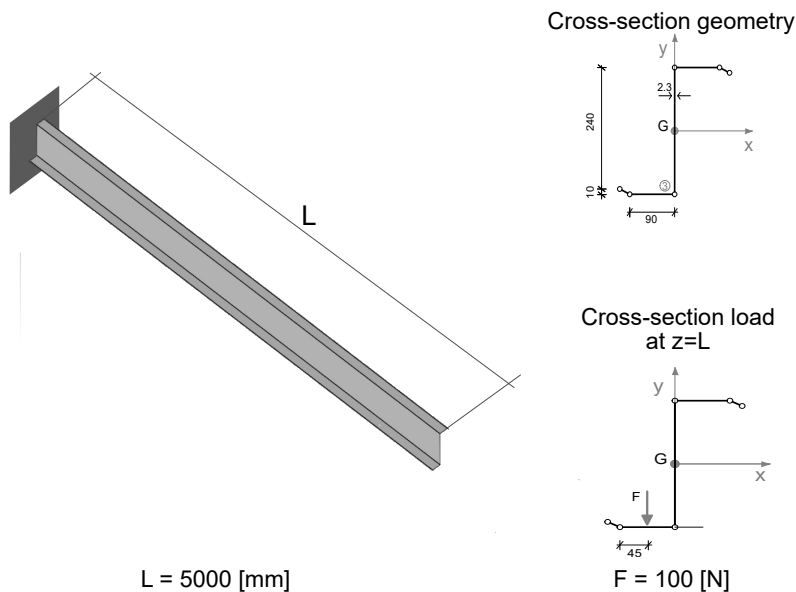


Figure 6.16: Z-section beam subjected cross-section distortion: geometry and load detail

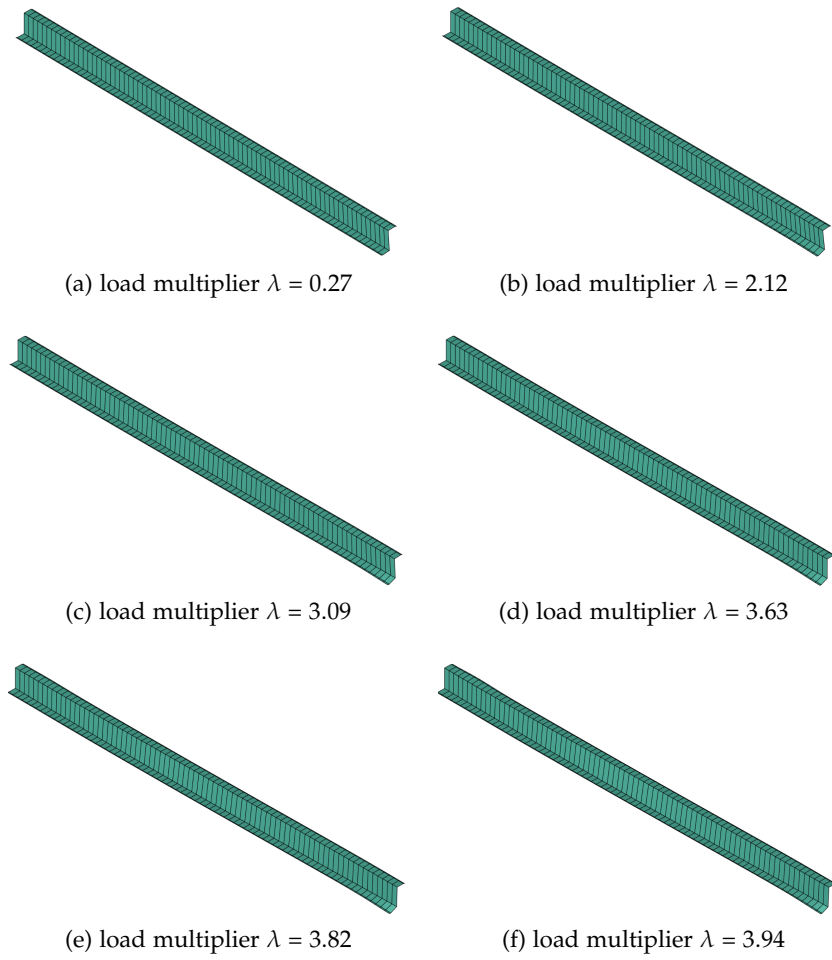


Figure 6.17: Z-section beam subjected to distortion: deformed shapes in the 3D space

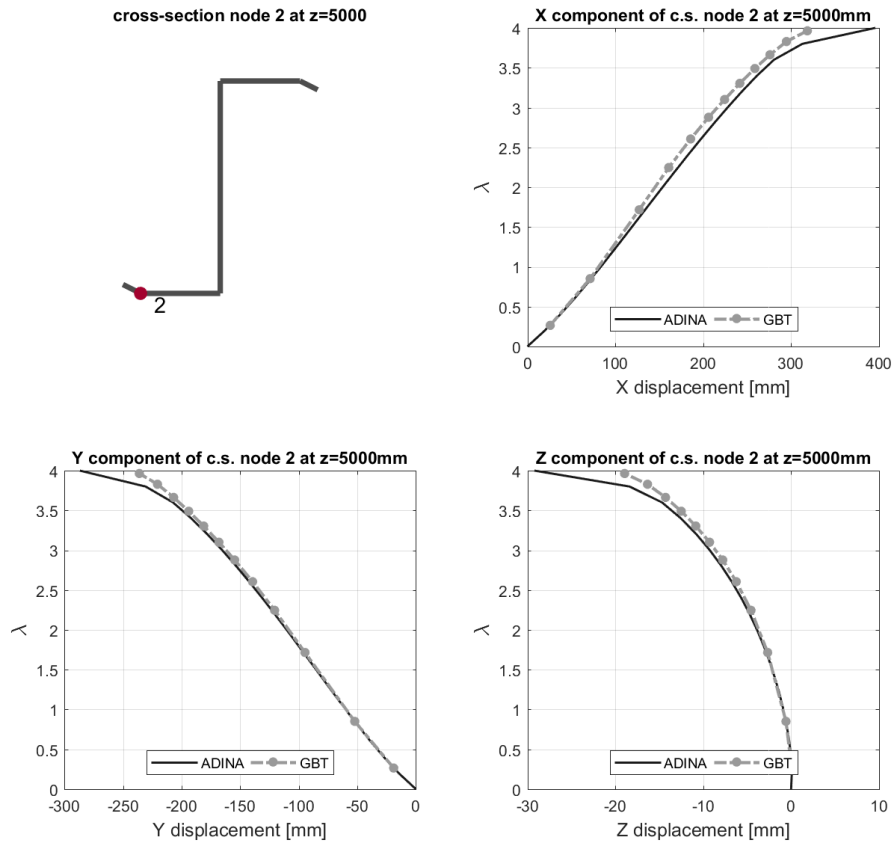


Figure 6.18: Stocky rack-section beam subjected distortional load: equilibrium path for node 2 at $z/L = 1$

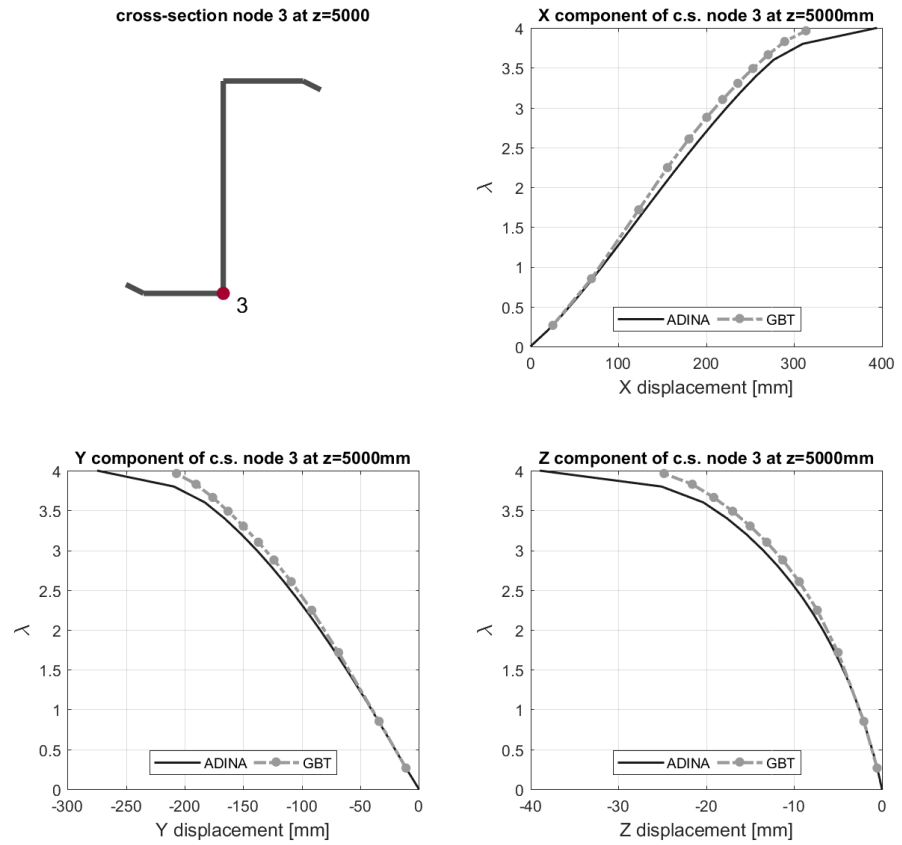


Figure 6.19: Stocky rack-section beam subjected distortional load: equilibrium path for node 3 at $z/L = 1$

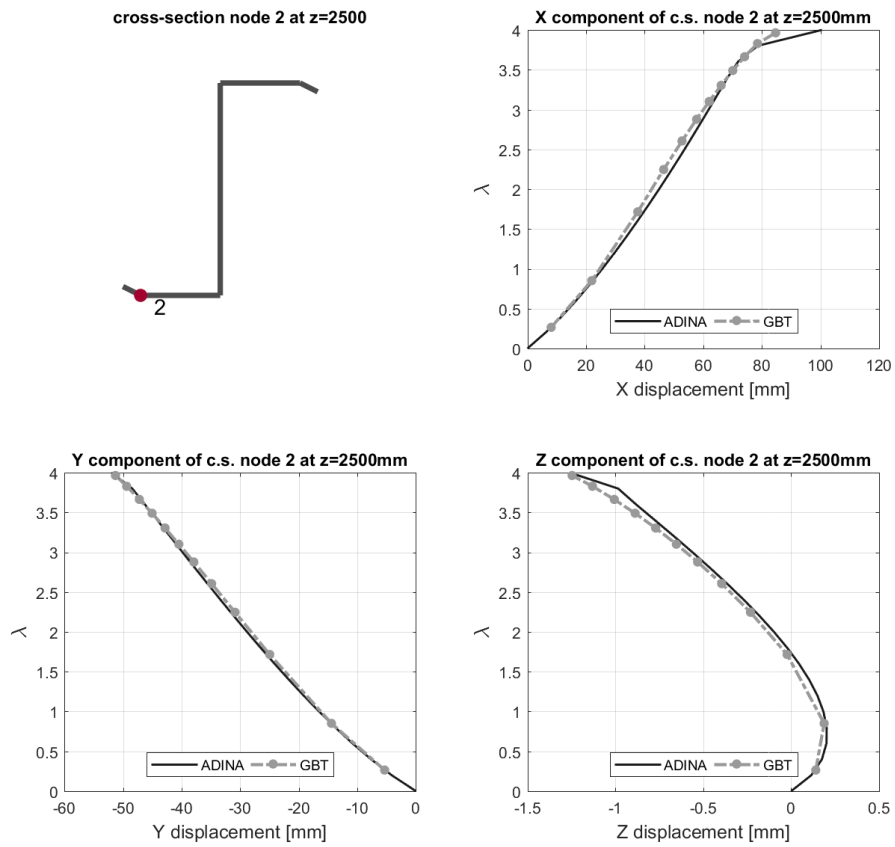


Figure 6.20: Stocky rack-section beam subjected distortional load: equilibrium path for node 2 at $z/L = 1/2$

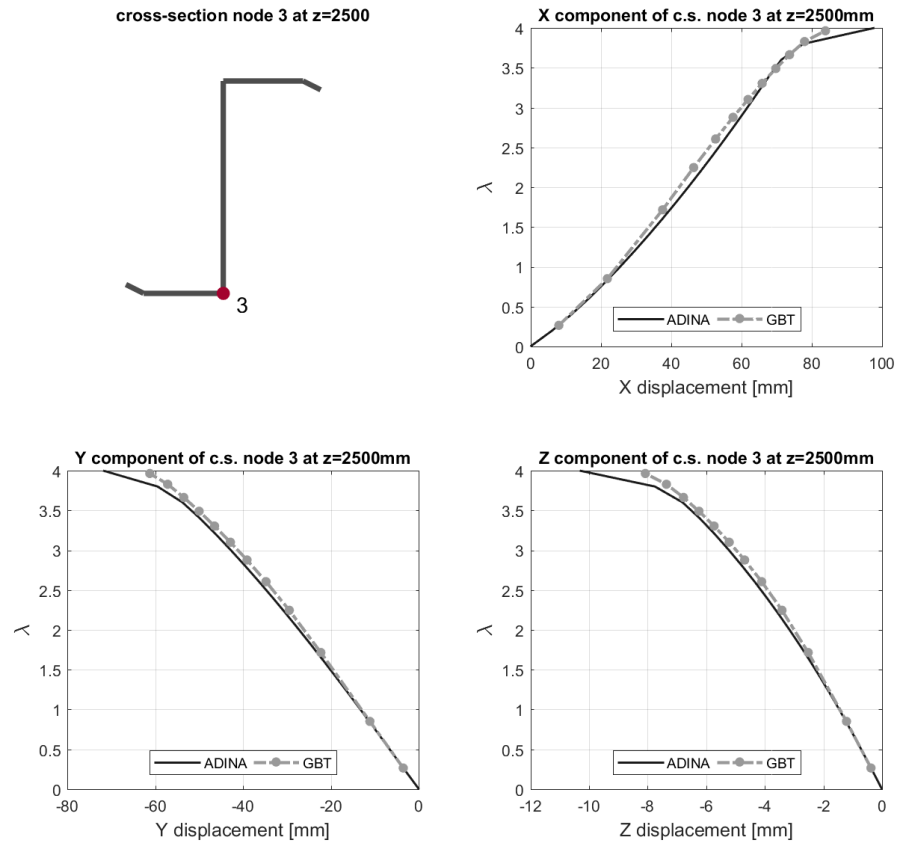


Figure 6.21: Stocky rack-section beam subjected distortional load: equilibrium path for node 3 at $z/L = 1/2$

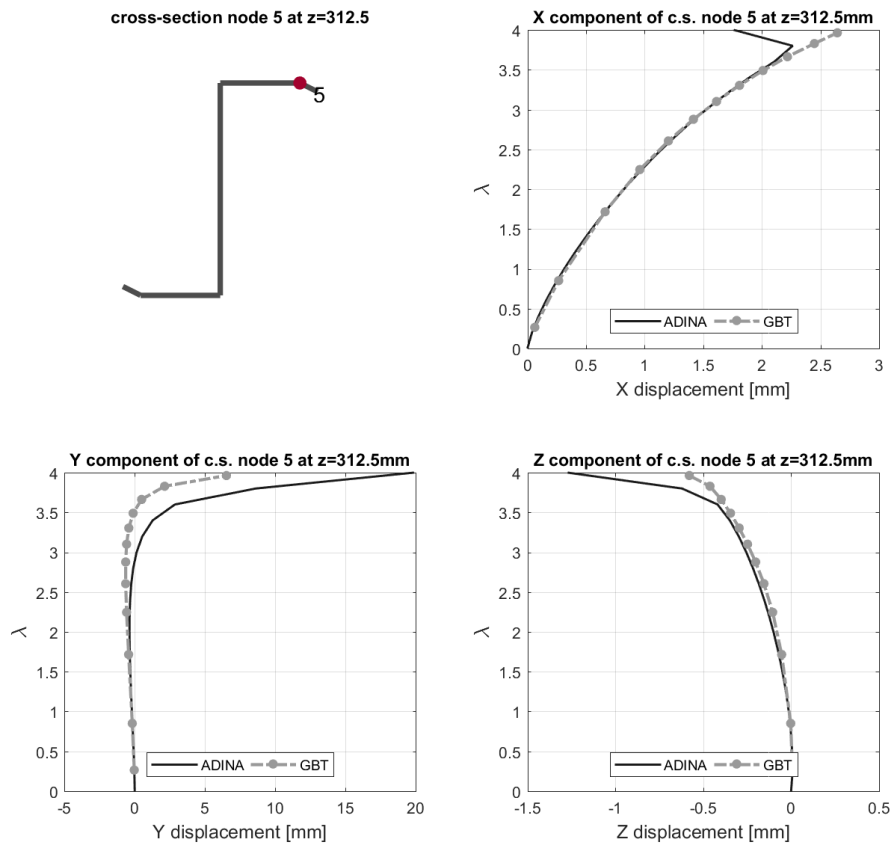


Figure 6.22: Stocky rack-section beam subjected distortional load: equilibrium path for node 5 at $z = 312\text{mm}$

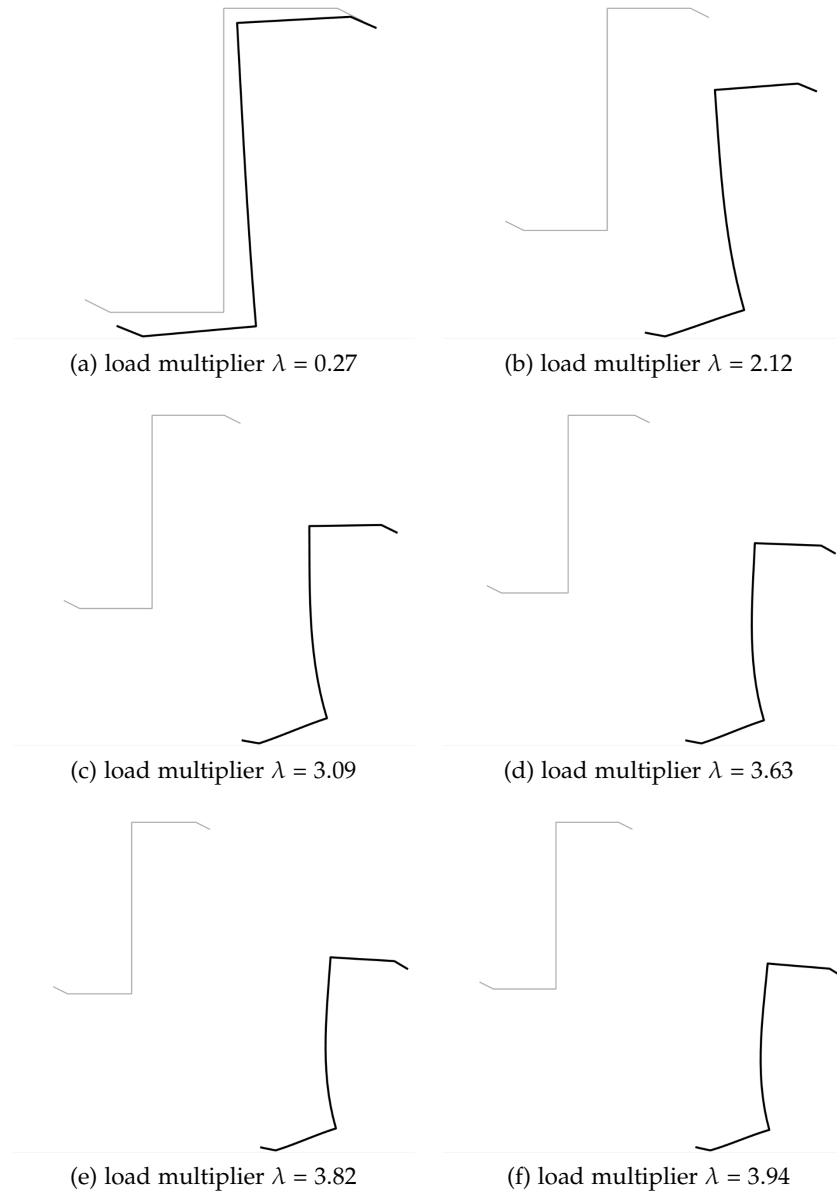


Figure 6.23: Z-section beam subjected to distortion: cross-section at $z/L = 1$

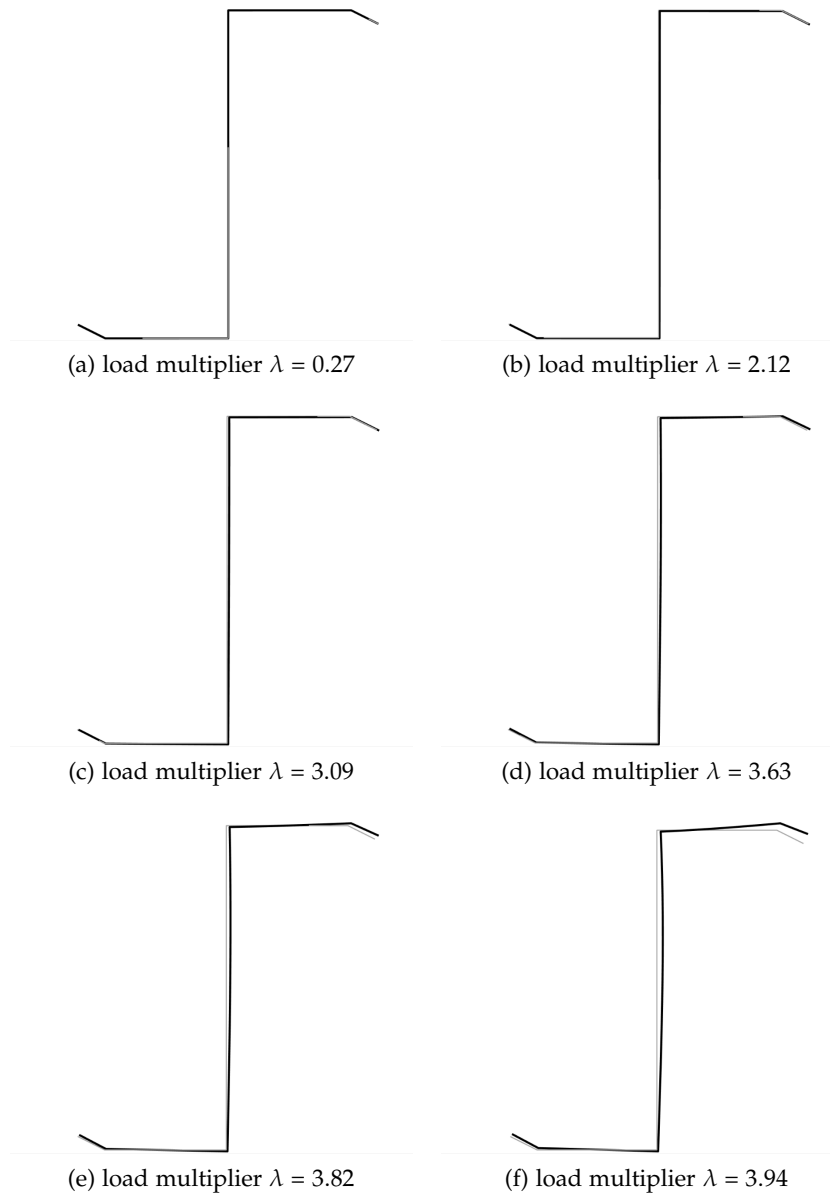


Figure 6.24: Z-section beam subjected to distortion: cross-section at $z = 312.5$ [mm]

“For such a model there is no need to ask the question “Is the model true?”. If “truth” is to be the “whole truth” the answer must be “No”. The only question of interest is “Is the model illuminating and useful?”.

— George Box

Thin-walled structural members exhibit a complex behavior, being affected both by material and geometrical nonlinearities. Modeling thin-walled members as inherently three-dimensional structures, as the nature of the involved phenomena would suggest, leads to rich and generalizable results. However, this might induce to abandon some physical intuition and the capability of conducting global analysis of structures.

An alternative approach can be found by resorting to higher order beam theories based on a one-dimensional representation. In this context, some phenomena affecting thin-walled beams, as section distortion, may be effectively described by the Generalized Beam Theory (GBT).

Starting from the observation that exists a gap among the analysis and the design of thin-walled beams, the aim of the thesis is to provide a contribution in the geometrical analysis of these by the using GBT. After an exemplification on how the GBT theory can be integrated in the design process of roofing systems, thanks to its direct relationship with classical beam theories, the main topic addressed is the formulation of a geometrically nonlinear GBT finite element able to deal with global phenomena and cross-section distortion.

Corotational methods are good candidates for this purpose, allowing to reuse existing linear theories. In particular, the Implicit Corotational Method (ICM) is a powerful tool to obtain the geometrically nonlinear model from the corresponding linear one, relying on a the description of the problem in terms of Biot stresses and strains. However, the application of the corotational description to higher order beam models is particularly challenging. A solution was found by placing more than one Corotational (CR) observer on partitions of the cross-section, uncovering the original interpretation of the theory of the GBT as in its “folded plate” nature, allowing to formulate a

geometrically nonlinear, CR-based, GBT. Once obtained, the GBT nonlinear model was implemented using a state-of-the-art mixed-stress finite element.

Several numerical results were presented, involving both buckling and path-following analyses. The linearized buckling analyses showed how the CR description is sufficient to obtain accurate buckling loads and deformed shapes when compared to a three-dimensional shell model, even for the complex cross-sectional shapes that can be found in real applications. Path-following analyses highlighted how the geometrical nonlinearity associated to highly distortional behaviors can be effectively addressed by the proposed ICM-based GBT.

RECOMMENDATIONS FOR FUTURE WORK

“Begin at the beginning,” the King said gravely, “and go on till you come to the end: then stop.”

— Lewis Carroll, Alice in Wonderland

Many recommendations may be devised for future work on the on the nonlinear GBT element and on the presented approach.

The nonlinear GBT implementation is suitable for further refinements in the treatment of 3D rotations, which may take advantage of a more efficient parametrization. Moreover, the introduction of local flexural GBT modes would probably further refine the results, bringing the opportunity to carry out a fair comparison with respect to 3D shell models. As far as the aspect of the technical applications, the implementation of more general cross-section shapes is certainly desirable. However, to fully exploit a nonlinear GBT finite element in practical applications, a very interesting feature would be the capability of handling general connections both with external elements (fasteners -point-wise compatibilities-, roofings -distributed springs-) and with other beams in the 3D space. Overcoming these practical limitations would make the model suitable for many problems engineering problems.

More in general, the theoretical and numerical development of the proposed approach has shown how to introduce multiple CR frames per GBT finite element, based on a full reparametrization of the GBT degrees of freedom. A further theoretically attractive development resides in developing a GBT nonlinear finite element based on a partial reparametrization, with the advantage of devising mechanically clearer corotational transformations for the classical beam generalized displacements.

Finally, the approach to the geometrically nonlinear GBT was firstly motivated by the ability to analyze cross-section deformable GBT beams, however, its application to other high-order beam theories would be of great interest.

DETAILS OF THE LINEAR GBT

A.1 SUBMATRICES OF THE CROSS-SECTION STIFFNESS MATRIX

The submatrices of the cross-section included in eq. 3.14 are:

$$\begin{aligned} \mathbf{C}_S = & \int_A n^2 \mathbf{C}_{11}^{(B)} \partial_{ss} \boldsymbol{\psi}^T \partial_{ss} \boldsymbol{\psi} \, dA + \int_A \mathbf{C}_{11}^{(M)} \partial_s \boldsymbol{\mu}^T \partial_s \boldsymbol{\mu} \, dA + \\ & - \int_A n \left(\mathbf{C}_{11}^{(M)} \partial_{ss} \boldsymbol{\psi}^T \partial_s \boldsymbol{\mu} + \mathbf{C}_{11}^{(B)} \partial_s \boldsymbol{\mu}^T \partial_{ss} \boldsymbol{\psi} \right) \, dA, \end{aligned} \quad (\text{A.1})$$

$$\mathbf{C}_{SM} = \int_A n^2 \mathbf{C}_{12}^{(B)} \partial_{ss} \boldsymbol{\psi}^T \boldsymbol{\psi} \, dA - \int_A n \mathbf{C}_{12}^{(B)} \partial_s \boldsymbol{\mu}^T \boldsymbol{\psi} \, dA, \quad (\text{A.2})$$

$$\begin{aligned} \mathbf{C}_M = & \int_A n^2 \mathbf{C}_{22}^{(B)} \boldsymbol{\psi}^T \boldsymbol{\psi} \, dA + \int_A \mathbf{C}_{22}^{(M)} \boldsymbol{\varphi}^T \boldsymbol{\varphi} \, dA + \\ & - \int_A n \left(\mathbf{C}_{22}^{(B)} \boldsymbol{\varphi}^T \boldsymbol{\psi} + \mathbf{C}_{22}^{(M)} \boldsymbol{\psi}^T \boldsymbol{\varphi} \right) \, dA, \end{aligned} \quad (\text{A.3})$$

$$\begin{aligned} \mathbf{C}_T = & \int_A 4n^2 \mathbf{C}_{33}^{(B)} \partial_s \boldsymbol{\psi}^T \partial_s \boldsymbol{\psi} \, dA + \\ & + \int_A \left(\mathbf{C}_{33}^{(M)} \boldsymbol{\mu}^T \boldsymbol{\mu} + \mathbf{C}_{33}^{(M)} \partial_s \boldsymbol{\varphi}^T \boldsymbol{\mu} + \right. \\ & + \mathbf{C}_{33}^{(M)} \boldsymbol{\mu}^T \partial_s \boldsymbol{\varphi} + \mathbf{C}_{33}^{(M)} \partial_s \boldsymbol{\varphi}^T \partial_s \boldsymbol{\varphi} \left. \right) \, dA + \\ & - \int_A 2n \left(\mathbf{C}_{33}^{(B)} \boldsymbol{\mu}^T \partial_s \boldsymbol{\psi} + \mathbf{C}_{33}^{(B)} \partial_s \boldsymbol{\varphi}^T \partial_s \boldsymbol{\psi} + \right. \\ & + \mathbf{C}_{33}^{(M)} \partial_s \boldsymbol{\psi}^T \boldsymbol{\mu} + \mathbf{C}_{33}^{(M)} \partial_s \boldsymbol{\psi}^T \partial_s \boldsymbol{\varphi} \left. \right) \, dA, \end{aligned} \quad (\text{A.4})$$

$$\begin{aligned} \mathbf{C}_{TV} = & \int_A \frac{1}{2} \left(\mathbf{C}_{33}^{(M)} \partial_s \boldsymbol{\varphi}^T \boldsymbol{\mu} - \mathbf{C}_{33}^{(M)} \partial_s \boldsymbol{\varphi}^T \partial_s \boldsymbol{\varphi} + \right. \\ & + \mathbf{C}_{33}^{(M)} \boldsymbol{\mu}^T \boldsymbol{\mu} - \mathbf{C}_{33}^{(M)} \boldsymbol{\mu}^T \partial_s \boldsymbol{\varphi} \left. \right) \, dA + \\ & + \int_A n \left(\mathbf{C}_{33}^{(M)} \partial_s \boldsymbol{\psi}^T \partial_s \boldsymbol{\varphi} - \mathbf{C}_{33}^{(M)} \partial_s \boldsymbol{\psi}^T \boldsymbol{\mu} \right) \, dA, \end{aligned} \quad (\text{A.5})$$

$$\begin{aligned} \mathbf{C}_V = & \int_A \frac{1}{4} \left(\mathbf{C}_{33}^{(M)} \boldsymbol{\mu}^T \boldsymbol{\mu} - \mathbf{C}_{33}^{(M)} \boldsymbol{\mu}^T \partial_s \boldsymbol{\varphi} + \right. \\ & - \mathbf{C}_{33}^{(M)} \partial_s \boldsymbol{\varphi}^T \boldsymbol{\mu} + \mathbf{C}_{33}^{(M)} \partial_s \boldsymbol{\varphi}^T \partial_s \boldsymbol{\varphi} \left. \right) \, dA + \\ & + \int_A \mathbf{C}_{44}^{(M)} \boldsymbol{\psi}^T \boldsymbol{\psi} \, dA. \end{aligned} \quad (\text{A.6})$$

A.2 GENERAL FORM FOR THE CROSS-SECTION STIFFNESS MATRIX

In the most general case, whenever the cross-section m deformation modes are used, $(\psi_1, \varphi_1, \mu_1) \dots (\psi_m, \varphi_m, \mu_m)$, the cross-section stiffness matrix can be defined by the expression 3.13. It is nonetheless instructive looking at the expression of the cross-section stiffness matrix in the hypothetical case when only two deformation modes $(\psi_i, \varphi_i, \mu_i), (\psi_j, \varphi_j, \mu_j)$ discretize a cross-section made only by 1 wall with thickness t and length l_w . This simplification avoid introducing some summations and lightens the text, without any loss of generality.

Let the cross-section stiffness matrix be formed by the submatrices of equation 3.14, which are rewritten explicitly hereinafter for the membrane:

$$\mathbf{C}_S = \begin{bmatrix} c_S^{ii} & c_S^{ij} \\ c_S^{ji} & c_S^{jj} \end{bmatrix}, \quad \mathbf{C}_M = \begin{bmatrix} c_M^{ii} & c_M^{ij} \\ c_M^{ji} & c_M^{jj} \end{bmatrix}, \quad \mathbf{C}_{SM} = \begin{bmatrix} c_{SM}^{ii} & c_{SM}^{ij} \\ c_{SM}^{ji} & c_{SM}^{jj} \end{bmatrix}, \quad (\text{A.7})$$

and bending part,

$$\mathbf{C}_T = \begin{bmatrix} c_T^{ii} & c_T^{ij} \\ c_T^{ji} & c_T^{jj} \end{bmatrix}, \quad \mathbf{C}_V = \begin{bmatrix} c_V^{ii} & c_V^{ij} \\ c_V^{ji} & c_V^{jj} \end{bmatrix}, \quad \mathbf{C}_{TV} = \begin{bmatrix} c_{TV}^{ii} & c_{TV}^{ij} \\ c_{TV}^{ji} & c_{TV}^{jj} \end{bmatrix}, \quad (\text{A.8})$$

where:

$$\begin{aligned} c_S^{ij} &= \frac{1}{12} \int_0^{l_w} Et (\partial_{ss} \psi_i \partial_{ss} \psi_j t^2 + 12 (\partial_s \mu_i) \partial_s \mu_j) ds \\ c_{SM}^{ij} &= \frac{1}{12} v \bar{E} t^3 \int_0^{l_w} (\partial_{ss} \psi_i) \psi_j ds \\ c_M^{ij} &= \frac{1}{12} \int_0^{l_w} Et (t^2 \psi_i \psi_j + 12 \varphi_i \varphi_j) ds \\ c_T^{ij} &= \frac{1}{3} \int_0^{l_w} 3 t G \left((\partial_s \varphi_j + \mu_j) \partial_s \varphi_i + \frac{1}{3} (\partial_s \psi_i) (\partial_s \psi_j) t^2 + \mu_i \partial_s \varphi_j + \mu_i \mu_j \right) ds \\ c_{TV}^{ij} &= \frac{1}{2} G t \int_0^{l_w} (\partial_s \varphi_i + \mu_i) (\mu_j - \partial_s \varphi_j) ds \\ c_V^{ij} &= \frac{1}{4} \int_0^{l_w} t \left((\partial_s \varphi_j - \mu_j) \partial_s \varphi_i - \mu_i \partial_s \varphi_j + \mu_i \mu_j + 4 \psi_i \psi_j \right) G ds. \end{aligned} \quad (\text{A.9})$$

Consider that the generic term c_*^{jj} can be obtained by the corresponding c_*^{ii} simply by a proper substitution of the indexes in the relevant integral. The provided expressions exemplify the high coupling across GBT modes in the natural base. The pictorial view a cross-section stiffness matrix in the natural and modal space is provided in figure for a C-shaped cross-section 3.2. Moreover, notice that the expressions in this paragraph are valid for generic form of the modes ζ, θ, ψ .

A.3 MODAL DECOMPOSITION

It has been discussed that the submatrices of C are in full, in the most general case. This fact determines high coupling among different generalized stresses and deformations, rendering the final governing equations difficult to be solved and to interpret.

The mechanical meaning of the equation coefficients cannot be referred to standard quantities, since the arbitrary kinematic hypothesis do not reflect any standard beam kinematic field.

The fundamental process in the GBT theory is the modal decomposition: the objective is to express the governing equations in a more appropriate base through a generalized eigenvalue problem that diagonalizes the cross-section stiffness matrix allowing not only for a partial uncoupling of the equations. The generalized displacements in the diagonalized base will turn to be the one of a standard beam theory. Let $\delta[z]$ be the generalized displacements as expressed in the modal space, and $\hat{\delta}[z]$ the ones in the natural one, then the matrix Λ allows for the base change:

$$\delta[z] = \Lambda \hat{\delta}[z].$$

The matrix Λ is defined so that the modal space is meaningful. For fundamental flexural modes, the following generalized eigenvalue problem provides the change of basis:

$$(C_S - \lambda_i C_M) \Lambda_i = \mathbf{0},$$

where Λ_i are the columns of Λ . It is worth to notice that, whichever the shape of the cross-section, fundamental modes will be associated to 4 null eigenvalues, physically representing a generic combination of the cross-section rigid body motion: out of plane translation, rotations about principal inertial axes, torsional rotation. Correspondingly, the matrix Λ can be split into two parts, where Λ_R identifies the part associated to null eigenvalues:

$$\Lambda = [\Lambda_R \quad \Lambda_F].$$

The identification of Λ_R can be carried out automatically according to standard procedures, as showed in [50].

Moreover, it is interesting to notice that the terms on the diagonal of the cross-section stiffness matrices expressed in the modal space are:

$$\{C_S\}_{ii} = \bar{E} \left(\int_A n^2 \partial_{ss} \psi_i dA \right), \quad \{C_M\}_{ii} = E \left(\int_A \omega_i^2 dA \right).$$

To provide a pictorial view of fundamental GBT modes in the modal space, reference can be made to figure 3.3 showing the mode in a 3D view for a C-shaped cross-section.

A.4 SELF-EQUILIBRATED INTERPOLATIONS FOR GENERALIZED STRESSES

One of the advantages of finite elements based on mixed stress interpolations is the possibility of providing an appropriate discrete space for the stress field which, satisfying the equilibrium equation pointwise optimizes performance and the number of degrees of freedom needed for the solution.

The homogeneous equilibrium equations in term of generalized stresses can be written by expanding equation 3.10:

$$\begin{aligned} S - \frac{1}{2}\partial_z T - \partial_z V &= \mathbf{0}, \\ \partial_z M + \frac{1}{2}T - V &= \mathbf{0}. \end{aligned} \quad (\text{A.10})$$

When dealing with GBT formulations, care must be taken to correctly locate the a-priori null generalized stresses for each class of modes. For sake of clarity, without loss of generality, refer to Fig. 3.3 for a C-shaped cross-section.

It is to be noticed in particular that, after the diagonalization of GBT modes, being s_n the vector of generalized stresses associated to the n -th GBT deformation mode:

$$s_i^T = \left[S_i \quad M_i \quad T_i \quad V_i \right],$$

a few basic elastokinematic observations can be performed for fundamental flexural modes for the stress resultants:

- the components S_1, S_2, S_3, S_4 are null
- T_1, T_2, T_3 are null
- V_1 is null

hence self-equilibrated, complete interpolation up to the third order polynomial for the first 4 modes can be synthetically written in matrix form as:

$$\begin{bmatrix} M_1 \\ M_2 \\ M_3 \\ M_4 \\ T_4 \\ V_2 \\ V_3 \\ V_4 \end{bmatrix} = \begin{bmatrix} 1 & 0 & 0 & 0 & 0 & 0 & 0 & 0 & 0 & 0 \\ 0 & 1 & -z & 0 & 0 & 0 & 0 & 0 & 0 & 0 \\ 0 & 0 & 0 & 1 & -z & 0 & 0 & 0 & 0 & 0 \\ 0 & 0 & 0 & 0 & 0 & 1 & z/2 & -z & -z^2 & -2/3 z^3 \\ 0 & 0 & 0 & 0 & 0 & 0 & 1 & -2z & -2z^2 & 0 \\ 0 & 0 & 1 & 0 & 0 & 0 & 0 & 0 & 0 & 0 \\ 0 & 0 & 0 & 0 & 1 & 0 & 0 & 0 & 0 & 0 \\ 0 & 0 & 0 & 0 & 0 & 0 & 0 & 1 & z & z^2 \end{bmatrix} \boldsymbol{\beta}_f, \quad (\text{A.11})$$

where $\boldsymbol{\beta}_f$ is the vector collecting the 8 interpolation parameters for the 4 fundamental [GBT](#) modes.

On the contrary, higher order modes as wall extension, local and distortional ones exhibit non-null generalized stresses, consequently the relevant interpolation is, for the given local or distortional or extension mode i :

$$\begin{bmatrix} S_i \\ M_i \\ T_i \\ V_i \end{bmatrix} = \begin{bmatrix} 6z & 2 & 0 & 0 & 6z^2 & 4z & 2 & 0 \\ z^3 & z^2 & z & 1 & 0 & 0 & 0 & 0 \\ 6z^2 & 4z & 2 & 0 & 2z^3 & 2z^2 & 2z & 2 \\ 0 & 0 & 0 & 0 & z^3 & z^2 & z & 1 \end{bmatrix} \boldsymbol{\beta}_i \quad (\text{A.12})$$

and the equilibrium may be readily checked by plugging the terms into equation [A.10](#).

SELECTED EXAMPLES FOR GA AND TA APPROACHES

To better illustrate the analysis results of the comparison among GA and TA approaches, some boards are presented in subsequent pages for selected examples subjected to the most critical load combination alt ULS, which is the one that generates the maximum fibre stress 4.1. Boards are chosen to be representative of the investigated population of examples, encompassing different boundary and load conditions and showing the detail on how the hypotheses described in 4.1 are reflected onto the stress check. The boards are made of:

- a structural scheme on top, that shows the acting load direction and intensity (the lengths of the bays is reported at scale).
- A left hand side, named “FE ANALYSIS”, that includes the diagram of v, w, θ , the generalized displacements associated to the centroid of the Z-section (see Fig. B.1) and the moment diagrams M_v, M_w, M_θ . For this section quantitative differences have essentially to be attributed to the different underlying numerical model,
- A right hand side, named “Stress Check”, that shows the axial fibre stress σ_{zz} over the cross section when adopting the hypotheses of the GA and TA approaches to the verification. The place where the maximum occurs is reported on the graph by a marker and distribution of stresses showed onto the cross section.

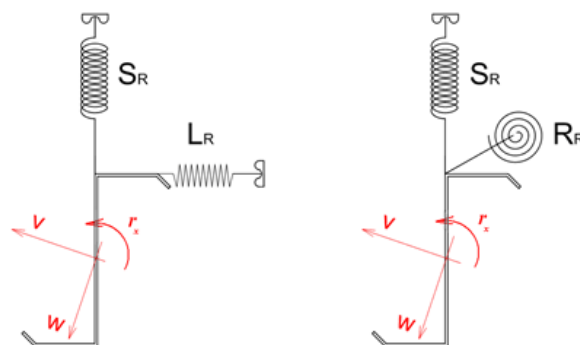
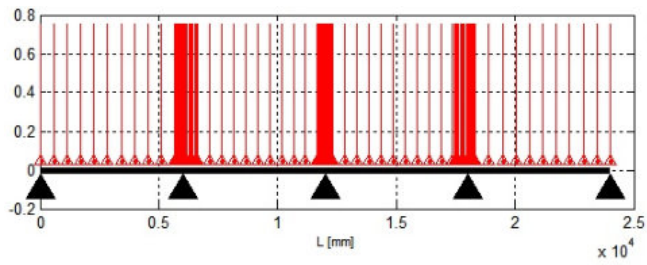


Figure B.1: Sketch of Z-sections analyzed and relevant elastic restraints: on the left hand side shear restraint and lateral one, on the right hand side shear and rotational restraints.

Moreover, since the for the [SLS](#) the verification process does not involve stress calculation and only pertains the beam models used, no board has been reported for [SLS](#) load cases.

EXAMPLE ID: 3

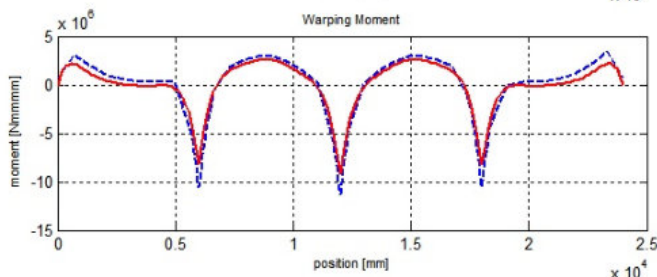
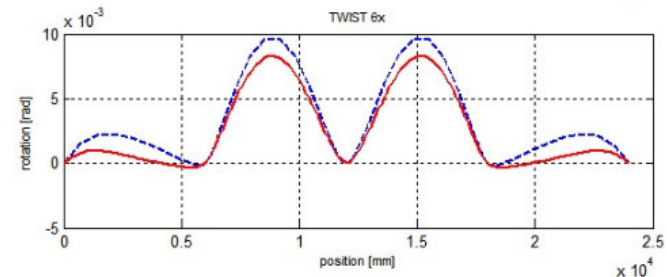
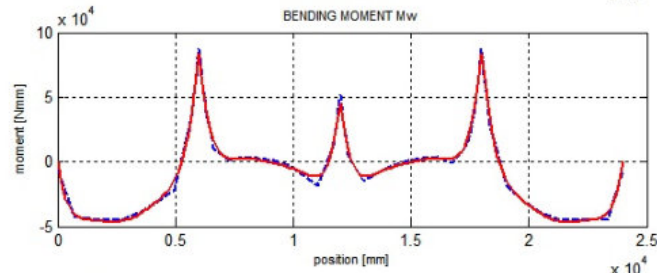
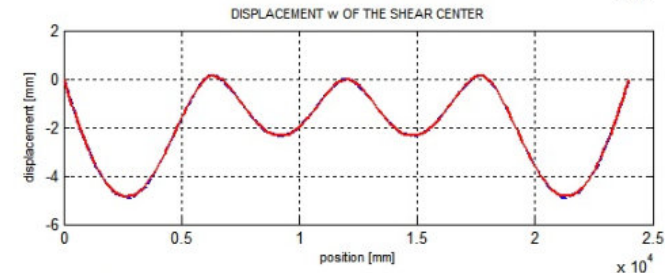
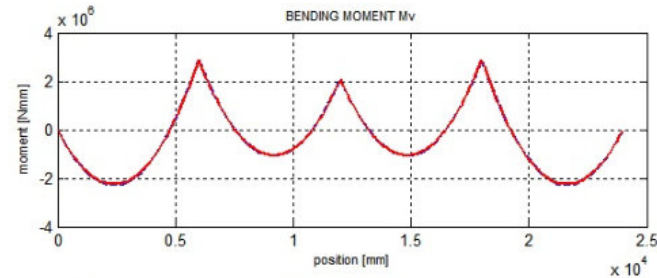
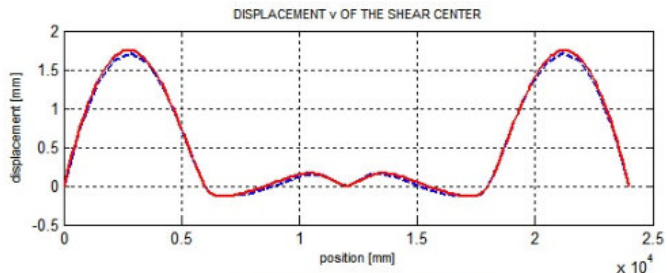


F.E. ANALYSIS

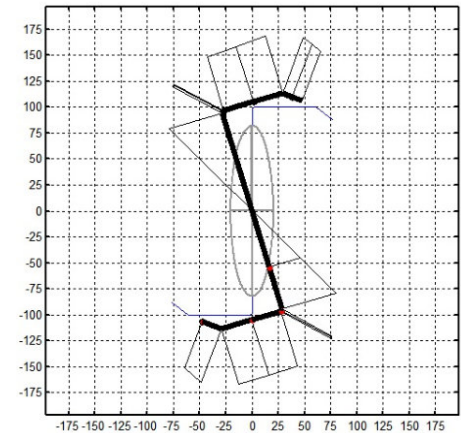
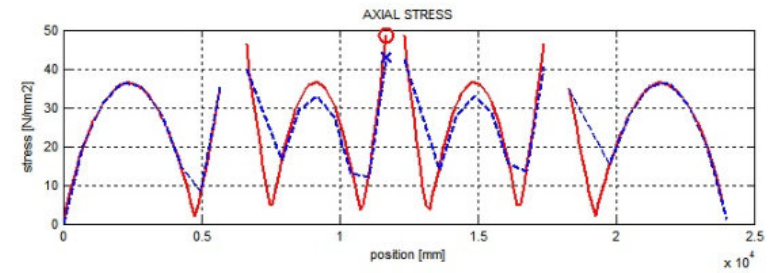
II order analysis
 Cross-section h: 200 [mm]
 Elastic restraints:
 SHEAR : N
 LATERAL : Y
 ROTATIONAL : N
 Load Combination: ULS2

LEGEND:

GBT ---
 Vlasov ---

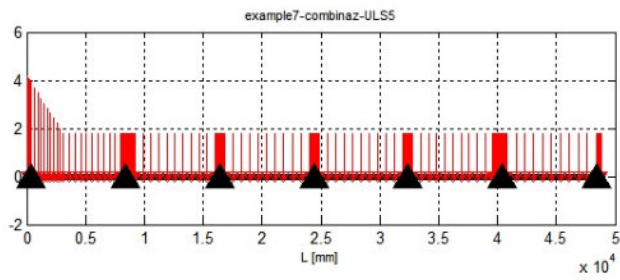


STRESS CHECK



Stress distribution over the cross-section (GA approach)

EXAMPLE ID: 7

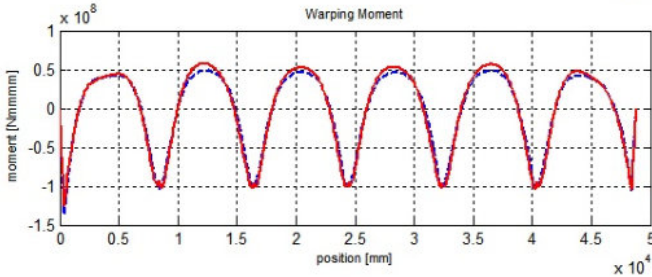
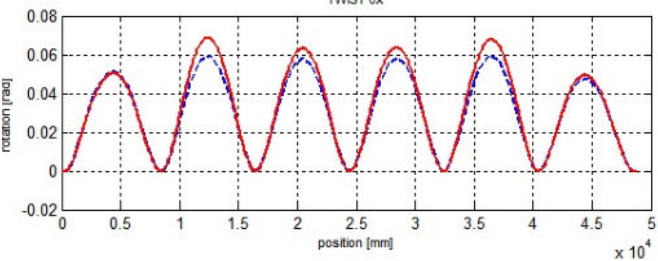
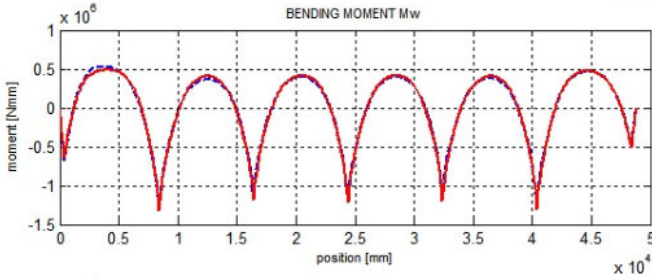
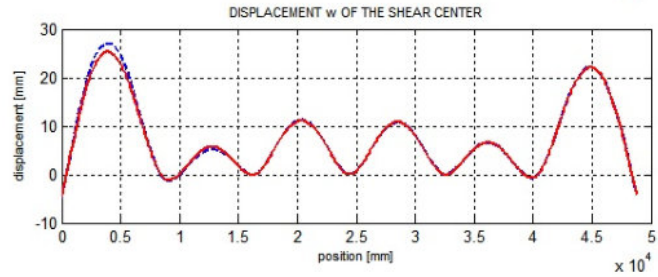
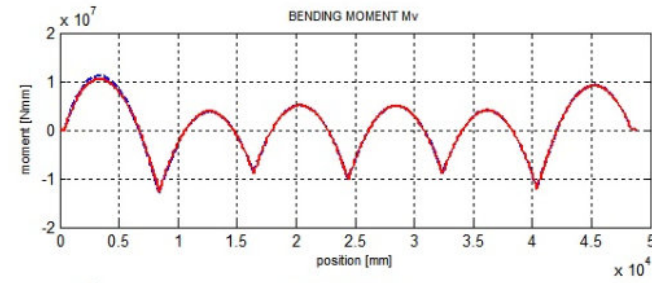
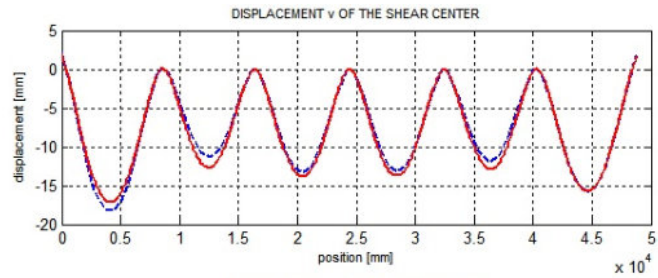


F.E. ANALYSIS

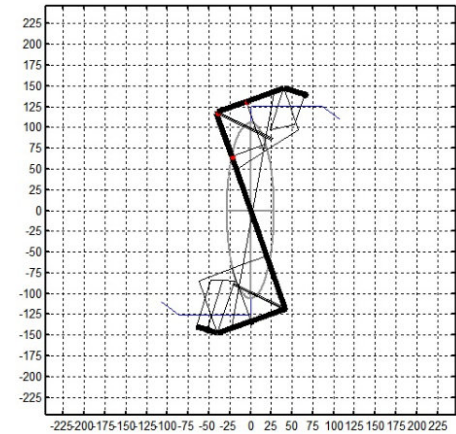
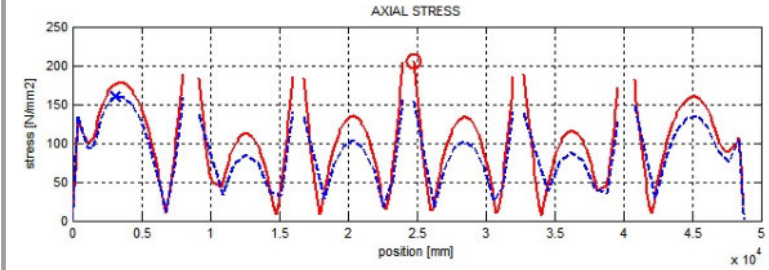
II order analysis
 Cross-section h: 200 [mm]
 Elastic restraints:
 SHEAR : Y
 LATERAL : N
 ROTATIONAL : Y
 Load Combination: ULS5

LEGEND:

GBT ---
 Vlasov —

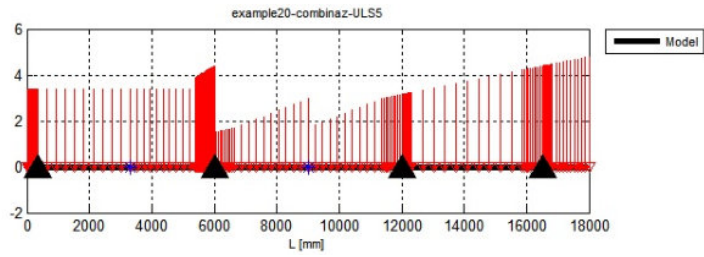


STRESS CHECK



Stress distribution over the cross-section (GA approach)

EXAMPLE ID: 20

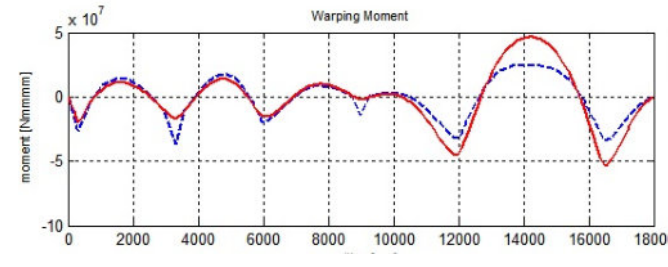
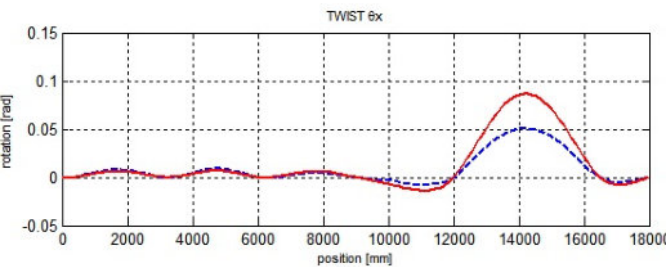
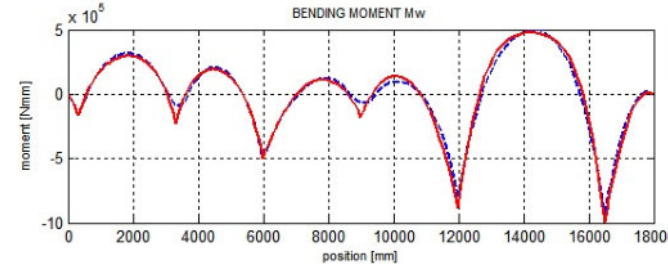
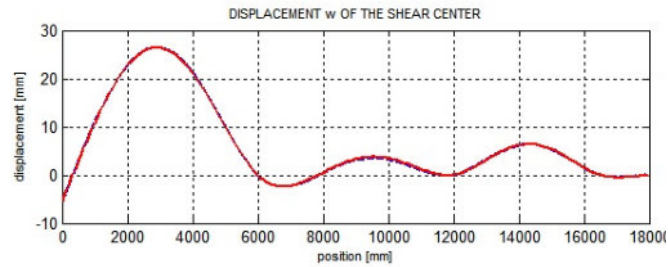
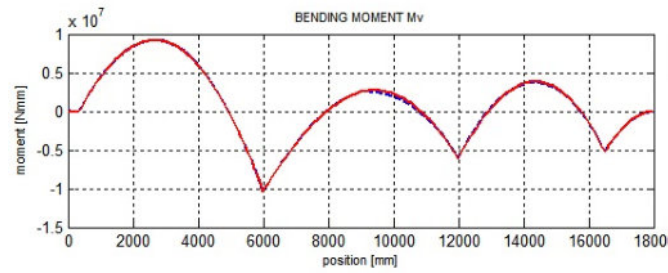
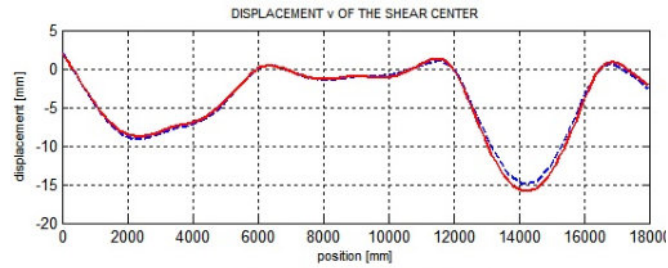


F.E. ANALYSIS

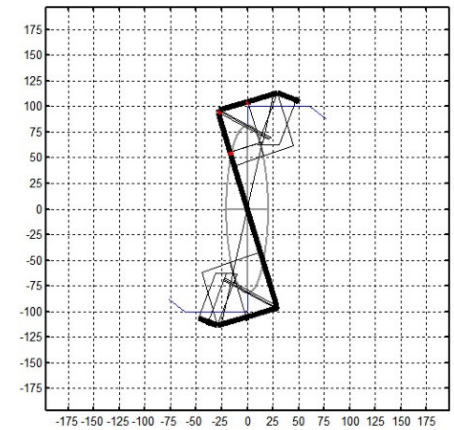
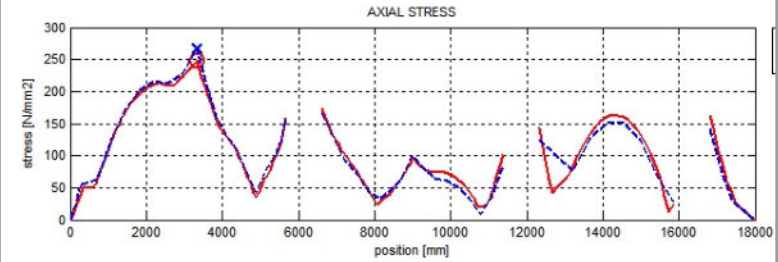
II order analysis
 Cross-section h: 200 [mm]
 Elastic restraints:
 SHEAR : Y
 LATERAL : N
 ROTATIONAL : Y
 Load Combination: ULS5

LEGEND:

GBT ---
 Vlasov ---

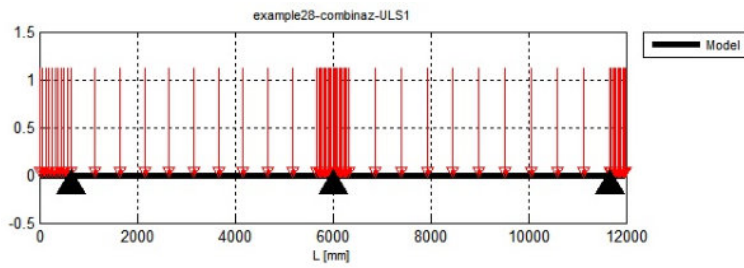


STRESS CHECK



Stress distribution over the cross-section (GA approach)

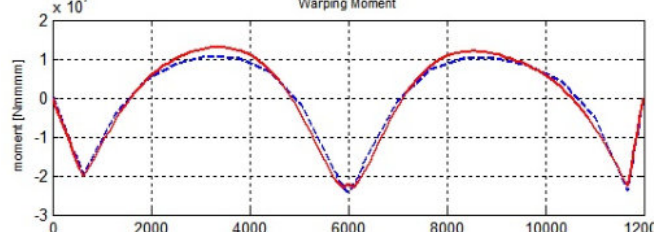
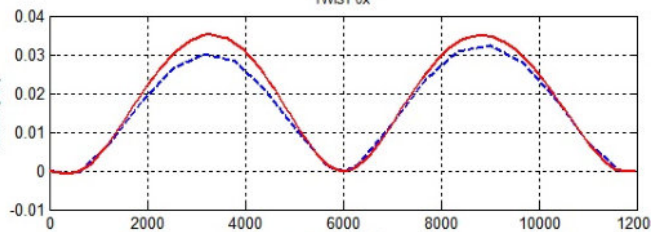
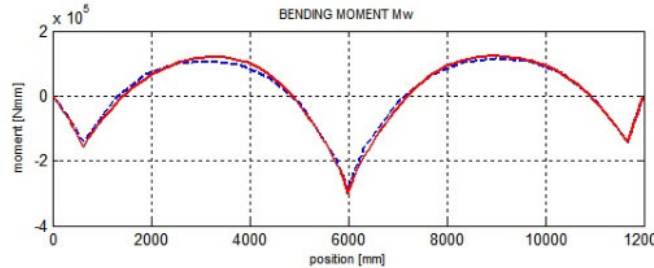
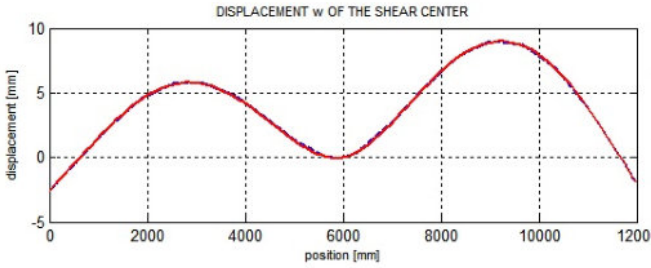
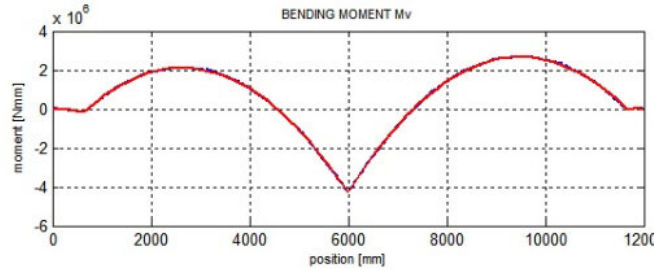
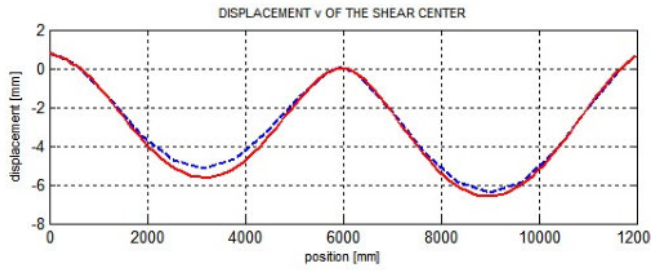
EXAMPLE ID: 28



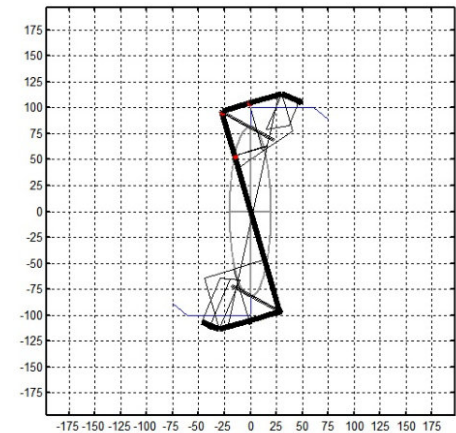
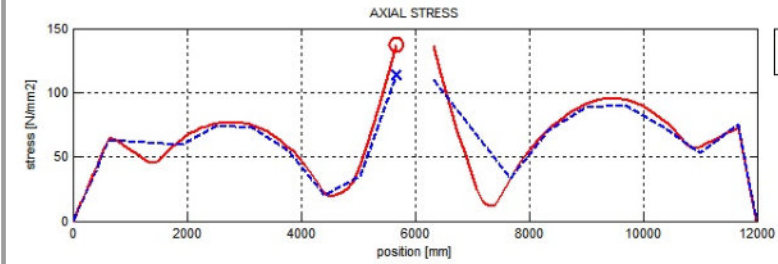
F.E. ANALYSIS

II order analysis
 Cross-section h: 200 [mm]
 Elastic restraints:
 SHEAR : Y
 LATERAL : N
 ROTATIONAL : Y
 Load Combination: ULS1

LEGEND:
 GBT ----
 Vlasov —

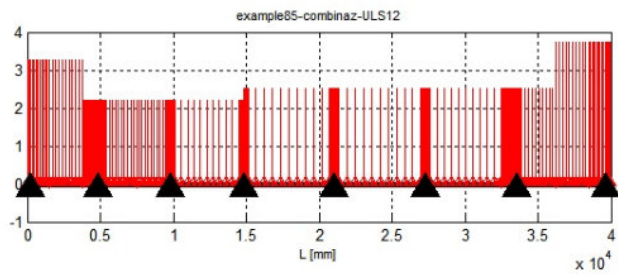


STRESS CHECK



Stress distribution over the cross-section (GA approach)

EXAMPLE ID: 85

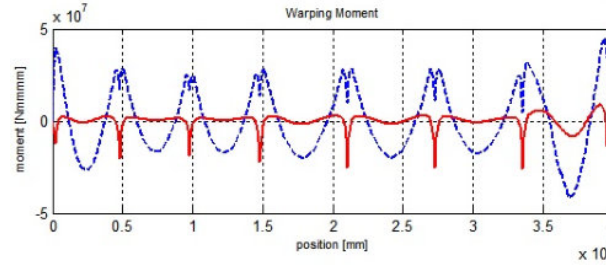
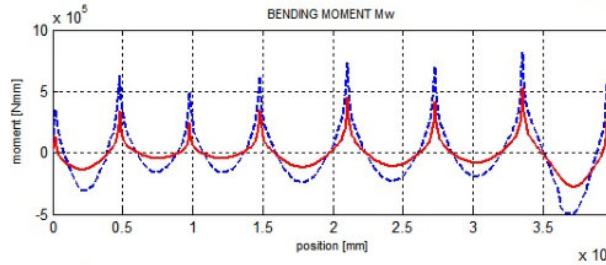
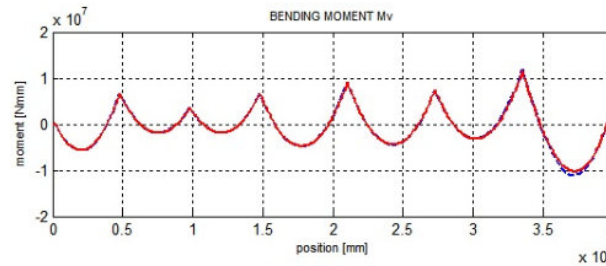
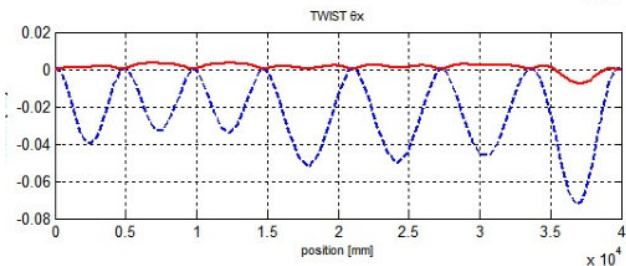
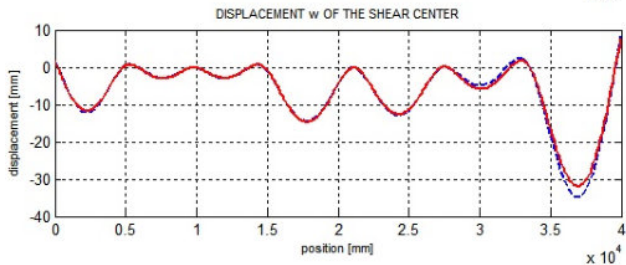
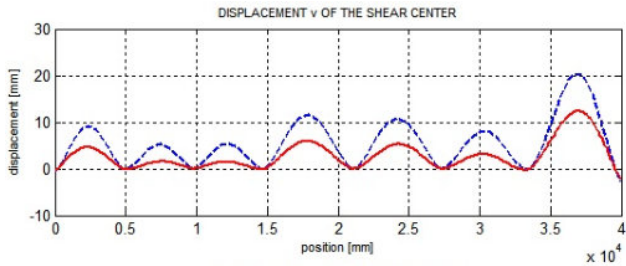


F.E. ANALYSIS

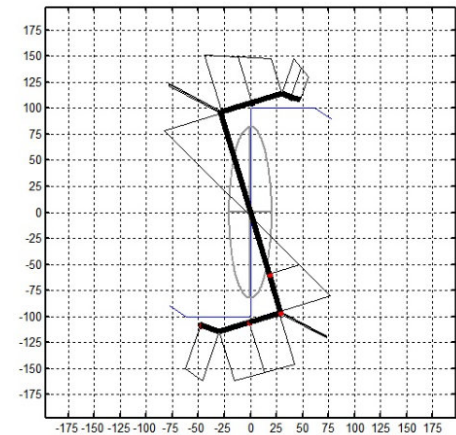
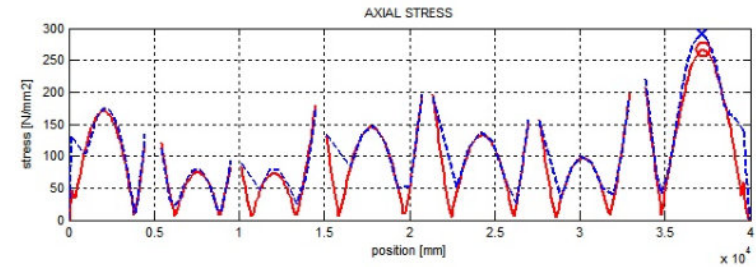
II order analysis
 Cross-section h: 200 [mm]
 Elastic restraints:
 SHEAR : Y
 LATERAL : N
 ROTATIONAL : Y
 Load Combination: ULS2

LEGEND:

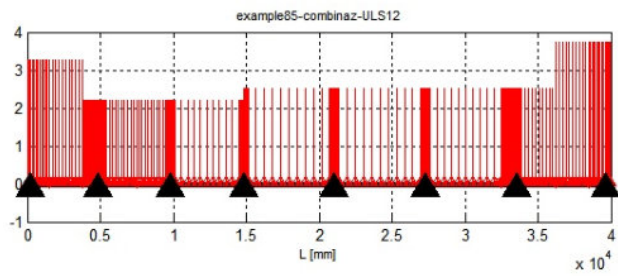
GBT ----
 Vlasov —



STRESS CHECK



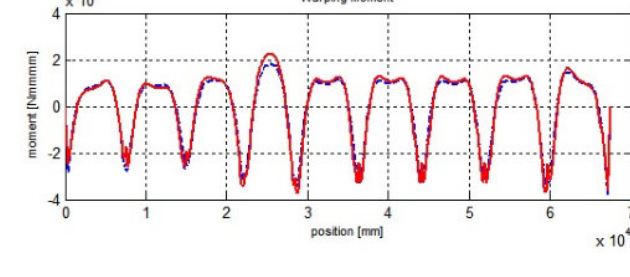
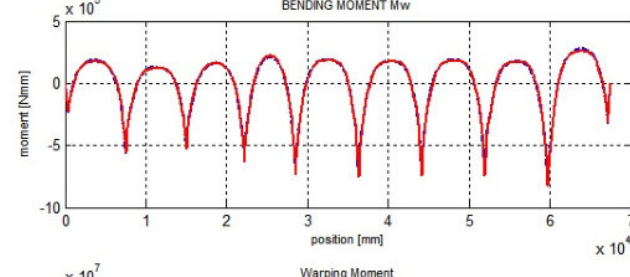
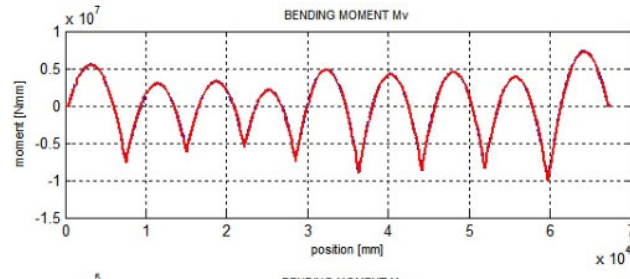
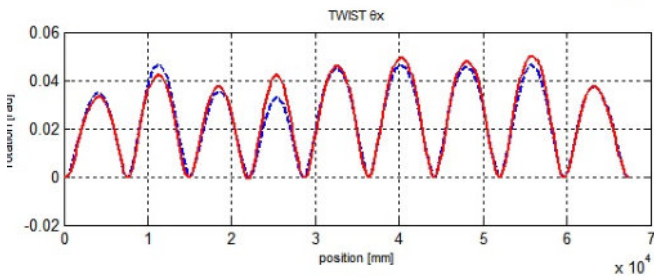
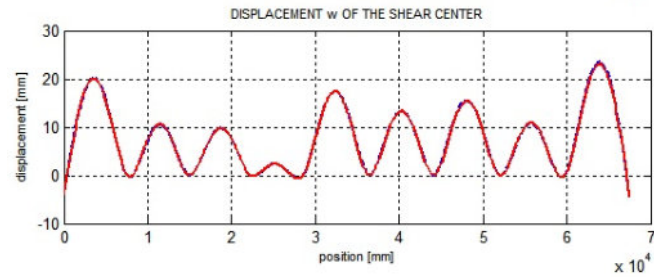
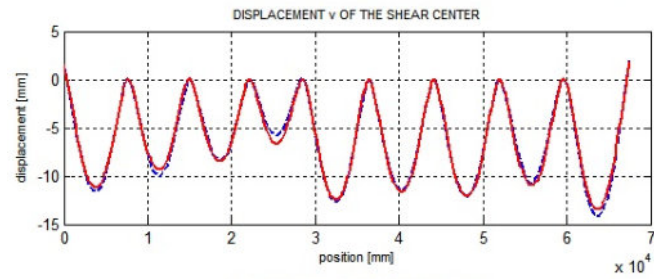
Stress distribution over the cross-section (GA approach)



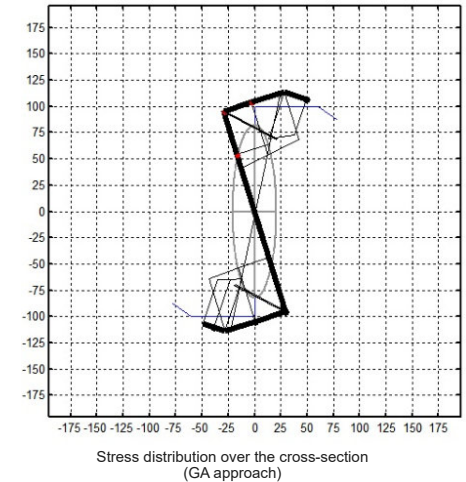
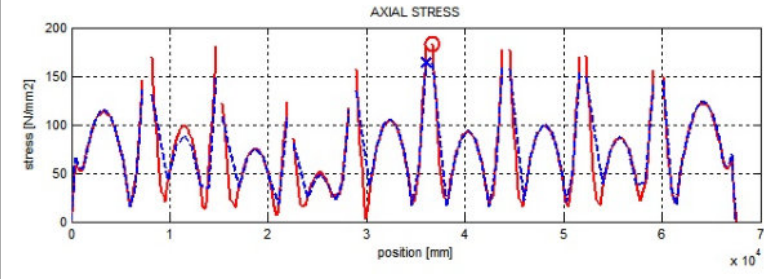
F.E. ANALYSIS

II order analysis
 Cross-section h: 200 [mm]
 Elastic restraints:
 SHEAR : Y
 LATERAL : N
 ROTATIONAL : Y
 Load Combination: ULS1

LEGEND:
 GBT ----
 Vlasov —



STRESS CHECK



SECOND ORDER STRAINS IN TERMS OF GBT MODES

This Appendix includes the expressions for the Biot strains in terms of generalized GBT parameters $\delta^T = \begin{bmatrix} v^T & w^T \end{bmatrix}$. Considering the non-null components of the three-dimensional linear stresses σ_l , only the corresponding Biot strain components, i.e. those relevant for the mixed strain energy evaluation, are considered: $\rho_l = [q_{l,ss}, q_{l,zz}, q_{l,sz}, q_{l,nz}]^T$. Following the same scheme of linear strains, these strains components are written by separating the membrane and bending contributions as follows:

$$\begin{aligned} q_{l,ss}[n, s, z] &= q_{l,ss}^{(M)}[s, z] + q_{l,ss}^{(B)}[n, s, z], \\ q_{l,zz}[n, s, z] &= q_{l,zz}^{(M)}[s, z] + q_{l,zz}^{(B)}[n, s, z], \\ q_{l,zs}[n, s, z] &= q_{l,zs}^{(M)}[s, z] + q_{l,zs}^{(B)}[n, s, z], \\ q_{l,zn}[s, z] &= q_{l,zn}^{(M)}[s, z], \end{aligned}$$

where

$$\begin{aligned} q_{l,ss}^{(M)} &= \frac{1}{2}v^T \partial_s \psi^T \partial_s \psi v + \frac{3}{8}w^T \partial_s \varphi^T \partial_s \varphi w - \frac{1}{4}w^T \partial_s \varphi^T \mu \partial_z v - \frac{1}{8} \partial_z v^T \mu^T \mu \partial_z v, \\ q_{l,zz}^{(M)} &= \frac{3}{8} \partial_z v^T \mu^T \mu \partial_z v - \frac{1}{4}w^T \partial_s \varphi^T \mu \partial_z v - \frac{1}{8}w^T \partial_s \varphi^T \partial_s \varphi w + \frac{3}{8} \partial_z v^T \psi^T \psi \partial_z v \\ &\quad + \frac{1}{4}w^T \psi^T \psi \partial_z v - \frac{1}{8}w^T \psi^T \psi w, \\ q_{l,zs}^{(M)} &= \frac{1}{2}v^T \partial_s \mu^T \mu \partial_z v - \frac{1}{2}v^T \partial_s \mu^T \partial_s \varphi w + v^T \partial_s \psi^T \psi \partial_z v - \frac{1}{2} \partial_z v^T \mu^T \varphi \partial_z w \\ &\quad + \frac{1}{2}w^T \partial_s \varphi^T \varphi \partial_z w, \\ q_{l,zn}^{(M)} &= -v^T \partial_s \psi^T \mu \partial_z v - \frac{1}{2} \partial_z w^T \varphi^T \psi \partial_z v - \frac{1}{2} \partial_z w^T \varphi^T \psi w, \end{aligned}$$

and

$$\begin{aligned}
\varrho_{l,ss}^{(B)} &= \frac{3}{8}n^2w^T\partial_s\psi^T\partial_s\psi w - \frac{3}{4}nw^T\partial_s\psi^T\partial_s\varphi w - \frac{1}{4}n^2w^T\partial_s\psi^T\partial_s\psi\partial_z v \\
&\quad + \frac{1}{4}nw^T\psi^T\mu\partial_z v + \frac{1}{4}nw^T\partial_s\varphi^T\partial_s\psi\partial_z v - \frac{1}{8}n^2\partial_z v^T\partial_s\psi^T\partial_s\psi\partial_z v \\
&\quad + \frac{1}{4}n\partial_z v^T\partial_s\psi^T\mu\partial_z v, \\
\varrho_{l,zz}^{(B)} &= \frac{1}{4}n\partial_z v^T\partial_z\psi^T\partial_s\varphi w + \frac{1}{4}nw^T\partial_s\psi^T\partial_s\varphi w - \frac{3}{4}n\partial_z v^T\partial_s\psi^T\mu\partial_z v \\
&\quad + \frac{1}{4}nw^T\partial_s\psi^T\mu\partial_z v + \frac{3}{8}n^2\partial_z v^T\partial_s\psi^T\partial_s\psi\partial_z v - \frac{1}{4}n^2w^T\partial_s\psi^T\partial_s\psi\partial_z v \\
&\quad - \frac{1}{8}n^2w^T\partial_s\psi^T\partial_s\psi w, \\
\varrho_{l,zs}^{(B)} &= \frac{1}{2}n^2v^T\partial_{ss}\psi^T\partial_s\psi\partial_z v - \frac{1}{2}nv^T\partial_s\mu^T\partial_s\psi\partial_z v - \frac{1}{2}nv^T\partial_{ss}\psi^T\mu\partial_z v \\
&\quad + \frac{1}{2}n^2v^T\partial_{ss}\psi^T\partial_s\psi w + \frac{1}{2}nv^T\partial_s\mu^T\partial_s\psi w + \frac{1}{4}nv^T\partial_{ss}\psi^T\partial_s\varphi w \\
&\quad - \frac{1}{2}n^2\partial_z v^T\partial_s\psi^T\psi\partial_z w + \frac{1}{2}n\partial_z v^T\partial_s\psi^T\varphi\partial_z w + \frac{1}{2}n\partial_z v^T\mu^T\psi\partial_z w \\
&\quad + \frac{1}{2}n^2w^T\partial_s\psi^T\psi\partial_z w - \frac{1}{2}nw^T\partial_s\psi^T\varphi\partial_z w - \frac{1}{2}nw^T\partial_s\varphi^T\psi\partial_z w \\
&\quad - \frac{1}{4}n^2w^T\partial_s\psi^T\partial_{ss}\psi v, \\
\varrho_{l,zn}^{(B)} &= n\partial_z v^T\partial_s\psi^T\partial_s\psi v + \frac{1}{2}n\partial_z w^T\psi^T\psi\partial_z v + \frac{1}{2}n\partial_z w^T\psi^T\psi w.
\end{aligned}$$

The above expressions can be computed to obtain the nonlinear term in the strain energy in eq. 5.6.

ROTATOR APPROXIMATION

The Taylor series expansion in eq. 6.2 is essential to obtain the first energy variation of the corotational transformations g_i which depends on Q_i . The term $V_{i,1}^{(1)}$ was reported at the end of Chapter 5. Higher order terms become increasingly complex, for sake of completeness the term $V_{i,2}^{(1)}$ is here reported. Let

$$\mathbf{V}_i^{(2)} = \begin{bmatrix} V_i^{11} & V_i^{12} & V_i^{13} \\ V_i^{21} & V_i^{22} & V_i^{23} \\ V_i^{31} & V_i^{32} & V_i^{33} \end{bmatrix},$$

its components are:

$$\begin{aligned} V_i^{11} = & -\frac{1}{8L_p^2 L^2} \left[L_p^2 \check{d}_{Ax}^2 + 2L_p^2 \check{d}_{Ax} \check{d}_{Bx} - 2L_p^2 \check{d}_{Ax} \check{d}_{Cx} - 2L_p^2 \check{d}_{Ax} \check{d}_{Dx} \right. \\ & + L_p^2 \check{d}_{Bx}^2 - 2L_p^2 \check{d}_{Bx} \check{d}_{Cx} - 2L_p^2 \check{d}_{Bx} \check{d}_{Dx} + L_p^2 \check{d}_{Cx}^2 + 2L_p^2 \check{d}_{Cx} \check{d}_{Dx} \\ & + L_p^2 \check{d}_{Dx}^2 + L^2 \check{d}_{Ay}^2 - 2L^2 \check{d}_{Ay} \check{d}_{By} - 2L^2 \check{d}_{Ay} \check{d}_{Cy} + 2L^2 \check{d}_{Ay} \check{d}_{Dy} + L^2 \check{d}_{By}^2 \\ & \left. + 2L^2 \check{d}_{By} \check{d}_{Cy} - 2L^2 \check{d}_{By} \check{d}_{Dy} + L^2 \check{d}_{Cy}^2 - 2L^2 \check{d}_{Cy} \check{d}_{Dy} + L^2 \check{d}_{Dy}^2 \right], \end{aligned}$$

$$\begin{aligned} V_i^{21} = & -\frac{1}{4L_p^2 L^2} \left[L_p^2 \check{d}_{Ax} \check{d}_{Ay} + L_p^2 \check{d}_{Ax} \check{d}_{By} - L_p^2 \check{d}_{Ax} \check{d}_{Cy} - L_p^2 \check{d}_{Ax} \check{d}_{Dy} \right. \\ & + L_p^2 \check{d}_{Ay} \check{d}_{Bx} - L_p^2 \check{d}_{Ay} \check{d}_{Cx} - L_p^2 \check{d}_{Ay} \check{d}_{Dx} + L_p^2 \check{d}_{Bx} \check{d}_{By} - L_p^2 \check{d}_{Bx} \check{d}_{Cy} \\ & - L_p^2 \check{d}_{Bx} \check{d}_{Dy} - L_p^2 \check{d}_{By} \check{d}_{Cx} - L_p^2 \check{d}_{By} \check{d}_{Dx} + L_p^2 \check{d}_{Cx} \check{d}_{Cy} \\ & + L_p^2 \check{d}_{Cx} \check{d}_{Dy} + L_p^2 \check{d}_{Cy} \check{d}_{Dx} + L_p^2 \check{d}_{Dx} \check{d}_{Dy} - L_p L \check{d}_{Ay} \check{d}_{Az} \\ & + L_p L \check{d}_{Ay} \check{d}_{Bz} + L_p L \check{d}_{Ay} \check{d}_{Cz} - L_p L \check{d}_{Ay} \check{d}_{Dz} - L_p L \check{d}_{Az} \check{d}_{By} \\ & + L_p L \check{d}_{Az} \check{d}_{Cy} + L_p L \check{d}_{Az} \check{d}_{Dy} + L_p L \check{d}_{By} \check{d}_{Bz} + L_p L \check{d}_{By} \check{d}_{Cz} \\ & - L_p L \check{d}_{By} \check{d}_{Dz} - L_p L \check{d}_{Bz} \check{d}_{Cy} - L_p L \check{d}_{Bz} \check{d}_{Dy} - L_p L \check{d}_{Cy} \check{d}_{Cz} \\ & + L_p L \check{d}_{Cy} \check{d}_{Dz} - L_p L \check{d}_{Cz} \check{d}_{Dy} + L_p L \check{d}_{Dy} \check{d}_{Dz} + L^2 \check{d}_{Ax} \check{d}_{Ay} \\ & - L^2 \check{d}_{Ax} \check{d}_{By} - L^2 \check{d}_{Ax} \check{d}_{Cy} + L^2 \check{d}_{Ax} \check{d}_{Dy} - L^2 \check{d}_{Ay} \check{d}_{Bx} - L^2 \check{d}_{Ay} \check{d}_{Cx} \\ & + L^2 \check{d}_{Ay} \check{d}_{Dx} + L^2 \check{d}_{Bx} \check{d}_{By} + L^2 \check{d}_{Bx} \check{d}_{Cy} - L^2 \check{d}_{Bx} \check{d}_{Dy} + L^2 \check{d}_{By} \check{d}_{Cx} \\ & \left. - L^2 \check{d}_{By} \check{d}_{Dx} + L^2 \check{d}_{Cx} \check{d}_{Cy} - L^2 \check{d}_{Cx} \check{d}_{Dy} - L^2 \check{d}_{Cy} \check{d}_{Dx} + L^2 \check{d}_{Dx} \check{d}_{Dy} \right], \end{aligned}$$

$$\begin{aligned} V_i^{31} = & \frac{1}{4L^2 L_p} \left[L_p \check{d}_{Ax} \check{d}_{Az} + L_p \check{d}_{Ax} \check{d}_{Bz} - L_p \check{d}_{Ax} \check{d}_{Cz} - L_p \check{d}_{Ax} \check{d}_{Dz} \right. \\ & + L_p \check{d}_{Az} \check{d}_{Bx} - L_p \check{d}_{Az} \check{d}_{Cx} - L_p \check{d}_{Az} \check{d}_{Dx} + L_p \check{d}_{Bx} \check{d}_{Bz} - L_p \check{d}_{Bx} \check{d}_{Cz} \\ & - L_p \check{d}_{Bx} \check{d}_{Dz} - L_p \check{d}_{Bz} \check{d}_{Cx} - L_p \check{d}_{Bz} \check{d}_{Dx} + L_p \check{d}_{Cx} \check{d}_{Cz} + L_p \check{d}_{Cx} \check{d}_{Dz} \\ & + L_p \check{d}_{Cz} \check{d}_{Dx} + L_p \check{d}_{Dx} \check{d}_{Dz} + L \check{d}_{Ay}^2 - 2L \check{d}_{Ay} \check{d}_{Cy} - L \check{d}_{By}^2 \\ & \left. + 2L \check{d}_{By} \check{d}_{Dy} + L \check{d}_{Cy}^2 - L \check{d}_{Dy}^2 \right], \end{aligned}$$

$$\begin{aligned}
V_i^{12} = & -\frac{1}{4L_p^2 L} \left[L_p \check{d}_{Ay} \check{d}_{Az} - L_p \check{d}_{Ay} \check{d}_{Bz} - L_p \check{d}_{Ay} \check{d}_{Cz} + L_p \check{d}_{Ay} \check{d}_{Dz} \right. \\
& + L_p \check{d}_{Az} \check{d}_{By} - L_p \check{d}_{Az} \check{d}_{Cy} - L_p \check{d}_{Az} \check{d}_{Dy} - L_p \check{d}_{By} \check{d}_{Bz} - L_p \check{d}_{By} \check{d}_{Cz} \\
& + L_p \check{d}_{By} \check{d}_{Dz} + L_p \check{d}_{Bz} \check{d}_{Cy} + L_p \check{d}_{Bz} \check{d}_{Dy} + L_p \check{d}_{Cy} \check{d}_{Cz} - L_p \check{d}_{Cy} \check{d}_{Dz} \\
& + L_p \check{d}_{Cz} \check{d}_{Dy} - L_p \check{d}_{Dy} \check{d}_{Dz} - L \check{d}_{Ax} \check{d}_{Ay} + L \check{d}_{Ax} \check{d}_{By} + L \check{d}_{Ax} \check{d}_{Cy} \\
& - L \check{d}_{Ax} \check{d}_{Dy} + L \check{d}_{Ay} \check{d}_{Bx} + L \check{d}_{Ay} \check{d}_{Cx} - L \check{d}_{Ay} \check{d}_{Dx} - L \check{d}_{Bx} \check{d}_{By} \\
& - L \check{d}_{Bx} \check{d}_{Cy} + L \check{d}_{Bx} \check{d}_{Dy} - L \check{d}_{By} \check{d}_{Cx} + L \check{d}_{By} \check{d}_{Dx} - L \check{d}_{Cx} \check{d}_{Cy} \\
& \left. + L \check{d}_{Cx} \check{d}_{Dy} + L \check{d}_{Cy} \check{d}_{Dx} - L \check{d}_{Dx} \check{d}_{Dy} \right],
\end{aligned}$$

$$\begin{aligned}
V_i^{22} = & -\frac{1}{8L_p^2 L^2} \left[L_p^2 \check{d}_{Ay}^2 + 2 L_p^2 \check{d}_{Ay} \check{d}_{By} - 2 L_p^2 \check{d}_{Ay} \check{d}_{Cy} - 2 L_p^2 \check{d}_{Ay} \check{d}_{Dy} \right. \\
& + L_p^2 \check{d}_{By}^2 - 2 L_p^2 \check{d}_{By} \check{d}_{Cy} - 2 L_p^2 \check{d}_{By} \check{d}_{Dy} + L_p^2 \check{d}_{Cy}^2 + 2 L_p^2 \check{d}_{Cy} \check{d}_{Dy} \\
& + L_p^2 \check{d}_{Dy}^2 + L^2 \check{d}_{Ay}^2 - 2 L^2 \check{d}_{Ay} \check{d}_{By} - 2 L^2 \check{d}_{Ay} \check{d}_{Cy} + 2 L^2 \check{d}_{Ay} \check{d}_{Dy} + L^2 \check{d}_{By}^2 \\
& \left. + 2 L^2 \check{d}_{By} \check{d}_{Cy} - 2 L^2 \check{d}_{By} \check{d}_{Dy} + L^2 \check{d}_{Cy}^2 - 2 L^2 \check{d}_{Cy} \check{d}_{Dy} + L^2 \check{d}_{Dy}^2 \right],
\end{aligned}$$

$$\begin{aligned}
V_i^{32} = & \frac{1}{4L^2 L_p} \left[L_p \check{d}_{Ay} \check{d}_{Az} + L_p \check{d}_{Ay} \check{d}_{Bz} - L_p \check{d}_{Ay} \check{d}_{Cz} - L_p \check{d}_{Ay} \check{d}_{Dz} \right. \\
& + L_p \check{d}_{Az} \check{d}_{By} - L_p \check{d}_{Az} \check{d}_{Cy} - L_p \check{d}_{Az} \check{d}_{Dy} + L_p \check{d}_{By} \check{d}_{Bz} - L_p \check{d}_{By} \check{d}_{Cz} \\
& - L_p \check{d}_{By} \check{d}_{Dz} - L_p \check{d}_{Bz} \check{d}_{Cy} - L_p \check{d}_{Bz} \check{d}_{Dy} + L_p \check{d}_{Cy} \check{d}_{Cz} + L_p \check{d}_{Cy} \check{d}_{Dz} \\
& + L_p \check{d}_{Cz} \check{d}_{Dy} + L_p \check{d}_{Dy} \check{d}_{Dz} - L \check{d}_{Ax} \check{d}_{Ay} + L \check{d}_{Ax} \check{d}_{By} + L \check{d}_{Ax} \check{d}_{Cy} \\
& - L \check{d}_{Ax} \check{d}_{Dy} - L \check{d}_{Ay} \check{d}_{Bx} + L \check{d}_{Ay} \check{d}_{Cx} + L \check{d}_{Ay} \check{d}_{Dx} + L \check{d}_{Bx} \check{d}_{By} \\
& + L \check{d}_{Bx} \check{d}_{Cy} - L \check{d}_{Bx} \check{d}_{Dy} - L \check{d}_{By} \check{d}_{Cx} - L \check{d}_{By} \check{d}_{Dx} - L \check{d}_{Cx} \check{d}_{Cy} \\
& \left. + L \check{d}_{Cx} \check{d}_{Dy} - L \check{d}_{Cy} \check{d}_{Dx} + L \check{d}_{Dx} \check{d}_{Dy} \right],
\end{aligned}$$

$$\begin{aligned}
V_i^{13} = & -\frac{1}{4L^2} \left[\check{d}_{Az} \check{d}_{Ax} + \check{d}_{Bz} \check{d}_{Ax} - \check{d}_{Cz} \check{d}_{Ax} - \check{d}_{Dz} \check{d}_{Ax} + \check{d}_{Az} \check{d}_{Bx} - \check{d}_{Az} \check{d}_{Cx} \right. \\
& - \check{d}_{Az} \check{d}_{Dx} + \check{d}_{Bz} \check{d}_{Bx} - \check{d}_{Cz} \check{d}_{Bx} - \check{d}_{Dz} \check{d}_{Bx} - \check{d}_{Bz} \check{d}_{Cx} - \check{d}_{Bz} \check{d}_{Dx} \\
& \left. + \check{d}_{Cz} \check{d}_{Cx} + \check{d}_{Dz} \check{d}_{Cx} + \check{d}_{Cz} \check{d}_{Dx} + \check{d}_{Dz} \check{d}_{Dx} \right],
\end{aligned}$$

$$\begin{aligned}
V_i^{23} = & -\frac{1}{4L^2} \left[\check{d}_{Ay} \check{d}_{Az} + \check{d}_{Ay} \check{d}_{Bz} - \check{d}_{Ay} \check{d}_{Cz} - \check{d}_{Ay} \check{d}_{Dz} + \check{d}_{By} \check{d}_{Az} - \check{d}_{Az} \check{d}_{Cy} \right. \\
& - \check{d}_{Dy} \check{d}_{Az} + \check{d}_{By} \check{d}_{Bz} - \check{d}_{By} \check{d}_{Cz} - \check{d}_{By} \check{d}_{Dz} - \check{d}_{Cy} \check{d}_{Bz} - \check{d}_{Dy} \check{d}_{Bz} \\
& \left. + \check{d}_{Cy} \check{d}_{Cz} + \check{d}_{Cy} \check{d}_{Dz} + \check{d}_{Dy} \check{d}_{Cz} + \check{d}_{Dy} \check{d}_{Dz} \right],
\end{aligned}$$

$$\begin{aligned}
V_i^{33} = & -\frac{1}{8L^2} \left[\check{d}_{Ax}^2 + 2 \check{d}_{Ax} \check{d}_{Bx} - 2 \check{d}_{Cx} \check{d}_{Ax} - 2 \check{d}_{Dx} \check{d}_{Ax} + \check{d}_{Ay}^2 + 2 \check{d}_{Ay} \check{d}_{By} \right. \\
& - 2 \check{d}_{Cy} \check{d}_{Ay} - 2 \check{d}_{Dy} \check{d}_{Ay} + \check{d}_{Bx}^2 - 2 \check{d}_{Cx} \check{d}_{Bx} - 2 \check{d}_{Dx} \check{d}_{Bx} + \check{d}_{By}^2 \\
& - 2 \check{d}_{Cy} \check{d}_{By} - 2 \check{d}_{Dy} \check{d}_{By} + \check{d}_{Cx}^2 + 2 \check{d}_{Cx} \check{d}_{Dx} + \check{d}_{Cy}^2 + 2 \check{d}_{Cy} \check{d}_{Dy} + \check{d}_{Dx}^2 \\
& \left. + \check{d}_{Dy}^2 \right].
\end{aligned}$$

BIBLIOGRAPHY

- [1] Sándor Ádány. “Shell element for constrained finite element analysis of thin-walled structural members.” In: *Thin-Walled Structures* 105.Supplement C (2016), pp. 135–146. DOI: <https://doi.org/10.1016/j.tws.2016.04.012>. URL: <http://www.sciencedirect.com/science/article/pii/S0263823116301598> (cit. on p. 13).
- [2] Sándor Ádány. “Constrained shell Finite Element Method for thin-walled members, Part 1: constraints for a single band of finite elements.” In: *Thin-Walled Structures* (2017). DOI: <https://doi.org/10.1016/j.tws.2017.01.015>. URL: <http://www.sciencedirect.com/science/article/pii/S0263823116307054> (cit. on p. 13).
- [3] Sándor Ádány, Dávid Visy, and Róbert Nagy. “Constrained shell Finite Element Method, Part 2: application to linear buckling analysis of thin-walled members.” In: *Thin-Walled Structures* (2017). DOI: <https://doi.org/10.1016/j.tws.2017.01.022>. URL: <http://www.sciencedirect.com/science/article/pii/S0263823116307066> (cit. on p. 13).
- [4] Michael Joachim Andreassen and Jeppe Jönsson. “A distortional semi-discretized thin-walled beam element.” In: *Thin Walled Struct.* 62 (2013), pp. 142–157 (cit. on p. 10).
- [5] Cilmar Basaglia, Dinar Camotim, Rodrigo Gonçalves, and André Graça. “GBT-based assessment of the buckling behaviour of cold-formed steel purlins restrained by sheeting.” In: *Thin-walled structures* 72 (2013), pp. 217–229 (cit. on p. 30).
- [6] Klaus-Jürgen Bathe, Alexander Iosilevich, and Dominique Chapelle. “An evaluation of the MITC shell elements.” In: *Computers & Structures* 75.1 (2000), pp. 1–30. DOI: [https://doi.org/10.1016/S0045-7949\(99\)00214-X](https://doi.org/10.1016/S0045-7949(99)00214-X). URL: <http://www.sciencedirect.com/science/article/pii/S004579499900214X> (cit. on p. 72).
- [7] R. Bebiano, R. Gonçalves, and D. Camotim. “A cross-section analysis procedure to rationalise and automate the performance of GBT-based structural analyses.” In: *Thin-Walled Structures* 92 (2015), pp. 29–47. DOI: <http://dx.doi.org/10.1016/j.tws.2015.02.017> (cit. on p. 10).
- [8] Rui Bebiano, Dinar Camotim, and Rodrigo Gonçalves. “GBTUL 2.0- A New/Improved Version of the GBT-Based Code for the Buckling Analysis of Cold-Formed Steel Members.” In: *International Specialty Conference on Cold-Formed Steel Structures*

- (2014). URL: <http://scholarsmine.mst.edu/isccss/22iccfss/session01/1> (cit. on p. 10).
- [9] M.A. Biot. *Mechanics of Incremental Deformations*. J Wiley & Sons, New-York, 1995 (cit. on p. 40).
- [10] Marc Braham, Antonio Ruggerini, and Francesco Ubertini. "A numerical model for roof detailing of cold-formed purlin-sheeting systems." In: *Stahlbau* 4 (2008), pp. 238–246 (cit. on pp. 10, 30, 32).
- [11] D Camotim, C Basaglia, and N Silvestre. "GBT buckling analysis of thin-walled steel frames: a state-of-the-art report." In: *Thin Walled Struct.* 48.10 (2010), pp. 726–743 (cit. on p. 10).
- [12] M. Capurso. "Sul calcolo delle travi in parete sottile in presenza di forze e distorsioni." In: *La ricerca scientifica* 6 (1964), pp. 241–286 (cit. on p. 9).
- [13] M. Capurso. "Influenza delle componenti di scorrimento nella deformazione delle travi di parete sottile con sezione aperta." In: *Giornale del Genio Civile* 122 (1984), pp. 127–144 (cit. on p. 9).
- [14] Erasmo Carrera, Maria Cinefra, Marco Petrolo, and Enrico Zappino. *Finite element analysis of structures through unified formulation*. John Wiley & Sons, 2014 (cit. on p. 15).
- [15] Erasmo Carrera, Alfonso Pagani, Marco Petrolo, and Enrico Zappino. "Recent developments on refined theories for beams with applications." In: *Mechanical Engineering Reviews* 2.2 (2015), pp. 14–00298 (cit. on p. 15).
- [16] Y. K. Cheung. "THE FINITE STRIP METHOD IN THE ANALYSIS OF ELASTIC PLATES WITH TWO OPPOSITE SIMPLY SUPPORTED ENDS." In: *Proceedings of the Institution of Civil Engineers* 40.1 (1968), pp. 1–7. DOI: [10.1680/iicep.1968.7709](https://doi.org/10.1680/iicep.1968.7709). eprint: <https://doi.org/10.1680/iicep.1968.7709>. URL: <https://doi.org/10.1680/iicep.1968.7709> (cit. on p. 11).
- [17] Yau Kai Cheung. *Finite strip method in structural analysis*. Elsevier, 2013 (cit. on p. 11).
- [18] A.H. Chilver. "The Stability and Strength of Thin-Walled Steel Struts." In: *The Engineer* (193), pp. 180–183 (cit. on p. 8).
- [19] J.M. Davies and P. Leach. "First-order generalised beam theory." In: *Journal of Constructional Steel Research* 31.2 (1994), pp. 187–220. DOI: [https://doi.org/10.1016/0143-974X\(94\)90010-8](https://doi.org/10.1016/0143-974X(94)90010-8). URL: <http://www.sciencedirect.com/science/article/pii/S0143974X94900108> (cit. on p. 10).
- [20] JM Davies, P Leach, and D Heinz. "Second-order generalised beam theory." In: *J. Constr. Steel Res.* 31.2 (1994), pp. 221–241 (cit. on p. 10).

- [21] T.P. Desmond. “The Behavior and Strength of Thin-Walled Compression Elements with Longitudinal Stiffeners.” PhD thesis. Cornell University., 1977 (cit. on p. 8).
- [22] P Borges Dinis, D Camotim, and N Silvestre. “GBT formulation to analyse the buckling behaviour of thin-walled members with arbitrarily ‘branched’ open cross-sections.” In: *Thin Walled Struct.* 44.1 (2006), pp. 20–38 (cit. on p. 10).
- [23] Dan Dubina. “The ECBL approach for interactive buckling of thin-walled steel members.” In: *Steel and Composite Structures* 1.1 (2001), pp. 75–96 (cit. on p. 6).
- [24] Dan Dubina and Viorel Ungureanu. “Instability mode interaction: from Van Der Neut model to ECBL approach.” In: *Thin Walled Struct.* 81 (2014), pp. 39–49 (cit. on p. 6).
- [25] *EN 1993-1-3:2006 Eurocode 3 - Design of steel structures - Part 1-3: General rules - Supplementary rules for cold-formed members and sheeting.* CEN (cit. on pp. 7, 30, 31).
- [26] *Eurocode 3: Design of Steel Structures, Part 1.3:General Rules.* European Prestandard ENV 1993-1-3. Comité Européen de Normalisation (cit. on p. 8).
- [27] Giovanni Garcea, Antonio Madeo, and Raffaele Casciaro. “Non-linear FEM analysis for beams and plate assemblages based on the implicit corotational method.” In: *J. Mech. Mater. Struct.* 7.6 (2012), pp. 539–574 (cit. on pp. 40, 48, 68, 69).
- [28] Giovanni Garcea, Antonio Madeo, and Raffaele Casciaro. “The implicit corotational method and its use in the derivation of nonlinear structural models for beams and plates.” In: *J. Mech. Mater. Struct.* 7.6 (2012), pp. 509–538 (cit. on pp. 40, 42, 48).
- [29] Giovanni Garcea, Rodrigo Gonçalves, Antonio Bilotta, David Manta, Rui Bebiano, Leonardo Leonetti, Domenico Magisano, and Dinar Camotim. “Deformation modes of thin-walled members: A comparison between the method of Generalized Eigenvectors and Generalized Beam Theory.” In: *Thin-Walled Structures* 100.Supplement C (2016), pp. 192–212. DOI: <https://doi.org/10.1016/j.tws.2015.11.013>. URL: <http://www.sciencedirect.com/science/article/pii/S0263823115301518> (cit. on p. 14).
- [30] Leroy Gardner and David A Nethercot. *Designers’ Guide to Eurocode 3: Design of Steel Buildings.* second edition. ICE publishing, 2011. URL: <http://www.icevirtuallibrary.com/doi/book/10.1680/dsb.41721> (cit. on p. 7).
- [31] Alessandra Genoese, Andrea Genoese, Antonio Bilotta, and Giovanni Garcea. “Buckling analysis through a generalized beam model including section distortions.” In: *Thin Walled Struct.* 85 (2014), pp. 125–141 (cit. on p. 14).

- [32] Andrea Genoese, Alessandra Genoese, Antonio Bilotta, and Giovanni Garcea. "A geometrically exact beam model with non-uniform warping coherently derived from the Saint Venant rod." In: *Eng. Struct.* 68 (2014), pp. 33–46 (cit. on p. 14).
- [33] Rodrigo Gonçalves and Dinar Camotim. "Geometrically non-linear generalised beam theory for elastoplastic thin-walled metal members." In: *Thin-Walled Structures* 51.Supplement C (2012), pp. 121–129. DOI: <https://doi.org/10.1016/j.tws.2011.10.006>. URL: <http://www.sciencedirect.com/science/article/pii/S026382311100231X> (cit. on p. 10).
- [34] Rodrigo Gonçalves. "A geometrically exact approach to lateral-torsional buckling of thin-walled beams with deformable cross-section." In: *Comput. Struct.* 106 (2012), pp. 9–19 (cit. on p. 10).
- [35] Rodrigo Gonçalves, Manuel Ritto-Corrêa, and Dinar Camotim. "A large displacement and finite rotation thin-walled beam formulation including cross-section deformation." In: *Comput. Meth. Appl. Mech. Eng.* 199.23 (2010), pp. 1627–1643 (cit. on p. 10).
- [36] Rodrigo Gonçalves, Manuel Ritto-Corrêa, and Dinar Camotim. "A new approach to the calculation of cross-section deformation modes in the framework of generalized beam theory." In: *Computational Mechanics* 46.5 (2010), pp. 759–781. DOI: [10.1007/s00466-010-0512-2](https://doi.org/10.1007/s00466-010-0512-2). URL: <https://doi.org/10.1007/s00466-010-0512-2> (cit. on p. 10).
- [37] G. J. Hancock. "Distortional Buckling of Steel Storage Rack Columns." In: *Journal of Structural Engineering* (), pp. 2770–2783 (cit. on p. 8).
- [38] GJ Hancock. "Cold-formed steel structures: Research review 2013–2014." In: *Adv. Struct. Eng.* (2016), p. 1369433216630145 (cit. on p. 7).
- [39] K. Klöppel and B Unger. "Das Ausbeulen einer am freien Rand verstüfteten, dreiseitig momentenfrei gelagerten Platte unter Verwendung der nichtlinearen Beultheorie, Teil II: Experimentelle Untersuchungen, Vergleich der experimentellen mit den theoretischen Ergebnissen." In: *Der Stahlbau* 39 (1970), pp. 115–123 (cit. on p. 8).
- [40] Raffaele Landolfo, Luigi Fiorino, and Gaetano Della Corte. "Seismic Behavior of Sheathed Cold-Formed Structures: Physical Tests." In: *Journal of Structural Engineering* 132.4 (2006), pp. 570–581. DOI: [10.1061/\(ASCE\)0733-9445\(2006\)132:4\(570\)](https://doi.org/10.1061/(ASCE)0733-9445(2006)132:4(570)) (cit. on p. 6).
- [41] S.C.W. Lau and Hancock G.J. "Distortional Buckling Formulas for Channel Columns." In: *Journal of Structural Engineering* (1987) (cit. on p. 8).

- [42] Z. Li and B.W. Schafer. “Buckling analysis of cold-formed steel members with general boundary conditions using CUFSM: conventional and constrained finite strip methods.” In: *Proceedings of the 20th Int'l. Spec. Conf. on Cold-Formed Steel Structures, St. Louis, MO*. (Nov. 2010) (cit. on p. 11).
- [43] Zhanjie Li, Jean C Batista Abreu, Jiazhen Leng, Sándor Ádány, and Benjamin W Schafer. “Constrained finite strip method developments and applications in cold-formed steel design.” In: *Thin-Walled Structures* 81 (2014), pp. 2–18 (cit. on p. 12).
- [44] R.M. Lucas, F.G.A. Al-Bermani, and S. Kitipomchai. “Modelling of cold-formed purlin-sheeting systems— Part 1: Full model.” In: *Thin-Walled Structures* 27.3 (1997), pp. 223 –243. DOI: [https://doi.org/10.1016/S0263-8231\(96\)00038-9](https://doi.org/10.1016/S0263-8231(96)00038-9). URL: <http://www.sciencedirect.com/science/article/pii/S0263823196000389> (cit. on p. 30).
- [45] R.M. Lucas, F.G.A. Al-Bermani, and S. Kitipornchai. “Modelling of cold-formed purlin-sheeting systems—Part 2. Simplified model.” In: *Thin-Walled Structures* 27.4 (1997), pp. 263 –286. DOI: [https://doi.org/10.1016/S0263-8231\(96\)00039-0](https://doi.org/10.1016/S0263-8231(96)00039-0). URL: <http://www.sciencedirect.com/science/article/pii/S0263823196000390> (cit. on p. 30).
- [46] E.E. Lundquist and E.Z. Stowel. “Principles of Moment Distribution Applied to the Stability of Structures Composed of Bars or Plates.” In: *NACA L-326* (1943) (cit. on p. 8).
- [47] M Majowiecki, F Ossola, and Pinardi S. “The suspended roof of the new Juventus stadium in Turin.” In: *Costruzioni Metalliche* 4 (2011), pp. 35–50 (cit. on p. 60).
- [48] Rosario Miletta. “Travi in parete sottile con deformabilità a a taglio e distorsione di sezione: formulazione teorica, modellazione numerica e applicazioni.” PhD thesis. Università di Bologna, 2013 (cit. on p. 10).
- [49] Stefano de Miranda, Alejandro Gutierrez, and Rosario Miletta. “Equilibrium-based reconstruction of three-dimensional stresses in GBT.” In: *Thin Walled Struct.* 74 (2014), pp. 146–154 (cit. on p. 10).
- [50] Stefano de Miranda, Alejandro Gutiérrez, Rosario Miletta, and Francesco Ubertini. “A generalized beam theory with shear deformation.” In: *Thin Walled Struct.* 67 (2013), pp. 88–100 (cit. on pp. 10, 17, 18, 105).
- [51] Stefano de Miranda, Antonio Madeo, Rosario Miletta, and Francesco Ubertini. “On the relationship of the shear deformable Generalized Beam Theory with classical and non-classical theories.” In: *Int. J. Solids Struct.* 51.21 (2014), pp. 3698–3709 (cit. on pp. 10, 17, 18, 20, 23).

- [52] Stefano de Miranda, Antonio Madeo, Domenico Melchionda, and Francesco Ubertini. "A high performance flexibility-based GBT finite element." In: *Comput. Struct.* 158 (2015), pp. 285–307 (cit. on pp. 10, 17, 27).
- [53] Stefano de Miranda, Antonio Madeo, Domenico Melchionda, Luca Patruno, and Andrea Walter Ruggerini. "A corotational based geometrically nonlinear Generalized Beam Theory: buckling FE analysis." In: *International Journal of Solids and Structures* (2017) (cit. on p. 39).
- [54] NCCI. *Non-contradictory, complementary information*. URL: <http://www.steel-ncci.co.uk> (visited on 10/05/2017) (cit. on p. 7).
- [55] Eugenio Oñate. *Structural Analysis with the Finite Element Method: Linear Statics*. 1st. Vol. 2. International Center for Numerical Methods in Engineering (CIMNE), 2013 (cit. on p. 27).
- [56] A Pagani and E Carrera. "Unified formulation of geometrically nonlinear refined beam theories." In: *Mechanics of Advanced Materials and Structures* (2017), pp. 1–17 (cit. on p. 15).
- [57] Theodore H.H. Pian. "Hybrid Models." In: *Numerical and Computer Methods in Structural Mechanics*. Academic Press, 1973, pp. 59–78. DOI: <http://dx.doi.org/10.1016/B978-0-12-253250-4.50009-9> (cit. on p. 27).
- [58] Giuseppe Piccardo, Gianluca Ranzi, and Angelo Luongo. "A complete dynamic approach to the Generalized Beam Theory cross-section analysis including extension and shear modes." In: *Mathematics and Mechanics of Solids* 19.8 (2014), pp. 900–924. DOI: [10.1177/1081286513493107](https://doi.org/10.1177/1081286513493107). eprint: <https://doi.org/10.1177/1081286513493107>. URL: <https://doi.org/10.1177/1081286513493107> (cit. on p. 10).
- [59] E Riks. "An incremental approach to the solution of snapping and buckling problems." In: *Int. J. Solids Struct.* 15.7 (1979), pp. 529–551 (cit. on p. 70).
- [60] B. O. Rodrigues. "Des lois géométriques qui régissent les déplacements d'un système solide dans l'espace, et de la variation des coordonnées provenant de ces déplacements considérés indépendamment des causes qui peuvent les produire." In: *Journal des Mathématiques Pures et Appliquées* 5.1 (1840), pp. 380–440 (cit. on p. 68).
- [61] Benjamin W Schafer. "Cold-formed steel structures around the world." In: *Steel Construction* 4.3 (2011), pp. 141–149 (cit. on pp. 6, 7).

- [62] Benjamin W Schafer and S Ádány. “Buckling analysis of cold-formed steel members using CUFSM: conventional and constrained finite strip methods.” In: *Eighteenth international specialty conference on cold-formed steel structures*. 2006, pp. 39–54 (cit. on pp. 11, 12).
- [63] Benjamin William Schafer. “Developments in research and assessment of steel structures: Highlights from the perspective of an American researcher.” In: *ce/papers 1.2-3* (2017), pp. 95–114 (cit. on p. 7).
- [64] Benjamin Schafer and Gregory J. Hancock. “A Detailed History of Distortional Buckling of Columns A History of Distortional Buckling of Cold-Formed Steel Columns.” In: (). URL: https://www.researchgate.net/publication/237731433_A_Detailed_History_of_Distortional_Buckling_of_Columns_A_History_of_Distortional_Buckling_of_Cold-Formed_Steel_Columns (cit. on p. 7).
- [65] R. Schardt. “Eine Erweiterung der technischen Biegelehre für die Berechnung biegesteifer prismatischer Faltwerke.” In: (1966). URL: https://www.ernst-und-sohn.de/sites/default/files/uploads/aktuelles/news/st66s161_0.pdf (cit. on p. 9).
- [66] R. Schardt. “Generalized beam theory—an adequate method for coupled stability problems.” In: *Thin-Walled Structures* 19.2 (1994), pp. 161–180. DOI: [https://doi.org/10.1016/0263-8231\(94\)90027-2](https://doi.org/10.1016/0263-8231(94)90027-2). URL: <http://www.sciencedirect.com/science/article/pii/0263823194900272> (cit. on p. 9).
- [67] Richard Schardt. *Verallgemeinerte Technische Biegetheorie*. Springer Nature, 1989. DOI: [10.1007/978-3-642-52330-4](https://doi.org/10.1007/978-3-642-52330-4) (cit. on pp. 9, 17, 20).
- [68] M.L. Sharp. “Longitudinal Stiffeners for Compression Members.” In: *Journal of the Structural Division* (1966), pp. 187–211 (cit. on p. 8).
- [69] N Silvestre and D Camotim. “Nonlinear generalized beam theory for cold-formed steel members.” In: *Int. J. Struct. Stab. Dyn.* 3.04 (2003), pp. 461–490 (cit. on p. 10).
- [70] N. Silvestre and D. Camotim. “Distortional buckling formulae for cold-formed steel C and Z-section members: Part I—derivation.” In: *Thin-Walled Structures* 42.11 (2004), pp. 1567–1597. DOI: <https://doi.org/10.1016/j.tws.2004.05.001>. URL: <http://www.sciencedirect.com/science/article/pii/S0263823104000862> (cit. on p. 10).
- [71] Nuno Silvestre and Dinar Camotim. “Shear deformable generalized beam theory for the analysis of thin-walled composite members.” In: *J. Eng. Mech.* 139.8 (2012), pp. 1010–1024 (cit. on p. 10).

- [72] P. Simão. “GBT stability analysis of a slender LiteSteel beam section member.” In: *EUROSTEEL 2008 A* (Sept. 2008), pp. 111–116 (cit. on p. 10).
- [73] P. Simão and L. Simões da Silva. “A unified energy formulation for the stability analysis of open and closed thin-walled members in the framework of the generalized beam theory.” In: *Thin-Walled Structures* 42.10 (2004), pp. 1495–1517. DOI: <https://doi.org/10.1016/j.tws.2004.03.021>. URL: <http://www.sciencedirect.com/science/article/pii/S0263823104000631> (cit. on p. 10).
- [74] Gerard Taig, Gianluca Ranzi, and Angelo Luongo. “GBT pre-buckling and buckling analyses of thin-walled members under axial and transverse loads.” In: *Continuum Mechanics and Thermodynamics* 28.1 (2016), pp. 41–66. DOI: [10.1007/s00161-014-0399-9](https://doi.org/10.1007/s00161-014-0399-9). URL: <https://doi.org/10.1007/s00161-014-0399-9> (cit. on p. 10).
- [75] Various. *Steelconstruction: The free encyclopedia for UK steel construction information*. 2017. URL: <https://www.steelconstruction.info/> (visited on 02/11/2017) (cit. on p. 6).
- [76] Vasilii Z. Vlasov. *Thin-walled elastic beams (Tonkostenny uprugie sterzhni)*. Ed. by Israel Program for Scientific Translations. II edition, translated from Russian. S. Monson, 1961 (cit. on p. 9).
- [77] G. Winter. “Strength of Thin Steel Compression Flanges.” In: *Transactions of ASCE* 1.112 (1947) (cit. on p. 8).
- [78] Wei-Wen Yu. *Cold-formed steel design*. John Wiley & Sons, 2000. URL: <http://ccfsonline.org/cold-formed-steel-design-4th-ed/> (cit. on p. 7).
- [79] Wei bin Yuan, Shanshan Cheng, Long yuan Li, and Boksun Kim. “Web-flange distortional buckling of partially restrained cold-formed steel purlins under uplift loading.” In: *International Journal of Mechanical Sciences* 89 (2014), pp. 476–481. DOI: <http://dx.doi.org/10.1016/j.ijmecsci.2014.10.011>. URL: <http://www.sciencedirect.com/science/article/pii/S0020740314003476> (cit. on p. 30).
- [80] Congxiao Zhao, Jian Yang, Feiliang Wang, and Andrew H.C. Chan. “Rotational stiffness of cold-formed steel roof purlin–sheeting connections.” In: *Engineering Structures* 59.Supplement C (2014), pp. 284–297. DOI: <https://doi.org/10.1016/j.engstruct.2013.10.024>. URL: <http://www.sciencedirect.com/science/article/pii/S0141029613004914> (cit. on p. 30).
- [81] Ronald D. Ziemian. *Guide to Stability Design Criteria for Metal Structures*. 6th edition. Wiley, 2010 (cit. on p. 7).

“Disse: la filosofia sembra che si occupi solo della verità, e la letteratura sembra che si occupi solo di fantasie, ma forse dice solo la verità. Monteiro Rossi sorrise e disse che gli sembrava una bella definizione per le due discipline. ”

— Antonio Tabucchi, *Sostiene Pereira*

RINGRAZIAMENTI

Con queste poche righe desidero ringraziare chi, a diverso titolo, ha contribuito alla tesi di dottorato.

Ringrazio il prof. Francesco Ubertini – oggi magnifico rettore – e il prof. Stefano de Miranda rispettivamente per la fiducia in me riposta e per la discussione sull’attività di ricerca, le numerose revisioni e le opportunità fornite.

Ringraziamenti particolari vanno inoltre alle persone che mi hanno fatto sentire un po’ a casa anche quando ero molto lontano dall’Emilia per condurre l’attività di ricerca. Un grazie particolare quindi all’ing. Antonio Madeo, per l’accoglienza presso l’università della Calabria, il confronto costante sul corotazionale implicito e la sua simpatia.

Un altro ringraziamento speciale è dovuto inoltre al prof. Rodrigo Gonçalves, che ha supervisionato con generosità la mia attività presso l’FCT di Lisbona, fornendo spunti di riflessione essenziali per il successo dell’elemento finito GBT nonlineare.

Grazie anche ai miei colleghi del LAMC, per avere creato un ambiente lavorativo estremamente positivo.

Grazie infine a Giovanna, per avere sorriso sempre, anche durante i miei brontolii da tesi, e a tutta la mia famiglia, per essere stata sempre vicina.

COLOPHON

This document was typeset using the typographical look-and-feel classicthesis developed by André Miede. The style was inspired by Robert Bringhurst's seminal book on typography "*The Elements of Typographic Style*". classicthesis is available for both \LaTeX and \LyX :

<https://bitbucket.org/amiede/classicthesis/>

Happy users of classicthesis usually send a real postcard to the author, a collection of postcards received so far is featured at:

<http://postcards.miede.de/>

